# ABSTRACT

| | |
|---|---|
| Title of Document: | ACTIVE NONRECIPROCAL ACOUSTIC METAMATERIALS |
| | Bilal Baqai, Masters of Science, 2017 |
| Directed By: | Professor Amr Baz, Mechanical Engineering |

In this thesis, the emphasis is placed on the development of a class of active acoustic diodes and metamaterials in an attempt to control the flow and distribution of acoustic energy in acoustic cavities and systems. Such development departs radically from the currently available approaches where the non-reciprocities are generated by hard-wired designs, favoring one transmission direction which is dictated by the arrangement of the hardware and hence it cannot be reversed, or without the presentation of rigorous control theory analysis.

The proposed active nonreciprocal acoustic metamaterial (*ANAM*) cell consists of only one-dimensional acoustic cavity provided with active flexible boundaries. These boundaries are made from piezoelectric bimorphs with the inner layers which interact directly with cavity acting as sensors for monitoring the pressures of the propagating acoustic waves. The outer layers of the bimorphs provide the necessary control actions by direct application of the appropriate control voltage on each layer or by proper connection of nonlinearly activated shunted networks of electrical components such as the switching resistor networks. The control of the switching is carried out using the robust Sliding Mode Control (*SMC*) strategy. In this strategy, a lumped-parameter model of the *ANAM* cell is developed to control the strength of the nonreciprocal characteristics of the cell by proper selection of the slope of the

switching surfaces. Appropriate optimization strategies are developed to enable a rational selection of the characteristics of the switching surfaces.

Numerical examples are presented to demonstrate the effectiveness of the proposed *ANAM* in tuning and programming the directivity, flow, and distribution of acoustic energy propagating though the metamaterial.

Experimental demonstration of the proposed *ANAM* is presented and includes a comprehensive investigation of the effect of the parameters of the *SMC* on the system performance. Such investigations are carried out in an attempt to validate the capabilities of *ANAM* in controlling the non-reciprocity in magnitude and direction.

The presented theoretical and experimental techniques provide invaluable tools for designing and predicting the performance of this class of *ANAM*.

ACTIVE NONRECIPROCAL ACOUSTIC

METAMATERIALS


By

Bilal Baqai



Thesis submitted to the Faculty of the Graduate School of the

University of Maryland, College Park, in partial fulfillment

of the requirements for the degree of

Masters of Science

2017



Advisory Committee:

Professor Amr Baz, Chair

Professor Balakumar Balachandran

Professor Miao Yu

# Acknowledgements

# Table of Contents

# List of Figures

# List of Tables

# Chapter 1

# INTRODUCTION

Extensive efforts have been exerted in the fields of optics, electronics, and electromagnetics to breaking the reciprocity theorem that govern the propagation of waves in linear media as described by Lorentz (1896)[1], Helmholtz (1860)[2], and Rayleigh (1901, 1945)[3-4]. These efforts have focused on controlling the wave energy flow by developing a wide variety of approaches such as the simple semiconductor "*electrical diode*" which transmits energy differently along two opposite propagation directions. In optics, a device performing a similar function is the "*optical (Faraday) isolator*" which utilizes polarization rotation in a magnetic field to break reciprocity (Siegman, 1986 [5]; Jalas *et al.*, 2013[6]). Similarly, thermal rectifiers or diodes are developed to rectify the heat flow in solids. Such devices act as a thermal conductor when a positive thermal bias is applied, while in the opposite case of a negative thermal, these devices effectively behave as thermal insulators (Dames, 2009)[7].

## 1.1. Concept of Active Nonreciprocal Acoustic Metamaterial (*ANAM*):

The concept of the active nonreciprocal acoustic metamaterial (*ANAM*) can best be understood by considering its two possible configurations whereby it can be used either for interior noise mitigation or exterior noise mitigation.

### 1.1.1. Interior Noise Mitigation:

For interior noise mitigation, as shown in Figure 1.1, the acoustic cavity is manufactured from the *ANAM* to block the flow of the incoming acoustic waves while allowing the propagation of outgoing acoustic waves to flow out of the cavity. In this manner, the interior noise of the acoustic cavity can be minimized.
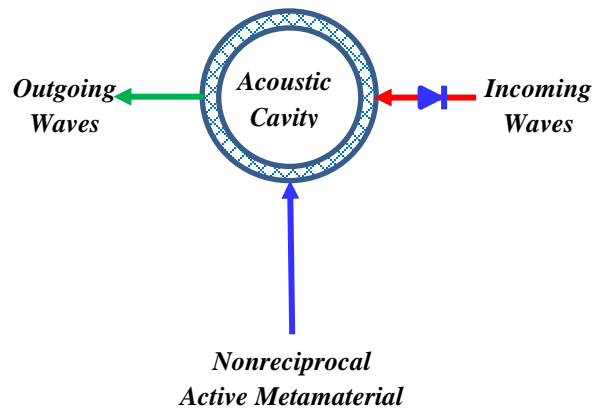


**Figure 1.1 - Nonreciprocal active metamaterial for interior noise mitigation**

### 1.1.2. Interior Noise Mitigation Application:

A typical application of this class of *ANAM* is shown in Figure 1.2 where the metamaterial can be used to manufacture or be a part of a composite fuselage of an aircraft in order to isolate the engine and flow noise from propagating to the interior of the fuselage and enabling any noise generated inside the fuselage to escape to the surrounding medium.
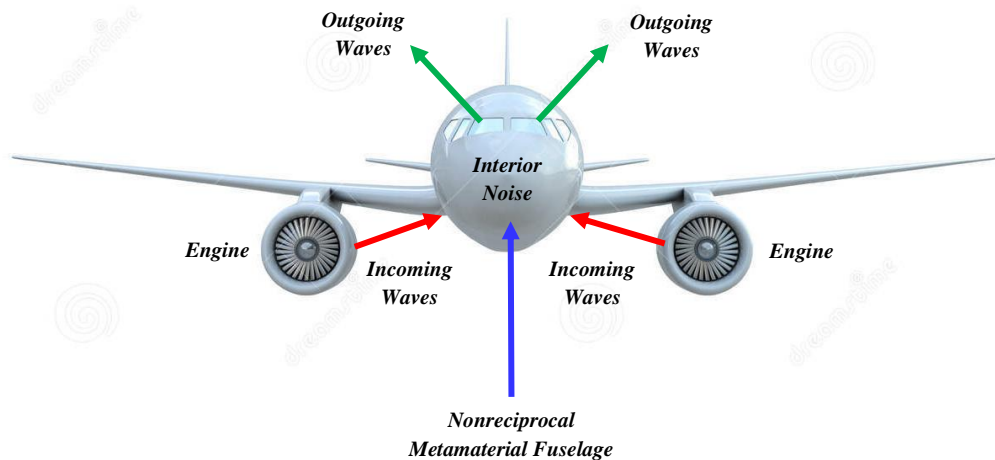


**Figure 1.2 – Application of interior noise mitigation by Nonreciprocal active metamaterial**

### 1.1.3. Exterior Noise Mitigation:

For exterior noise mitigation, as shown in Figure 1.3, the acoustic cavity is manufactured from the *ANAM* to block the flow of the outgoing acoustic waves while allowing the propagation of incoming acoustic waves into the cavity. Hence, the interior noise of the acoustic cavity is trapped.
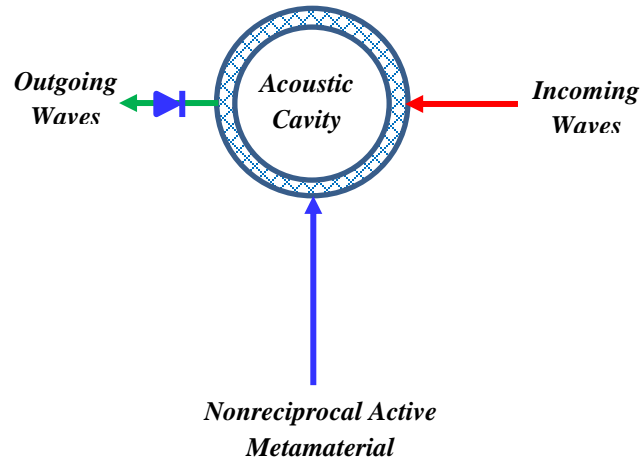
**Figure 1.3 - Nonreciprocal active metamaterial for exterior noise mitigation**

### 1.1.4. Exterior Noise Mitigation Application:

A typical application of this class of *ANAM* is shown in 1.4 where the metamaterial can be used to manufacture or be a part of a composite structure of an underwater vehicle. Using *ANAM* can isolate the engine and flow noise from propagating to the exterior of the vehicle to ensure stealth operation.
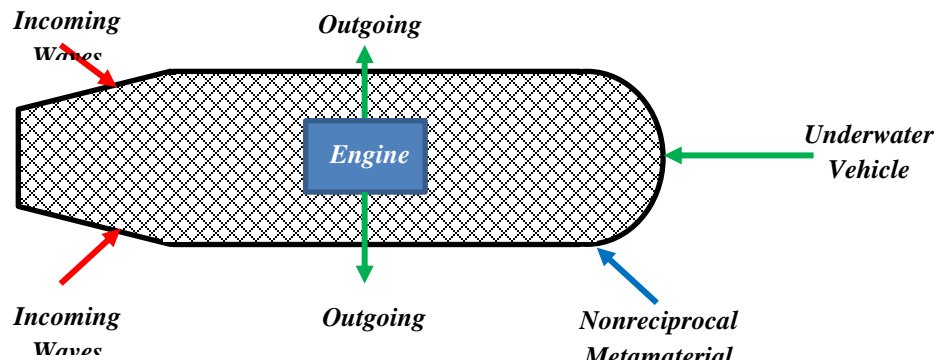


**Figure 1.4 – Applications of Nonreciprocal active metamaterial for exterior noise mitigation**

4

## 1.2. Active Nonreciprocal Acoustic Metamaterial *(ANAM):*

Considerable efforts have been exerted at the to develop active acoustic metamaterial (*AAMM*)[11-26], platforms which have tunable and programmable mechanical and acoustic properties. These *AAMM* are intended to enable the operation over wide frequency bands, adaptation to varying external environment, and more importantly morphing from one functional configuration to another based on the mission requirements of the *AAMM*. With such unique capabilities, acoustic cloaks, beam shifters, perfect absorbers, and/or perfect reflectors can be physically realizable by simply programming the same *AAMM* platform to acquire the appropriate mechanical and acoustic properties necessary to achieve the desired functionality without the need for any changes in the physical hardware of the platform itself.

The main emphasis had been placed on developing acoustic cloaks which can be configured to treat objects either externally or internally in order to render these objects acoustically invisible. The external cloaks can potentially be used in hiding acoustically critical objects whereas the internal cloak can be employed to make the fuselages of aircraft and helicopters quiet and improve the interior acoustics inside auditoriums and meeting rooms.

## 1.3. Vision of the thesis:

The thesis was envisioned for the following key points,

- Develop active nonreciprocal acoustic metamaterial platforms which have been provided with unique modeling, simulation, visualization and characterization tools

to study the fundamentals and discover the underlying phenomena governing the operation of this class of acoustic metamaterials.

- Develop rational design tools and approaches to enable the development and synthesis of active nonreciprocal acoustic metamaterials with desired functionality.

## 1.4. Developments:

Development of the following new concepts and designs for synthetic acoustic nonreciprocal acoustic metamaterials

- Develop lumped-parameter for modeling and simulation of 1D periodic acoustic nonreciprocal acoustic metamaterials with active and passive configurations.
- Study the physics of propagation of low frequency acoustic waves in active functional metamaterials.
- Develop various configurations of new nonreciprocal metamaterial with programmable acoustic properties
- Develop new device concepts and designs

## 1.5. Demonstration of functional acoustic metamaterials

- Develop active and passive nonreciprocal acoustic metamaterial platforms
- Fabrication techniques and processes
- Characterization of the acoustic wave propagation in the active and passive nonreciprocal acoustic metamaterial platforms

- Characterization of the impedance, transmissibility, scattering, and dispersion of active and passive nonreciprocal acoustic metamaterial platforms

- Develop demonstrators of active and passive nonreciprocal acoustic metamaterial devices with controllable directivity and dispersion characteristics

## 1.6. Innovations:

- Proposed active and passive nonreciprocal acoustic metamaterials (*ANAM*) have programmable characteristics to enable operation over broad frequency band unlike all available hard wired nonreciprocal metamaterials which operate over limited frequency bands.

- Proposed *ANAM* is realizable using smart materials & can have acoustic properties that can be tuned and configured according to the mission of the platform.

- Proposed *ANAM* metamaterials have unique mechanical structure but by virtue of novel interactions between neighboring cells, their acoustic properties can be tuned to operate over a wide frequency bandwidth.

- No one has any Nonreciprocal Acoustic Metamaterials that are comparable to the *ANAM* presented in this thesis.

Therefore the thesis appears in five chapters. Chapter 1 presented a brief overview of the literature of non-reciprocal propagation of acoustic waves as well as outlined the concept of Active Nonreciprocal Acoustic Metamaterials (*ANAM*). In chapter 2, the theory that governs the operation of the *ANAM* using the Sliding Mode Controller (*SMC*). The

experimental behavior of a prototype of a cell of the *ANAM* is investigated and presented, in chapter 3, when using an analog implementation of the *SMC* controller. A simulation of the theoretical behavior of the *ANAM* using *PSPICE* is carried out in chapter 4 in an attempt to validate the experimental results. A summary of the conclusions of the present study is presented in chapter 5 along with the possible recommendations for the future studies.

## 1.7. Summary

This chapter has presented the a brief overview of the literature of non-reciprocal propagation of acoustic waves as well as outlined the concept of Active Nonreciprocal Acoustic Metamaterials (*ANAM*). The significance and the objectives of the present work have been also discussed. This chapter has presented also the scope of the thesis and the topics discussed.

# Chapter 2

# THEORY

## 2.1. Active Nonreciprocal Acoustic Metamaterials (*ANAM*)

In this thesis, the approach which has been used was meant to mainly control the flow and the distribution of acoustic energy in acoustic systems and acoustic cavities. Emphasis is mainly placed on the development of a class of active acoustic diodes and metamaterials in an which can contribute towards controlling the flow and the distribution of acoustic energy in acoustic cavities and systems. The control of the non-reciprocity will be demonstrated by using the Sliding Mode Control (*SMC*).

## 2.2. Current Non-reciprocal Acoustic Metamaterial

Several configurations of nonreciprocal acoustic diode that have are either passive ( Liu *et al.*, 2015) [8] as shown in Figure 2.1 or active as proposed by Popa and Cummer (2014) [9] and Gu *et al.* (2015) [10] which are shown in Figures 2.2 and 2.3 respectively.
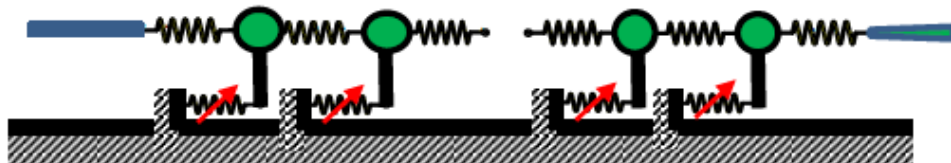


**Figure 2.1 - Mechanical analog of the acoustic diode metamaterial**
**(Liu *et al*., 2015)**

The acoustic diode proposed by Liu *et al.* one-dimensional Acoustic Diode had been manufactured using a series of spherical masses which have been connected by linear and weakly nonlinear springs. A uniform cross-section, linear elastic rod and another linear elastic rod with variable cross sectional area have been placed at the two ends to introduce asymmetry of the system is introduced by one. When an acoustic wave propagates through the non-uniform rod, its amplitude is changed because of the energy-conservation principle.
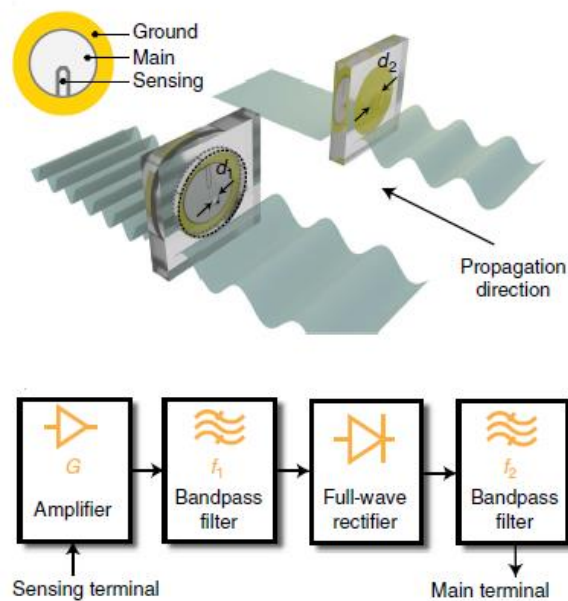


**Figure 2.2 - Non-reciprocal and highly nonlinear active acoustic metamaterials (Popa and Cummer, 2014)**

In the non-reciprocal metamaterials introduced by Popa and Cummer, a couple of Helmholtz cavities, which were tuned on different frequencies to create the asymmetry needed, were used for the non-reciprocal behavior. Both cavities had a shared common wall made up of piezoelectric membrane. The membrane senses the ambient acoustic field and generate an acoustic response which is controlled by the electronic circuit.
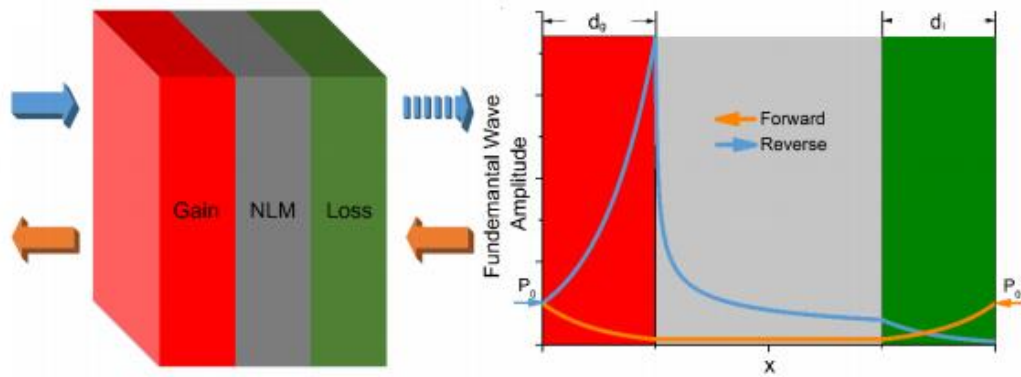


**Figure 2.3 - Broadband non-reciprocal transmission of sound**
**(Gu *et al.*, 2015)**

The model proposed by Gu *et al.* in 2015, comprises of an acoustical nonlinear material which is inserted between the gain and lost media. The presence of the gain and lossy media allows non-reciprocal manipulation of waves. The non-linear material is to provide the pressure-dependent response to the incident wave, in addition to provide the non-reciprocal characteristics.

The existing models of non-reciprocal acoustic metamaterial suffer from some of the serious limitations. Below are some of the common limitations from which these acoustic metamaterial suffer,

- The non-reciprocity is generated by hard-wired designs
- The non-reciprocity has favorable characteristics in one direction which is dictated by the arrangement of the hardware and hence it cannot be reversed
- No control theory, analysis, or synthesis has been presented

## 2.3. Configurations of the Active Nonreciprocal Acoustic Metamaterial

## 2.3.1. Configuration 1:

Basically *ANAM* is made up of an acoustic cavity which has been provided with flexible and controlled piezoelectric diaphragms. These piezoelectric diaphragms are capable of being used as an actuator or as a sensor ((2009, 2010) [11-12] and Akl and Baz (2009, 2010)[13-16]). Figure 2.4(a) shows the basic structure of the Active non-reciprocal acoustic cavity.
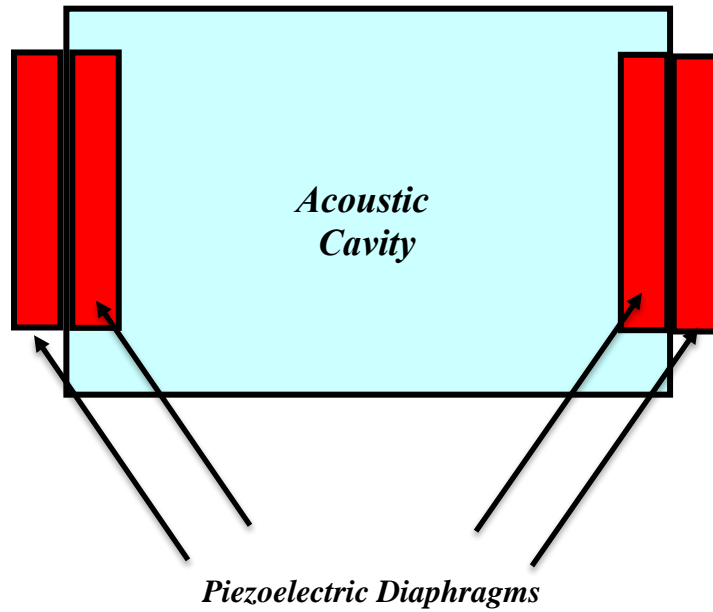
**Figure 2.4 – Basic Structure of Active Non-reciprocal Acoustic Metamaterial**

On using appropriate control laws and/or programmable electronic components, the energy dissipation distributions along the *ANAM* components can be manipulated. Figure 2.5 shows nonreciprocal and reversible wave propagation characteristics.

**(a) - transmission**



**(b) - attenuation**
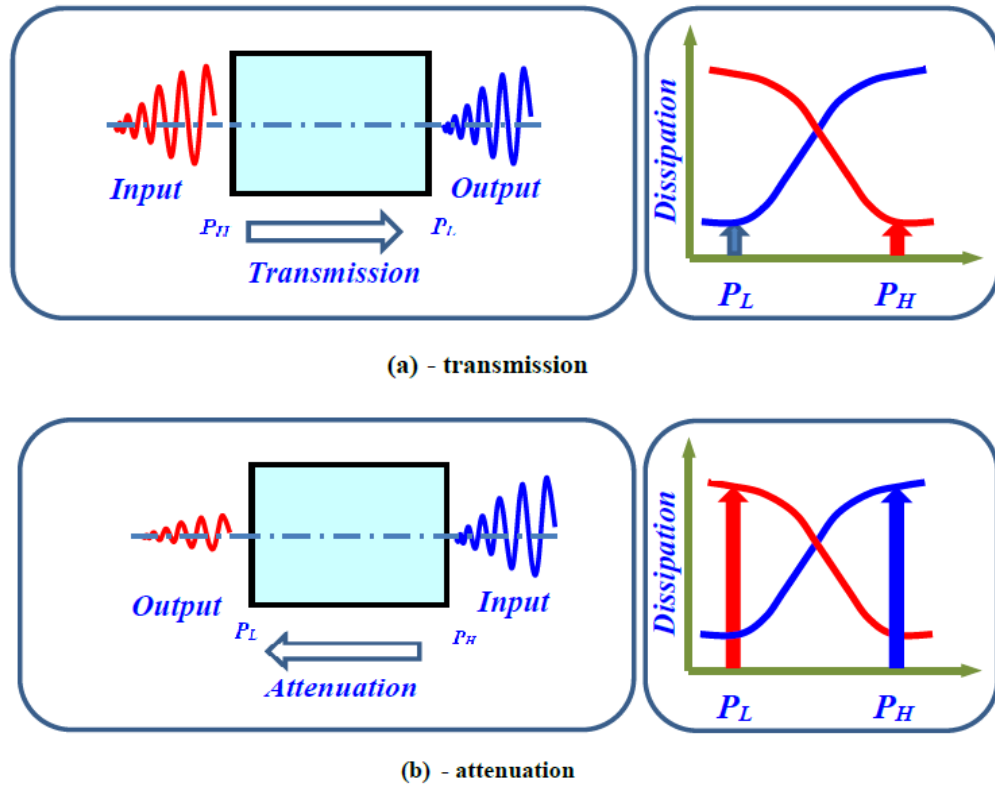
**Figure 2.5 – First configuration of Active acoustic
non-reciprocal metamaterial cell**

### 2.3.2. Configuration 2:

As mentioned earlier, Active nonreciprocal acoustic metamaterial (*ANAM*) cell consists of an acoustic cavity which is provided with active flexible boundaries. These boundaries are made from piezoelectric bimorphs. As shown in the figure 2.6, piezoelectric diaphragms can have the following two uses in this acoustic cavity

a. Actuator

b. Sensor

## a. Actuator:

There are two outer piezoelectric diaphragms in the acoustic cavity. Both of them acts as actuator. Basically, these layers of piezoelectric bimorphs provide the necessary control actions by direct application of the appropriate control voltage on each layer or by proper connection of nonlinearly activated shunted networks of electrical components such as the switching resistor network ($R_0$-$R_1$).

## b. Sensor:

As shown in the Figure 2.6, there are a couple of piezoelectric diaphragms which act as sensors in the acoustic cavity. These inner layers which interact directly with cavity which allows them to act as a sensor. These sensors are meant to monitor the pressure of the propagating acoustic waves.
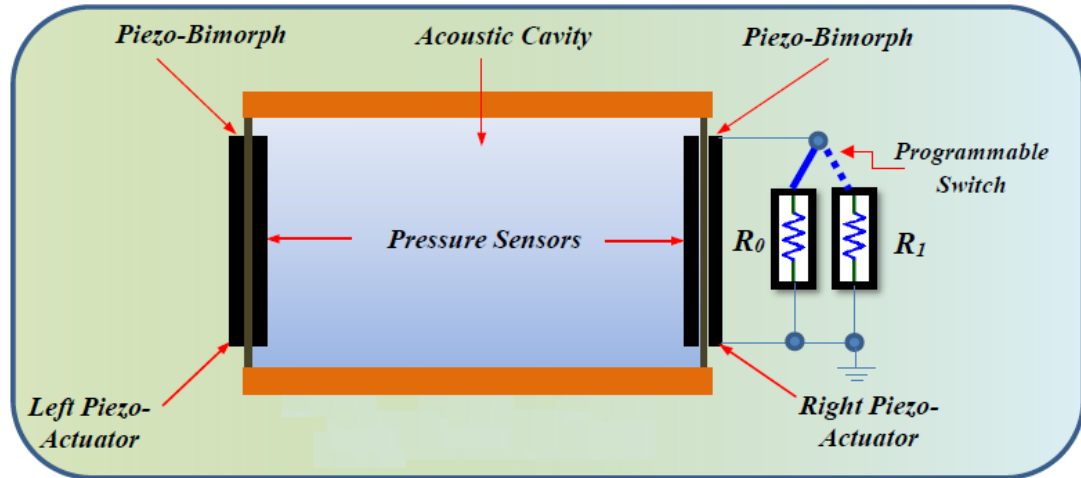
**Figure 2.6 – Second configuration of Active
acoustic non-reciprocal metamaterial cell**

## 2.4. Transmission line Analysis of Active non-reciprocal acoustic Metamaterial:

Electrical analogous circuits have been developed to simulate the lumped-parameter characteristics of the proposed *ANAM* cell. Such an analogy enables the accurate predictions of the *ANAM* behavior provided that the dimensions of the cell are much smaller than the smallest wavelength of the propagating waves.

For illustrative purposes, a one-dimensional model of an idealized and undamped *ANAM* cell has been represented as shown in Figure 2.7. The mass and stiffness of the acoustic cavity have been represented by the inductance and capacitance respectively. The dynamics of the piezo-bimorph is split into two parts. The first part is intended to account for the behavior of mechanical structure of the bimorph which consist of its mass and stiffness that are represented by the inductance and capacitance respectively. The second part accounts for the electrical behavior of the bimorph whereby the coupled-field nature of the bimorph is represented by a transformer with transformation ratio 1:φ, where φ is

16

the acoustic pressure/voltage transformation factor. Furthermore, the electric impedance of the bimorph is included to model the bimorph capacitance as well as any shunted electric network components which are connected to facilitate the control of the bimorph behavior. These ideas have been discussed earlier by Baz (2009, 2010) [11-12] and Akl and Baz (2009, 2010)[13-16].
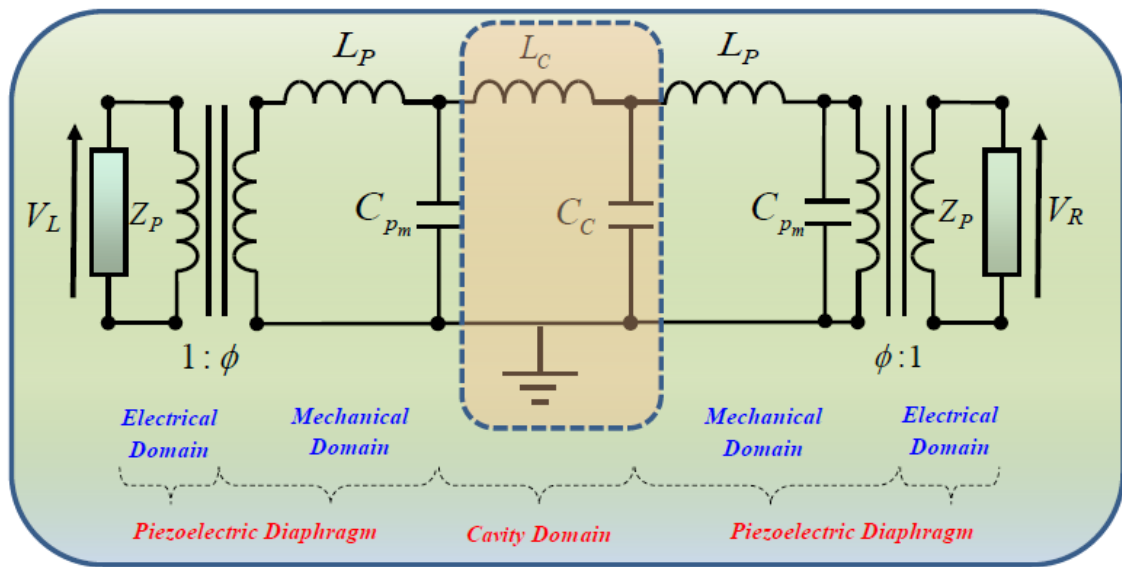


**Figure 2.7 – Electrical circuit analogy for the proposed active nonreciprocal acoustic metamaterial cell**

## 2.5. Active Control of the Nonreciprocal Acoustic Metamaterial Cell

The two configurations of the *ANAM*, which have been discussed earlier, enables the development of a wide range of scientifically rich active control strategies. The approach taken here, was to use a Sliding Mode control to actively control the cell, as employed on an idealized version of configuration 2 of the *ANAM*. The fast dynamics of the piezo-bimorphs are neglected relative to the slow dynamics of the acoustic cavity.

Such an idealized version is shown in Figure 2.8 where the control is achieved by a programmable switching between the two shunted resistors $R_0$ and $R_1$.
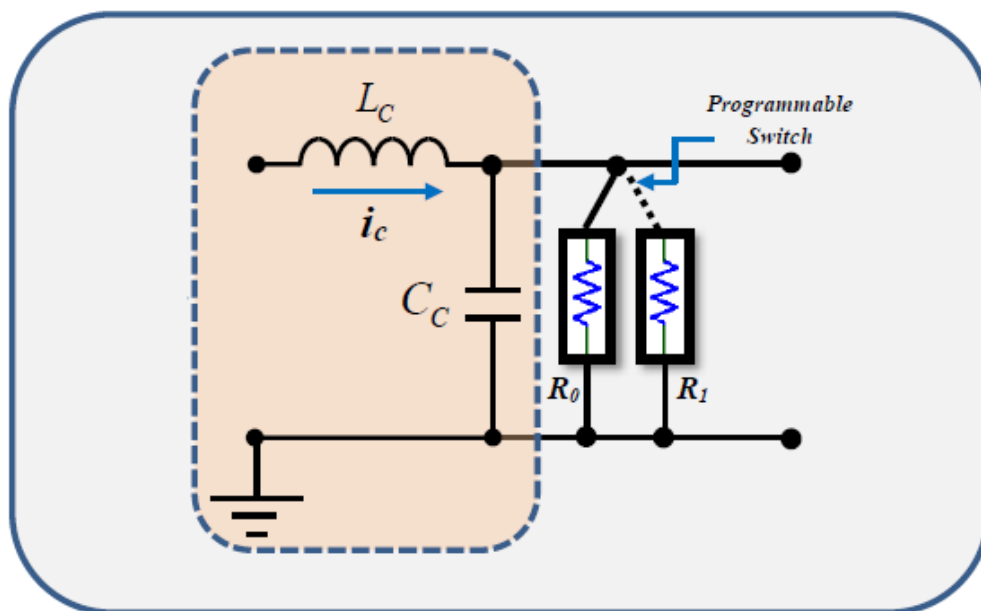


**Figure 2.8 – An idealized active nonreciprocal acoustic metamaterial cell**

The dynamics of the idealized *ANAM* cell are governed by the following state-space equations:

$$\frac{d}{dt}\begin{Bmatrix} i_c \\ u_c \end{Bmatrix} = \begin{bmatrix} 0 & -\dfrac{1}{L_C} \\ \dfrac{1}{C_C} & -\dfrac{1}{RC_C} \end{bmatrix} \begin{Bmatrix} i_c \\ u_c \end{Bmatrix} + \begin{Bmatrix} \dfrac{1}{L_C} \\ 0 \end{Bmatrix} U \tag{2.1}$$

where $R$ is a nonlinear shunting resistance that varies between $R_0$ and $R_1$ through switching.

Equation (2.1) can be rewritten in the following controllable canonical form:

$$\frac{d}{dt}\begin{Bmatrix} u_c \\ \dot{u}_c \end{Bmatrix} = \begin{bmatrix} 0 & 1 \\ -\dfrac{1}{C_C L_C} & -\dfrac{1}{RC_C} \end{bmatrix} \begin{Bmatrix} u_c \\ \dot{u}_c \end{Bmatrix} + \begin{Bmatrix} 0 \\ \dfrac{1}{C_C L_C} \end{Bmatrix} U \tag{2.2}$$

Hence, the switching between $R_0$ and $R_1$ by using the following switching line σ:

$$\sigma = \dot{u}_c + \alpha u_c \qquad \text{with } \alpha > 0 \tag{2.3}$$

To ensure stability of the switching controller, define a Lyapunov function $V$, such that:

$$V = \frac{1}{2}\sigma^2 \tag{2.4}$$

Stability requires that:

$$\dot{V} = \sigma\dot{\sigma} = \sigma\left(\ddot{u}_c + \alpha\dot{u}_c\right) \tag{2.5}$$

Now, on using the switching line equation, Eq. (2.3) and Eq. (2.2), we can obtain the following expression,

$$\dot{V} = \sigma\dot{\sigma} = -\left(\alpha^2 + \frac{1}{C_c L_c} - \frac{\alpha}{C_c R}\right)(\sigma u_c) \qquad (2.6)$$

Hence, the switching yields stable operation requires that $\dot{V} < 0$, hence the following switching laws must be satisfied:

$$\text{when } \sigma u_c > 0 \;\rightarrow\; R = R_0 = \frac{L_c}{\alpha} \;\rightarrow\; \dot{V} = -\alpha^2(\sigma u_c) < 0 \qquad (2.7)$$

$$\sigma u_c < 0 \;\rightarrow\; R = R_1 < \frac{\alpha}{C_c\left(\alpha^2 + \dfrac{1}{C_c L_c}\right)} < \frac{1}{\alpha C_c} \;\rightarrow\; \dot{V} < 0 \qquad (2.8)$$

From the above two expressions (Eq. 2.7 and Eq. 2.8), it can be concluded that a switching controller was required to be designed that can switch between two resistances depending whether $\sigma U_c$ terms is either greater than or less than zero.

In addition, the above expression also quantifies that the value of the resistances are related with the values of $\alpha$ from which it can also be concluded that the variation in alpha lead to changes in the resistance values. Furthermore, the changes occurring due to changes in $\alpha$ values are not only limited to the resistance changes, but it also affects the response in the output parameters.

To study the changes in the output parameters, different $\alpha$ values were considered to obtain the outputs. For illustrative purposes, an acoustic cavity was considered with

$C_C$=1 $m^4s^2/kg$ and $L_C$=1 $kg/m^4$.    For different values of the slope of the switching line α,

dynamic responses were obtained.    From Figure 2.9 it is evident that when α is large

(α=5), the strength of the input acoustic pressure wave, at the left side of the *ANAM*, is

attenuated considerably as it propagates to the output end at the right side of the *ANAM* as

shown in Figures 2.9 (a) and 2.9 (e). Such attenuation results from the application of the

switching controller which has the phase plane characteristics displayed in Figure 2.9 (c).

Note that reversing the direction propagation through the *ANAM* results in amplification of

the wave propagation strength as shown in Figure 2.9 (g). Under such inverse propagation

conditions, the *ANAM* acts in a manner similar to the classical "*Boost Voltage Converter*"

(King and Knight, 2009) whereby the input wave at the right side of the *ANAM* is amplified

as it propagates to the left side of the *ANAM*. Accordingly, the *ANAM* exhibits very clearly

distinct nonreciprocal characteristics.

On reducing the value of *α* to 0.8, is shown to not affect the propagation strength of

the input pressure wave as it propagates through the *ANAM* cell from the left to the right

sides of the cell as shown in Figures 2.9 (g) through Figure 2.9 (h).

Hence, the strength of the nonreciprocal characteristics of the *ANAM* cell can be

controlled by proper selection of the slope of the switching line α. Simulations and

experiments have been conducted which appears to confirm that the change in the values

of affects the non-reciprocal characteristics of the *ANAM* cell.
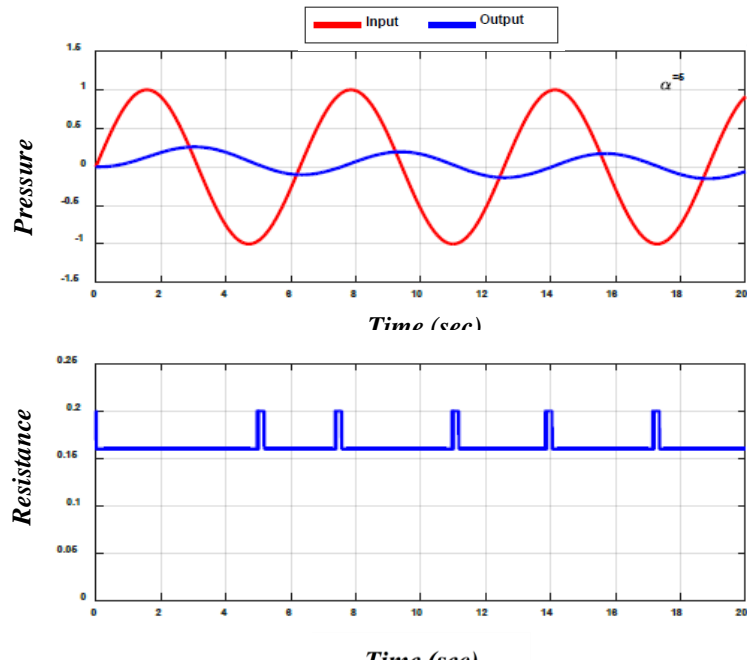
**(a) – Pressure vs Time and Resistance vs Time plots for higher values of α = 5**
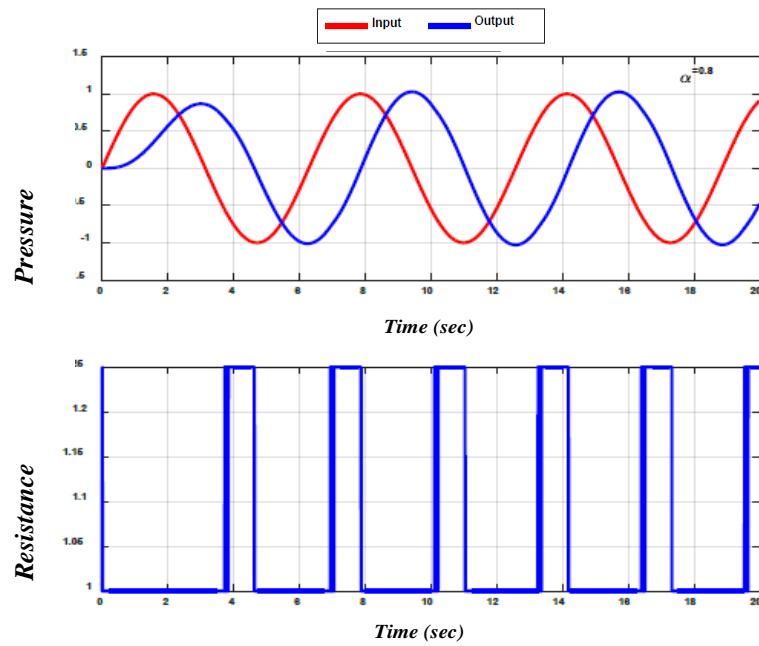


**Figure 2.9(b) – Pressure vs Time and Resistance vs Time plots for lower values of α=0.8**

22
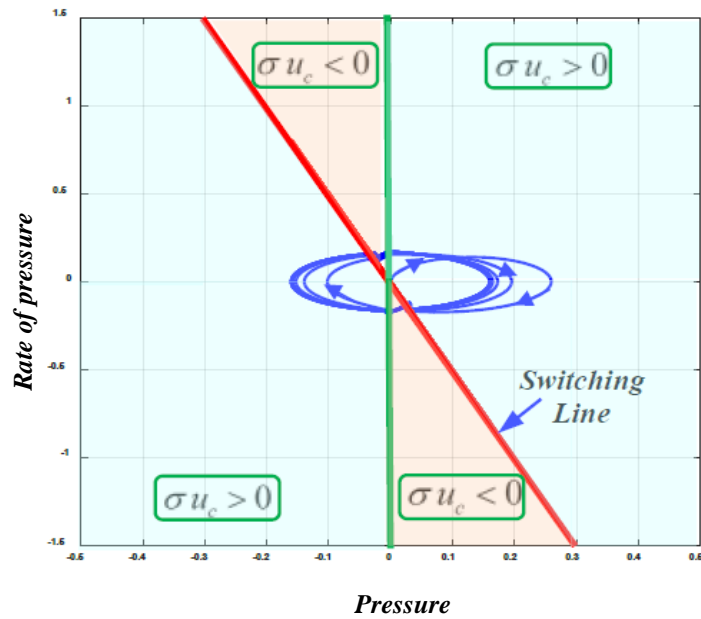
**Figure 2.9(c) – Pressure vs Pressure Rate**
**Higher values of α =5**
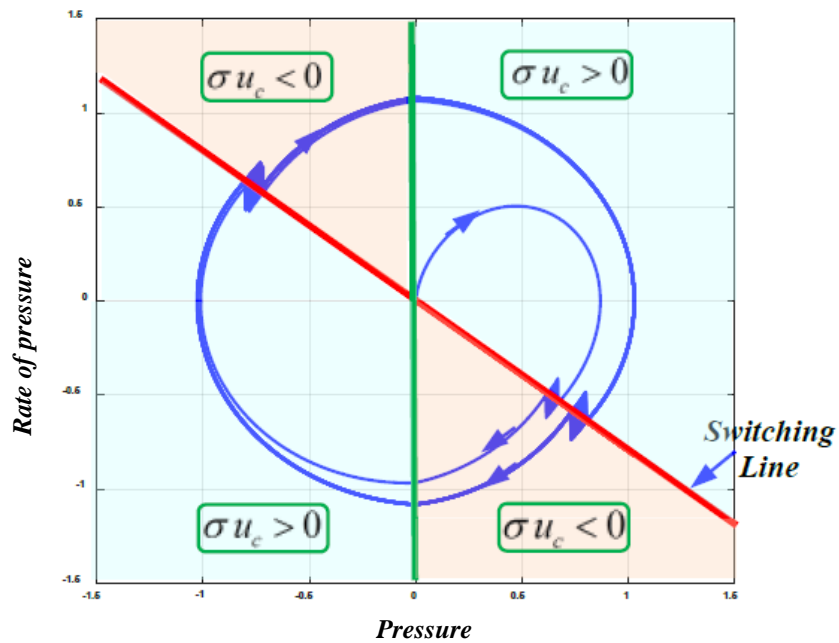


**Figure 2.9(d) – Pressure vs Pressure Rate**
**Lower values of α = 0.8**
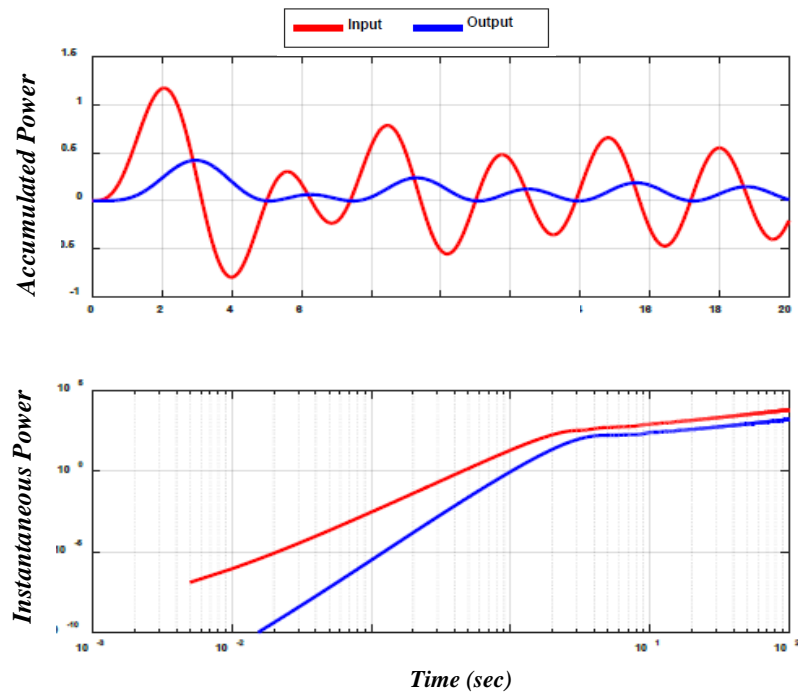
**Figure 2.9(e) – Instantaneous and acclimated Power vs Time for higher values α = 5**
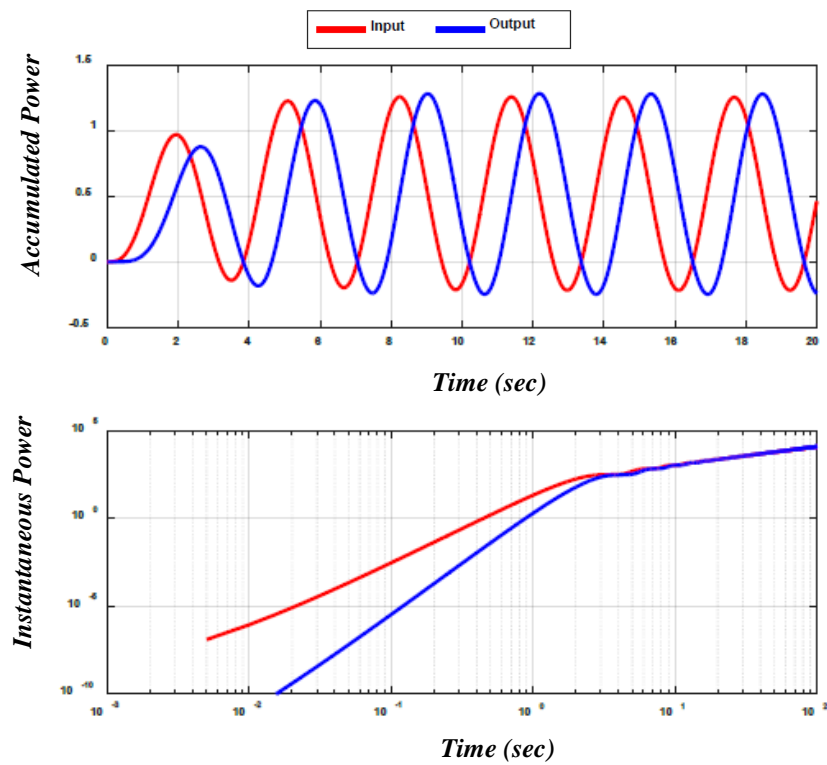


**Figure 2.9(f) – Instantaneous and acclimated Power vs Time for lower values of α =0.8**
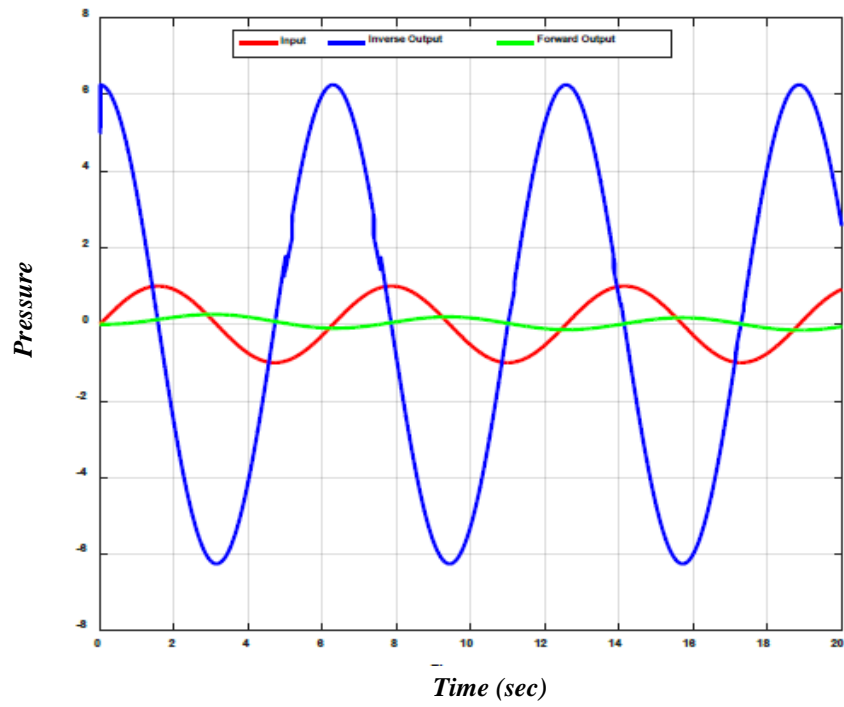
**Figure 2.9(g) – Time Response for higher α values**
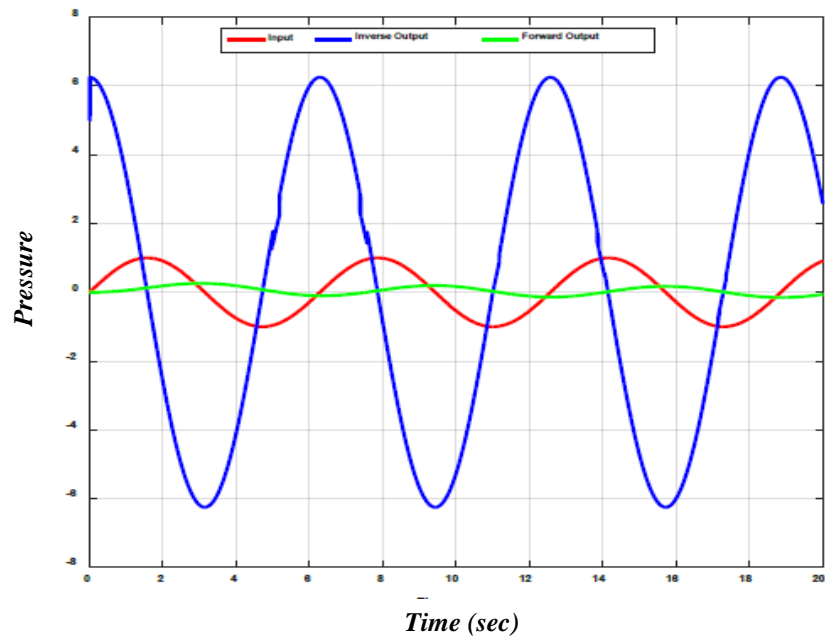


**Figure 2.9(h) – Time Response for lower α values**

**Figure 2.9 - Comparison of plots with different α values**

## 2.6. Summary

This chapter has presented a fundamental study of a new class of active nonreciprocal acoustic metamaterial (*ANAM*) platforms that can be programmed to achieve reversible transmission and/or attenuation of acoustic wave propagation in structures. The proposed *ANAM* can find its applications in interior and exterior noise mitigation. For example, the *ANAM* can be used to manufacture aircraft fuselage to isolate the engine and flow noise from propagating to the interior of the fuselage and enabling any noise generated inside the fuselage to escape to the surrounding medium. Also, the *ANAM* can be employed in underwater vehicles in order to isolate the engine and flow noise from propagating to the exterior of the vehicle to ensure stealth operation. Between these two extreme cases, there are many others that are only limited by our imagination.

# Chapter 3

# EXPERIMENTS

## 3.1. Introduction:

In order to fully understand and study the dynamic behavior of the Active non-reciprocal acoustic metamaterial cell, a comprehensive experimental investigation was done in order to determine the degree of accuracy of the theory. A variety of combinations of different parameters have been used in the experiments to observe the change in the outputs on changing those parameters.

## 3.2. Experimental Phases:

The experimental study was broken down into two steps. In the first step, the acoustic cavity was connected externally to a single resistance. Different combinations of the input parameters were used to determine the behavior of the circuit on connecting with a single external resistance.

In the second step the resistances were switched and then the output was observed. A programmable switching controller was designed which was able to control the switching of the resistances based on an equations which would be discussed in details in this chapter.

### 3.2.1. Phase I: Connecting single External Resistance:

One end of the acoustic cavity was given an *AC* input and the other end was connected with a resistance in parallel.   Figure 3.1 shows a circuit diagram of the circuit.
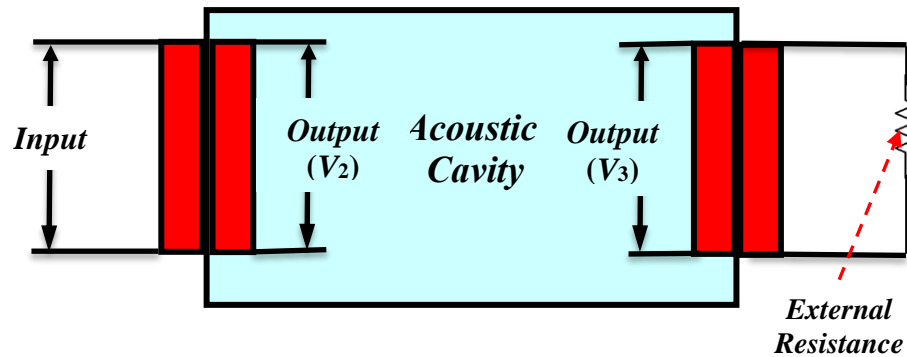


**Figure 3.1. – Schematic Diagram of the acoustic cell
connected with an external resistance**

### 3.2.1.1. Inputs and Outputs

Different combination of the following input quantities were used to observe the variation in the output.  These input quantities include: (a) Voltage Amplitude, (b) External Resistance, and (c) Input Frequency.  Such quantities are varied according to the values listed in Table 3.1.

**Table 3.1. – Matrix of Varied Experimental Parameters**

| Resistance Values | Frequency Values | Voltage Input |
|---|---|---|
| 100 Ω | 10 Hz | 250 mV |
| | | 500 mV |
| | | 1000 mV |
| | 100 Hz | 250 mV |
| | | 500 mV |
| | | 1000 mV |
| | 1000 Hz | 250 mV |
| | | 500 mV |
| | | 1000 mV |
| 1,000 Ω | 10 Hz | 250 mV |
| | | 500 mV |
| | | 1000 mV |
| | 100 Hz | 250 mV |
| | | 500 mV |
| | | 1000 mV |
| | 1000 Hz | 250 mV |
| | | 500 mV |
| | | 1000 mV |

| 10,000 Ω | 10 HZ | 250 MV |
|---|---|---|
| | | 500 mV |
| | | 1000 mV |
| | 100 Hz | 250 mV |
| | | 500 mV |
| | | 1000 mV |
| | 1000 Hz | 250 mV |
| | | 500 mV |
| | | 1000 mV |

The measured outputs, for the considered matrix of inputs are:

- Time Response across Second Piezoelectric diaphragm ($V_2$)

- Time Response across Third Piezoelectric diaphragm ($V3$)

The output data are obtained in the form of excel *ASCII* files which were then transformed for plotting and analysis in *MATLAB*.

### 3.2.1.2. The experimental setup:

The major equipment used in this study include:

### a. Signal Analyzer

A wave generator feature of *Dynamic Signal Analyzer,* by Stanford Research Systems*, Model SR785,* was used as an input and to monitor as well as recording the

outputs. This device has an option which enables the users to obtain an *AC* input which was used as input to the acoustic cavity. Specifically for this experiment, an *AC* sinusoidal wave with varying frequencies and amplitudes, were used to obtain multiple combinations. Figure 3.2 shows a photograph of the system device that served as a wave generator.



**Figure 3.2 – Photograph of the Dynamic Signal Analyzer**

The same device was used to extract the output of the circuit as this wave generator not only allows us to use it as a wave generator but also allows us to use the device to see multiple output across multiple channels. These channels just need to be connected to the circuit point from where we the output needs to be obtained.

**b.  *ANAM* Prototype:**

A prototype of the *ANAM* cell has been created which demonstrates the feasibility of the concept of *ANAM*. The cell is composed of two lead- zirconium-titanate (*PZT4*) piezoelectric bimorphs of 37*mm* diameter confining a water column of 50*mm* height as shown in Figure 3.3.

The input from the wave generator or function generator is connected to the first piezoelectric diaphragm of the acoustic cavity after which this piezo diaphragm acts as an actuator. The other two piezos (the one on the opposite side of the aluminum plate and the inner piezo of the other aluminum plate) are connected to the outputs as shown in the schematic diagrams of Figure 3.3(a) and (b). Also, a resistance is connected in parallel to the fourth piezoelectric diaphragm as shown in the figure.



*Piezo*

*Acoustic cavity*
*(Filled with*

*Figure 3.3 (a) – Schematic Drawing*     *Figure 3.3. (b) - Photograph*
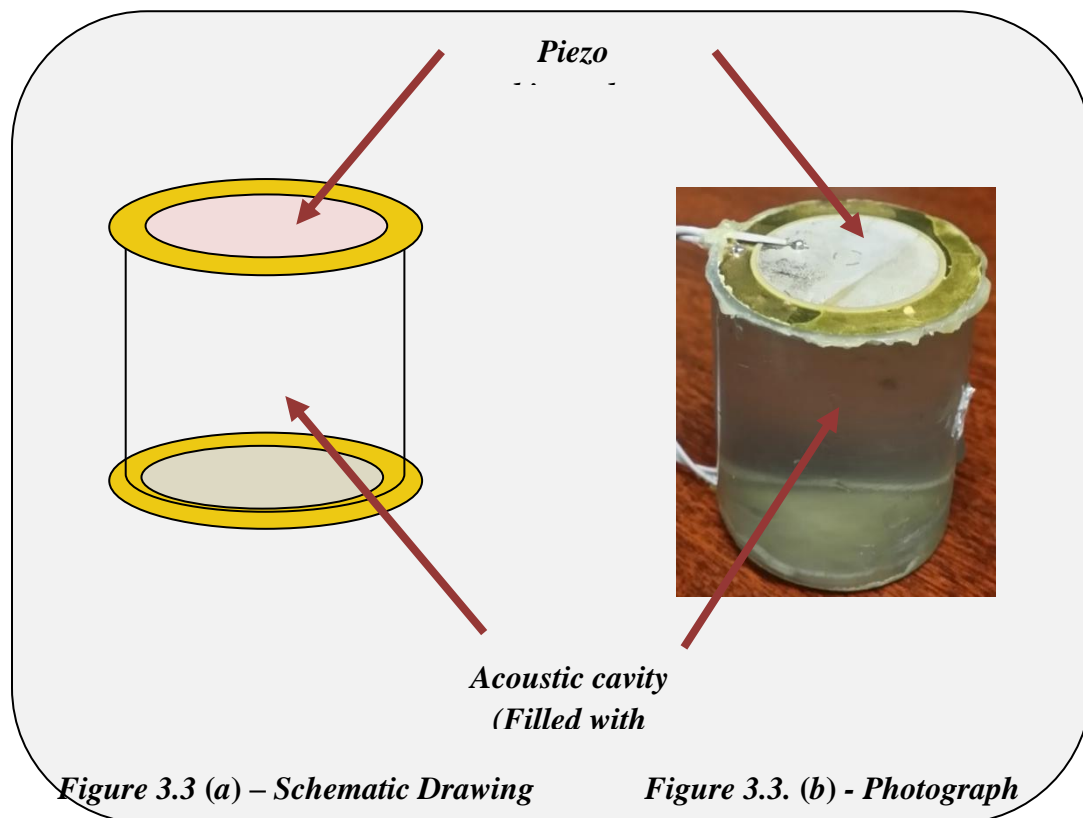
**Figure 3.3. – Prototype of the Active Nonreciprocal Acoustic
Metamaterial cell**

Extensive experimental have been carried on the *ANAM* cell, on an attempt to validate the theory. A series of different combinations of the parameters have been used to observe the pattern in the non-reciprocal acoustic metamaterial cell. These experimental techniques are followed by electrical simulations to obtain further confirmation. Both experimental techniques and the electrical simulations have been discussed in detail in the upcoming chapters.
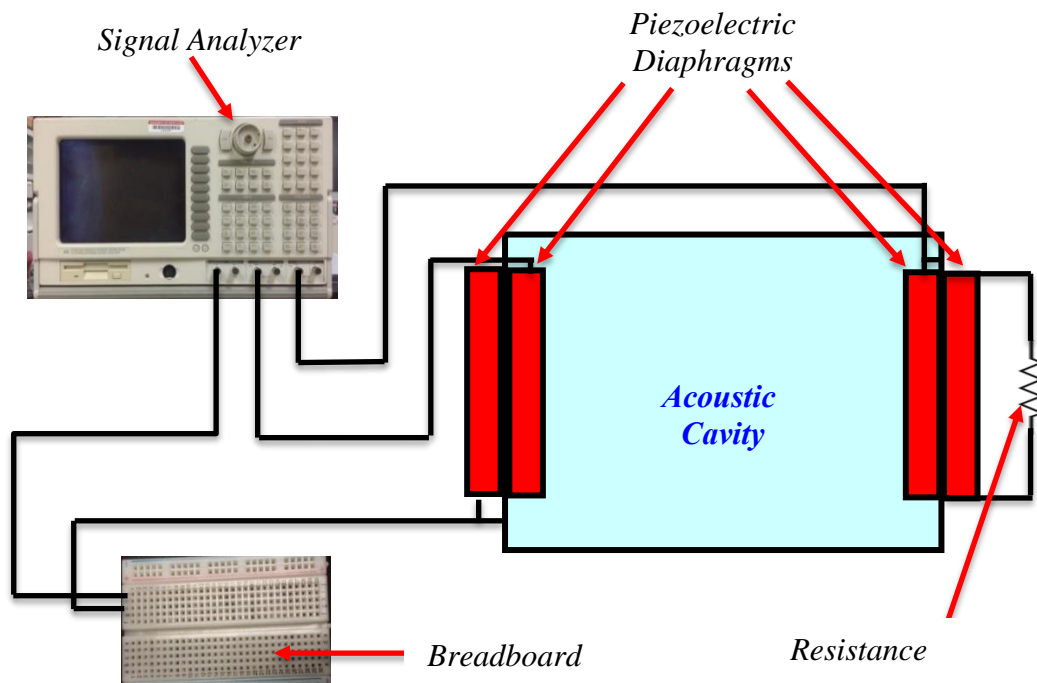


**Figure 3.4 - Schematic drawing of setup with
single resistance**

### 3.2.1.3. Experimental results from Phase I:

This section includes a summary of the obtained experimental results.
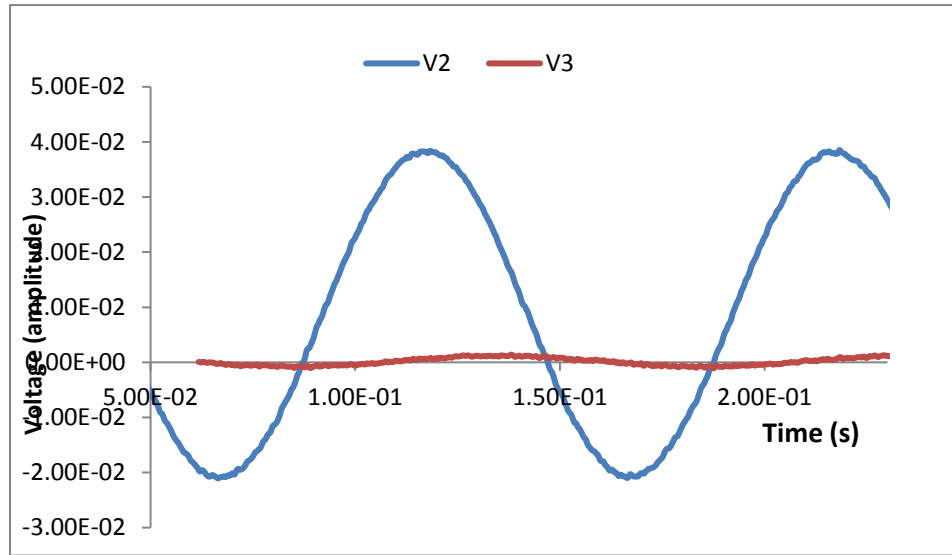


**Figure 3.5 -Time Response - (100 Ω - 10 Hz - 250 mV)**
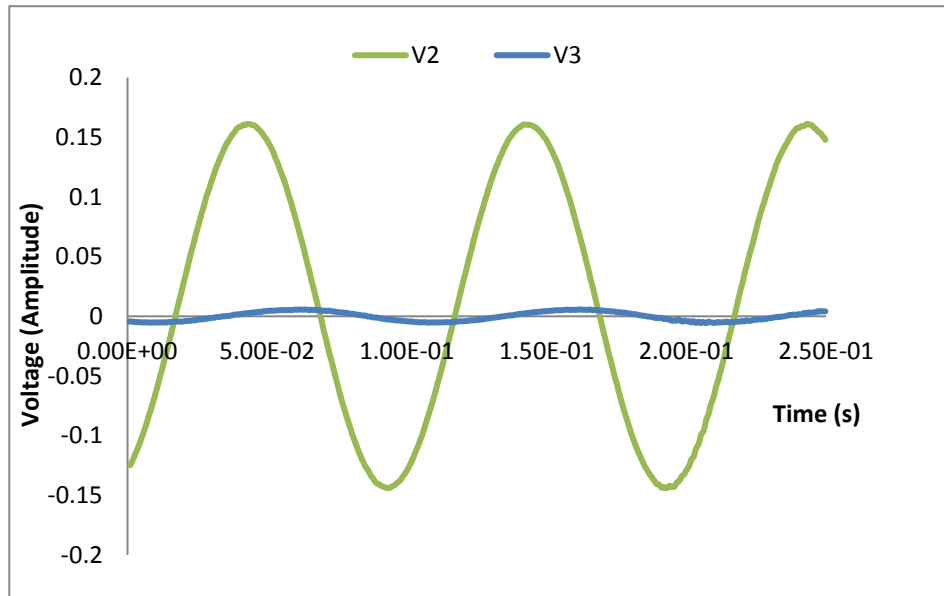


**Figure 3.6 – Time Response - (100 Ω- 10Hz - 500mV)**
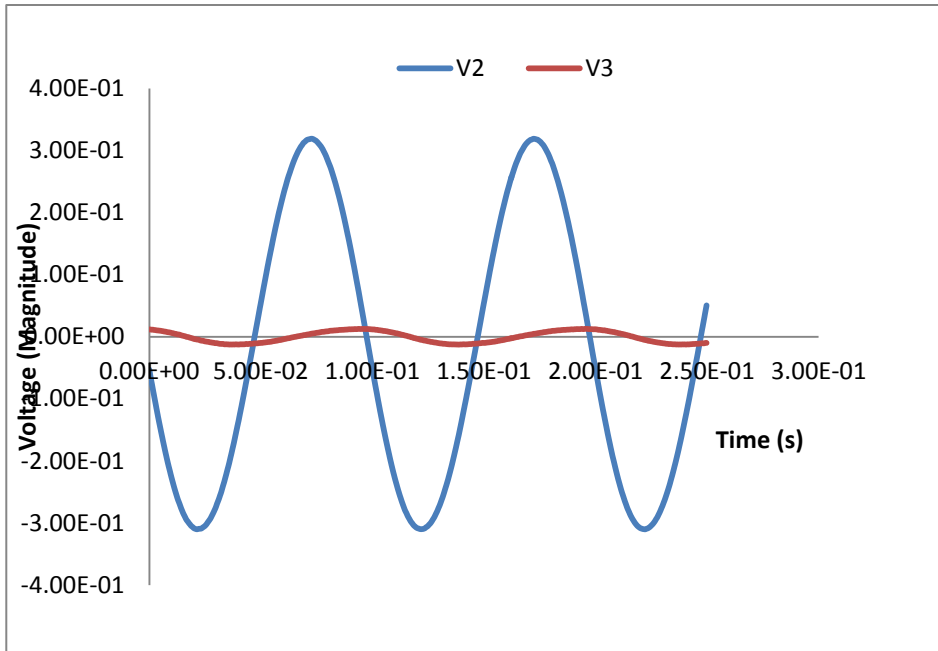
**Figure 3.7 – Time Response - (100 Ω - 10Hz - 1000mV)**
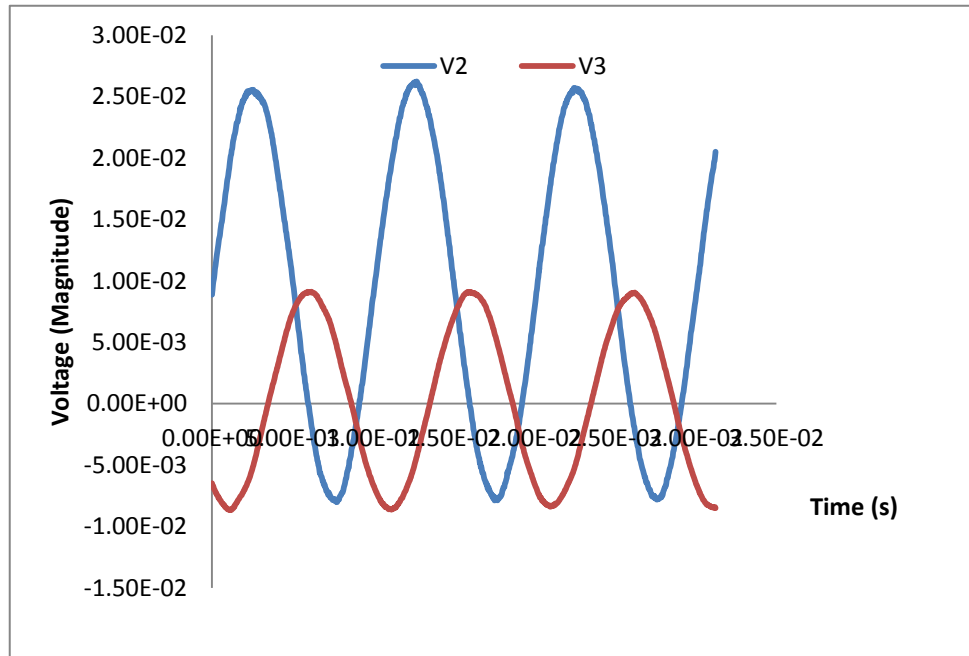


**Figure 3.8 – Time Response - (100 Ω - 100Hz - 250mV)**
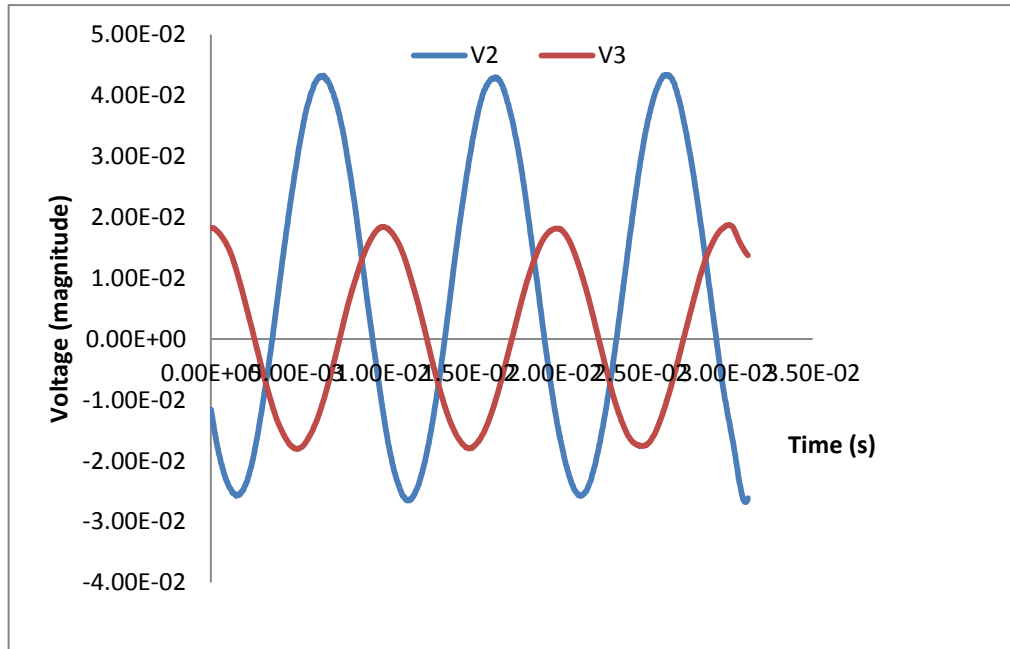
**Figure 3.9 – Time Response - (100 Ω - 100Hz - 500mV)**
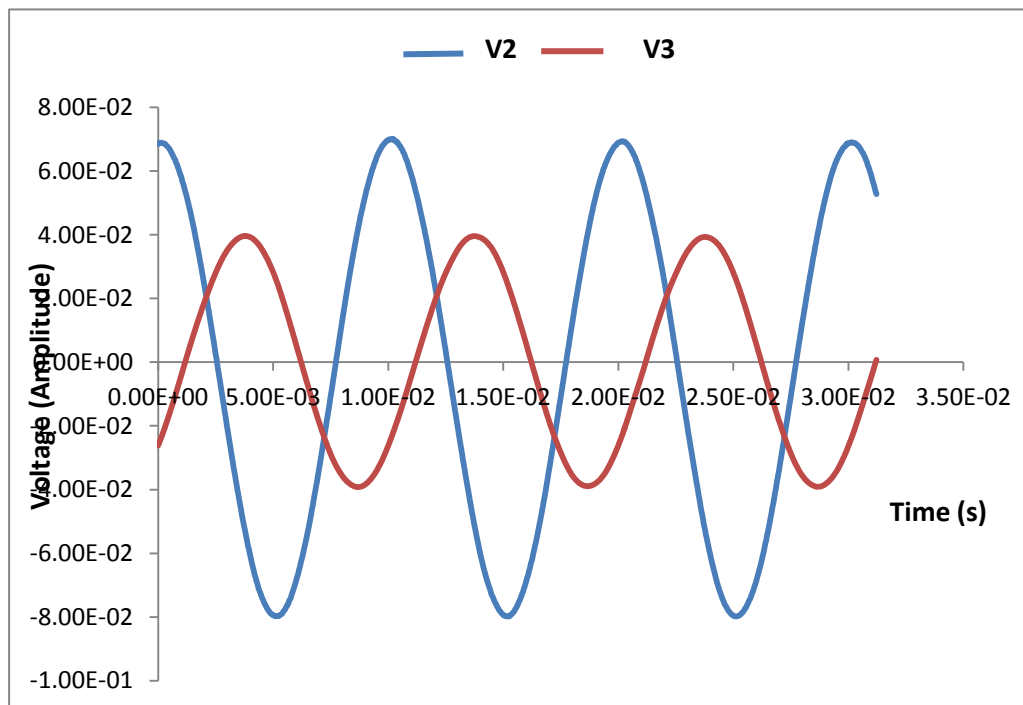


**Figure 3.10 – Time Response - (100 Ω - 100Hz - 1000mV)**
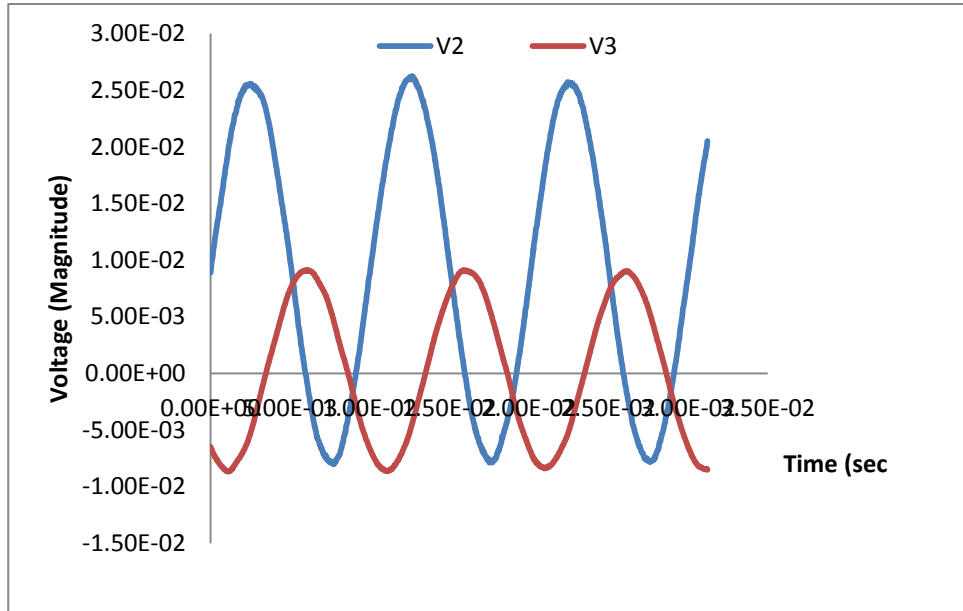
**Figure 3.11 -Time Response - (100 Ω - 1000Hz - 250mV)**
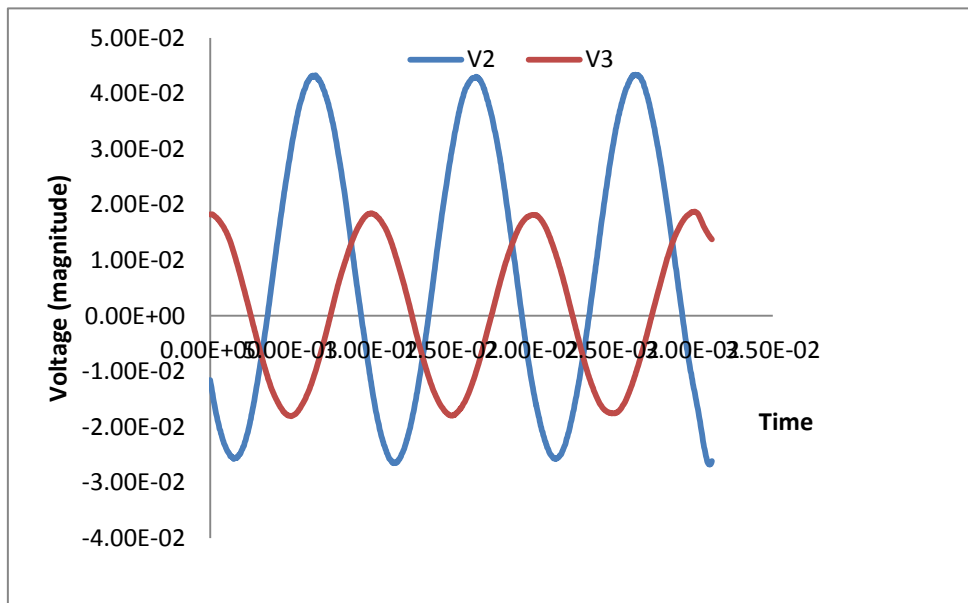


**Figure 3.12 – Time Response - (100 Ω - 1000Hz - 500mV)**
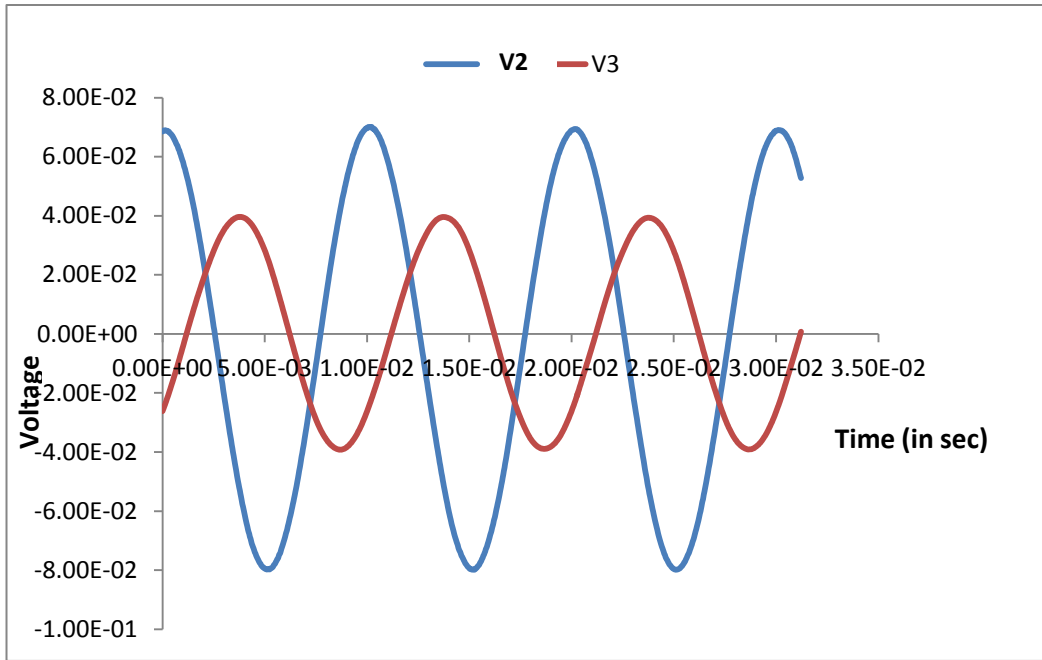
**Figure 3.13 - Time Response - (100 Ω - 1000Hz - 1000mV)**
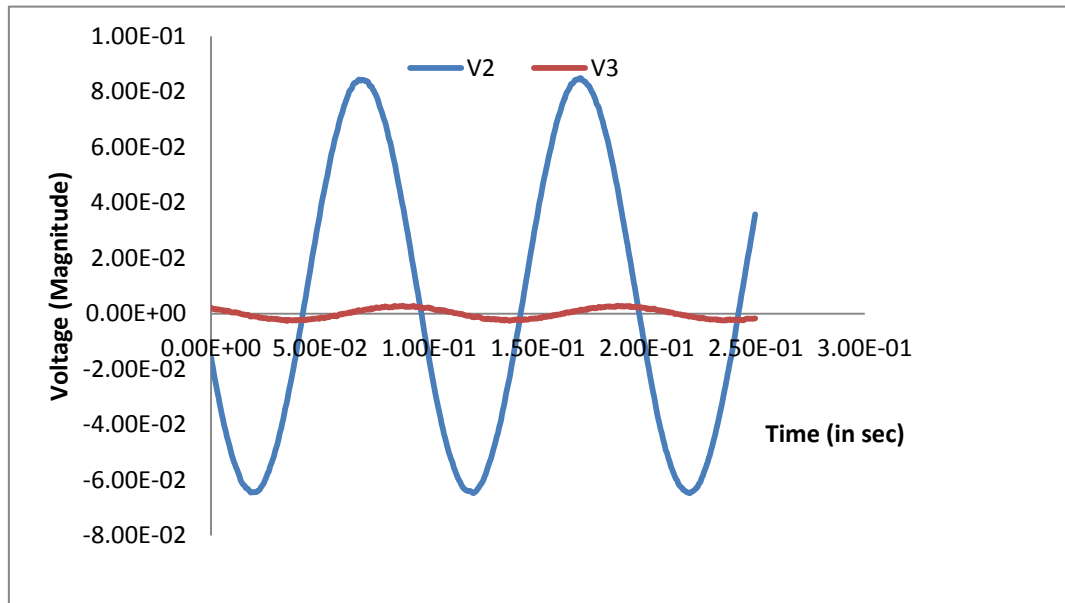


**Figure 3.14 – Time Response - (1,000 Ω - 10Hz - 250mV)**
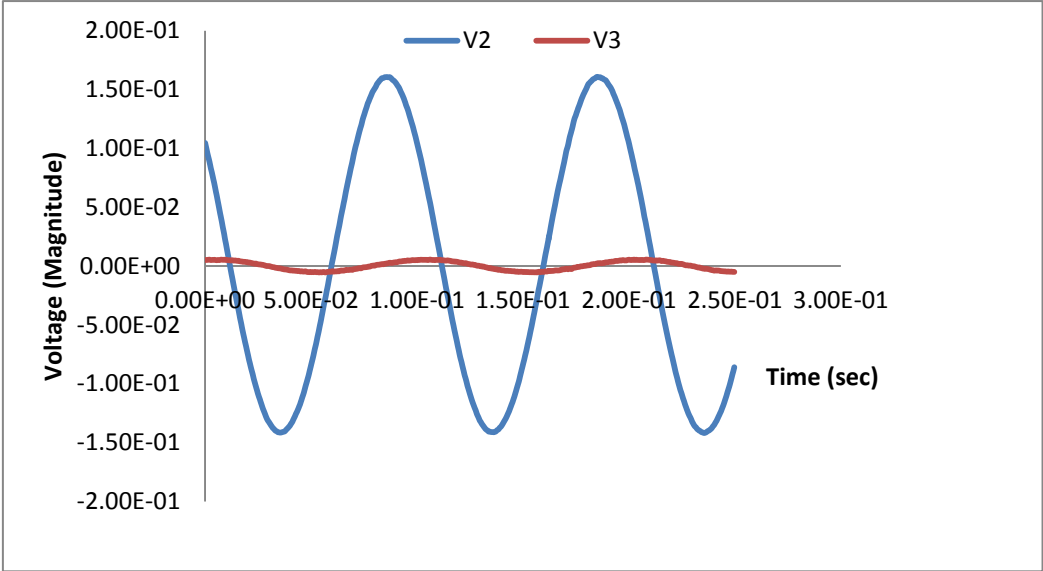
**Figure 3.15 – Time Response - (1,000 Ω - 10Hz - 500mV)**
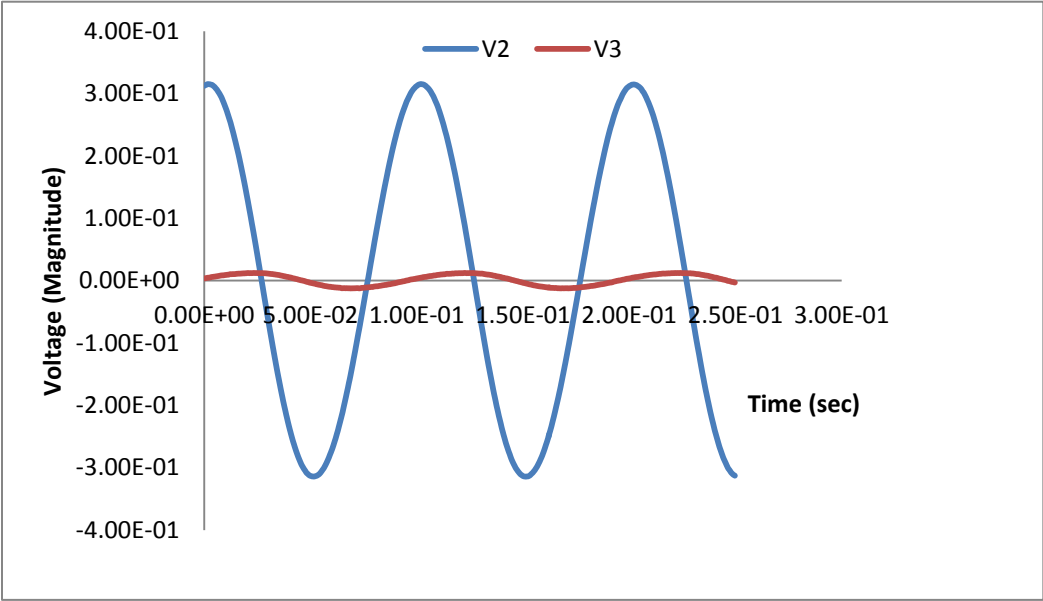


**Figure 3.16 – Time Response - (1,000 Ω - 10Hz - 1000mV)**
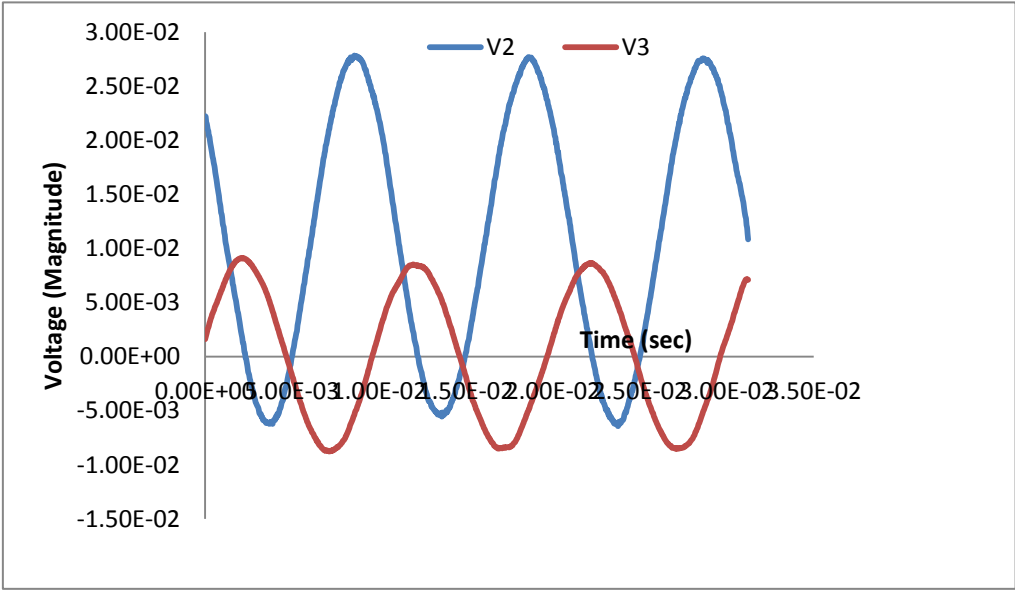
**Figure 3.17 – Time Response - (1,000 Ω - 100Hz - 250mV)**
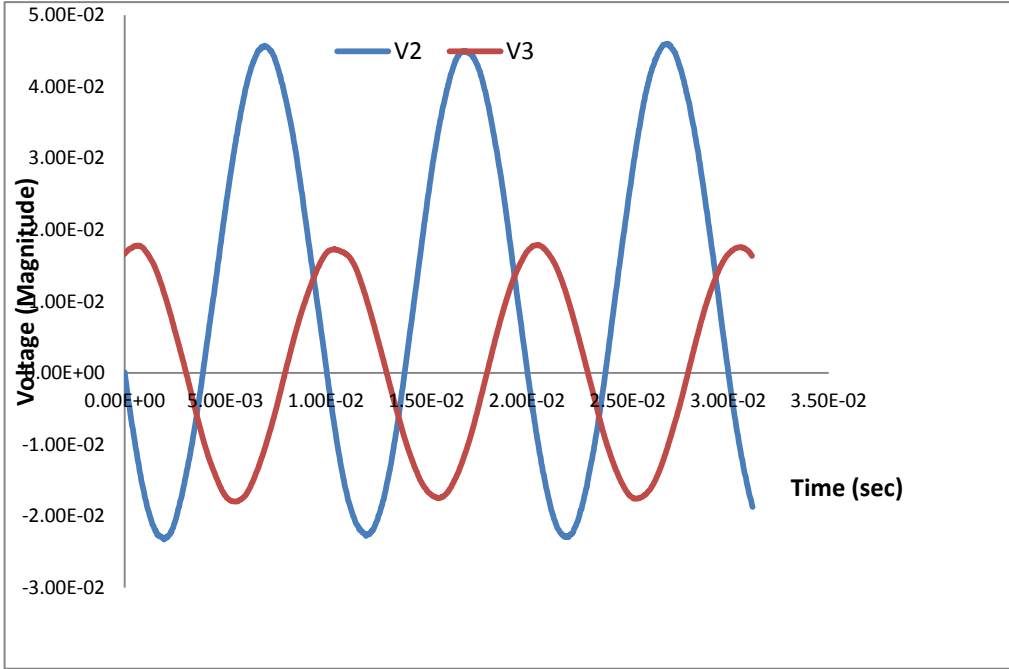


**Figure 3.18 – Time Response - (1,000 Ω - 100Hz - 500mV)**
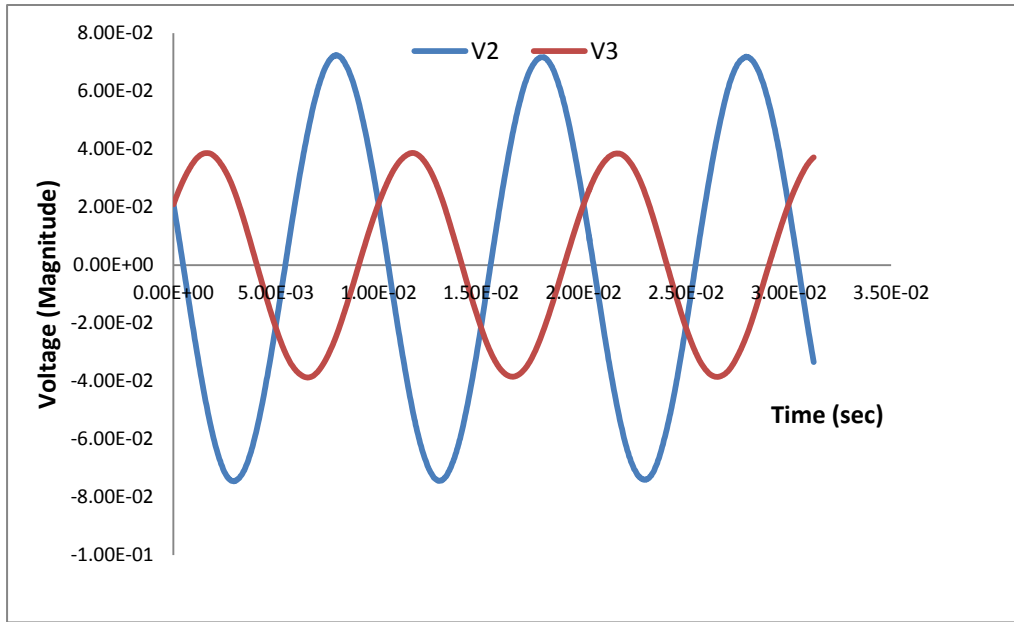
**Figure 3.19 – Time Response - (1,000 Ω - 100Hz - 1,000mV)**
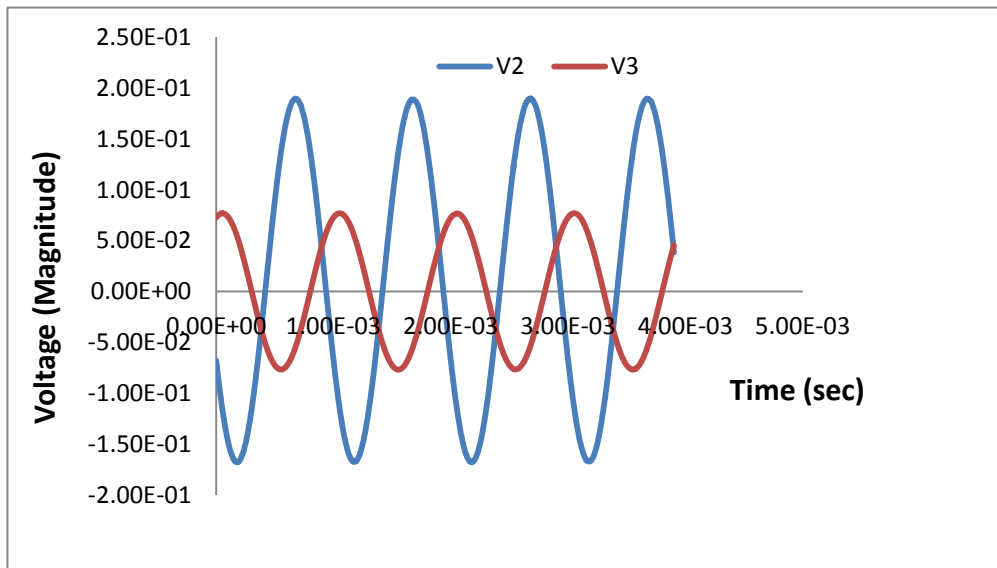


**Figure 3.20 – Time Response - (1,000 Ω - 1000Hz - 250mV)**
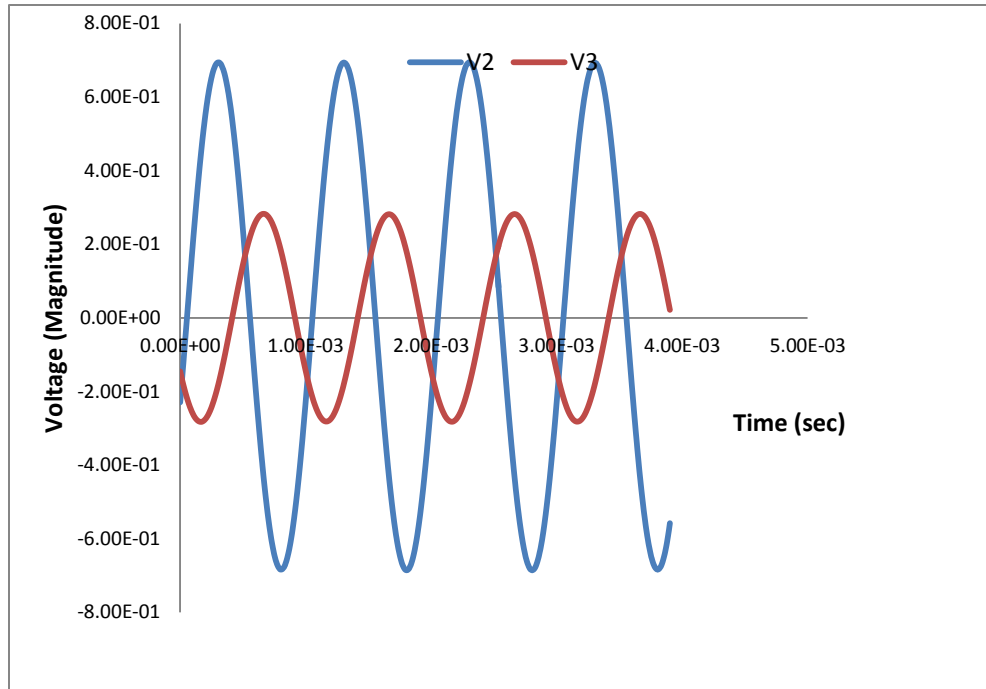
**Figure 3.21 – Time Response - (1,000 Ω - 1000Hz - 500mV)**
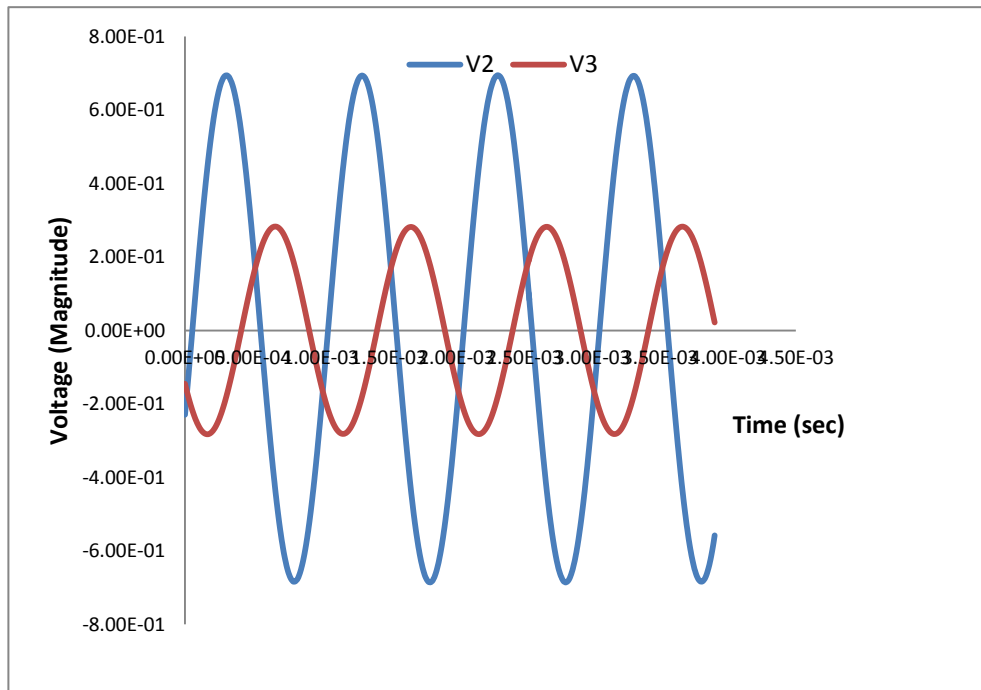


**Figure 3.22 – Time Response - (1,000 Ω - 1000Hz - 1000mV)**
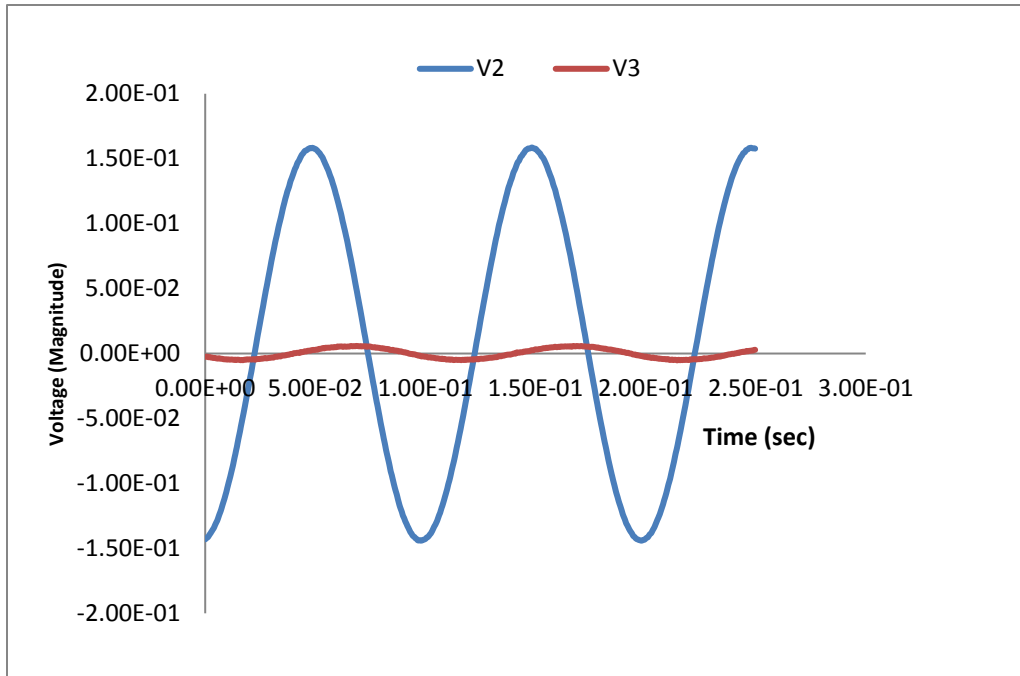
**Figure 3.23 – Time Response - (10,000 Ω - 10Hz - 250mV)**
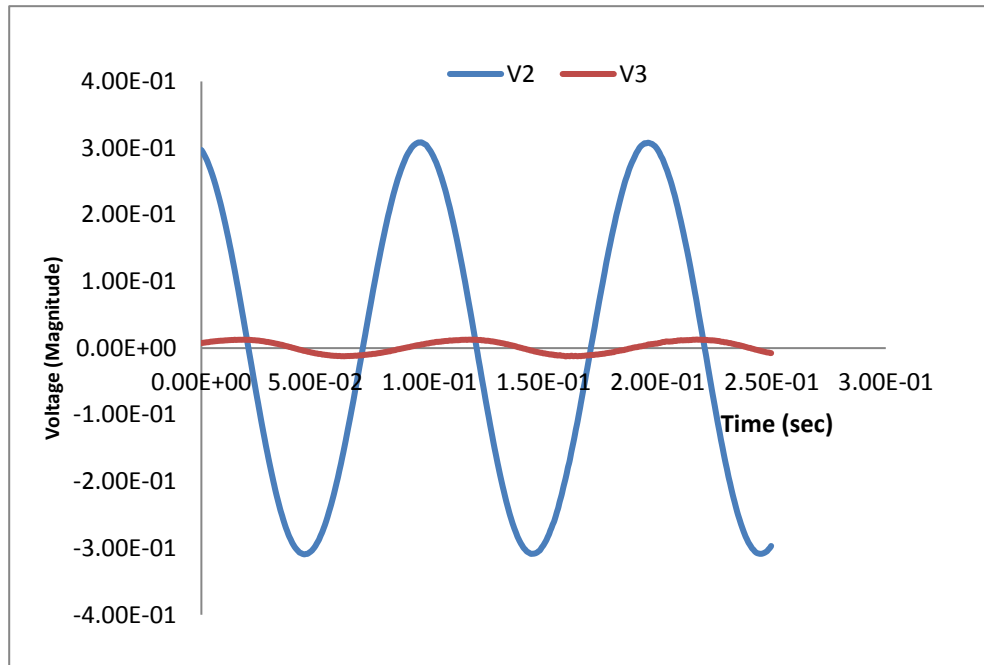


**Figure 3.24 – Time Response - (10,000 Ω - 10Hz - 500mV)**
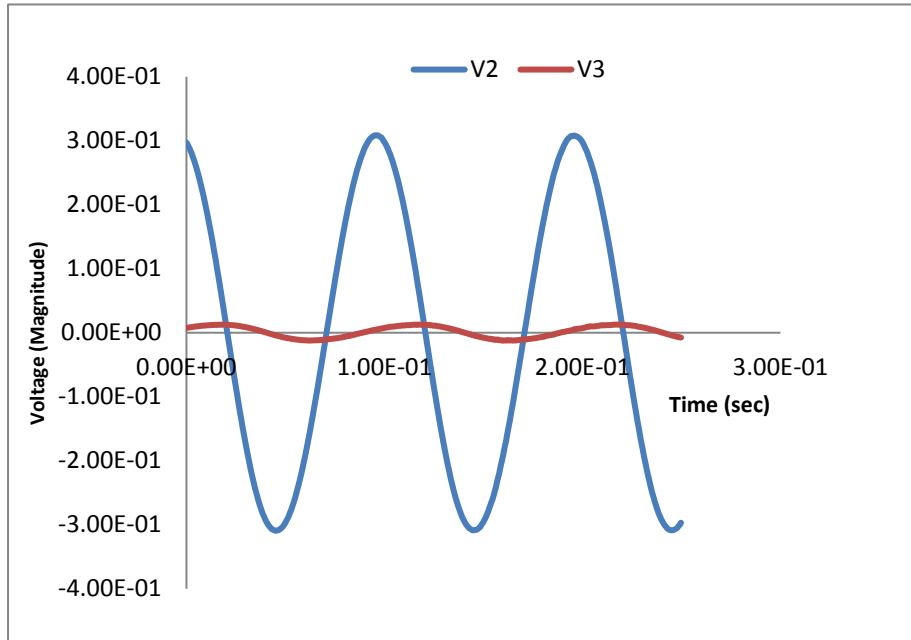
**Figure 3.25 – Time Response - (10,000 Ω - 10Hz – 1,000mV)**
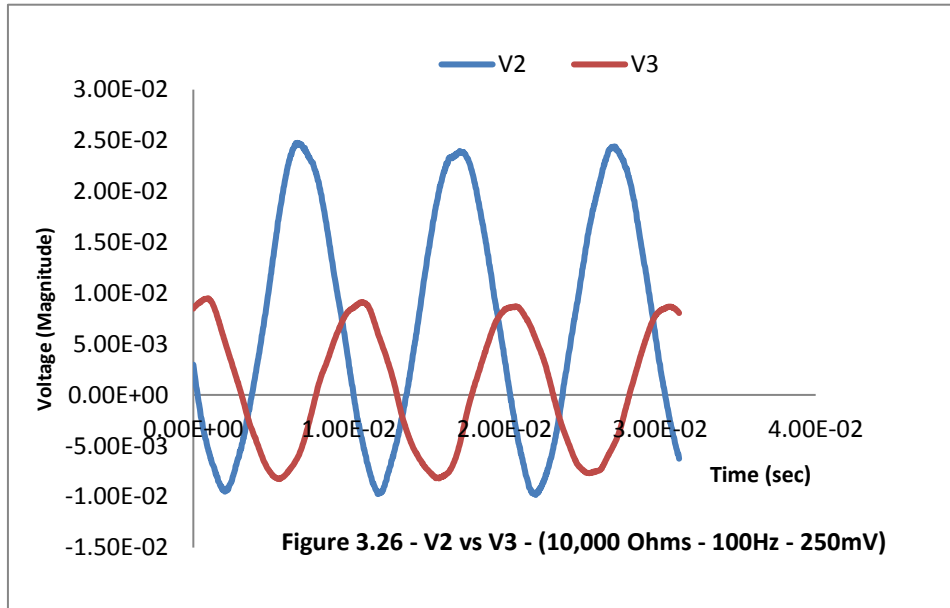


Figure 3.26 - V2 vs V3 - (10,000 Ohms - 100Hz - 250mV)

**Figure 3.26 – Time Response - (10,000 Ω - 100Hz – 250mV)**
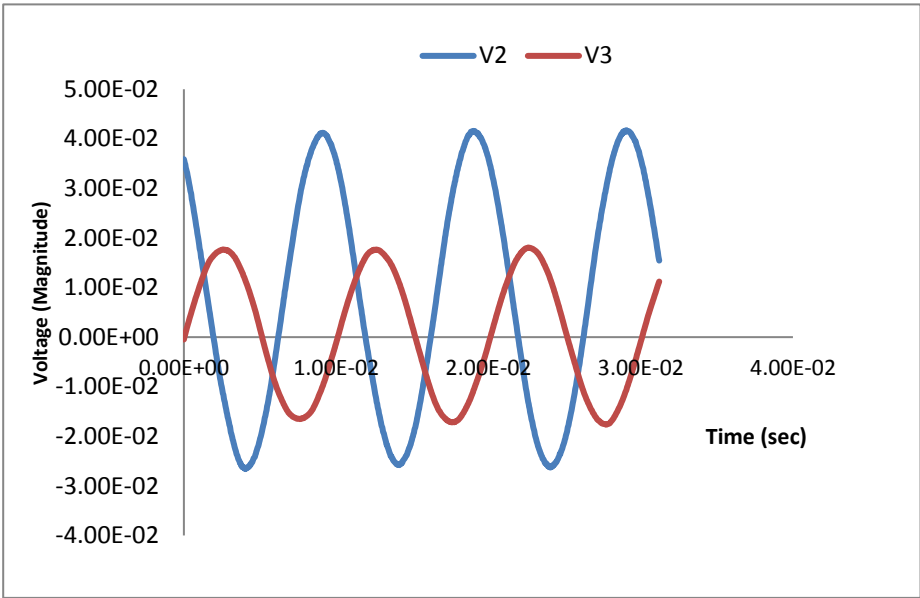
**Figure 3.27 – Time Response - (10,000 Ω - 100Hz - 500mV)**
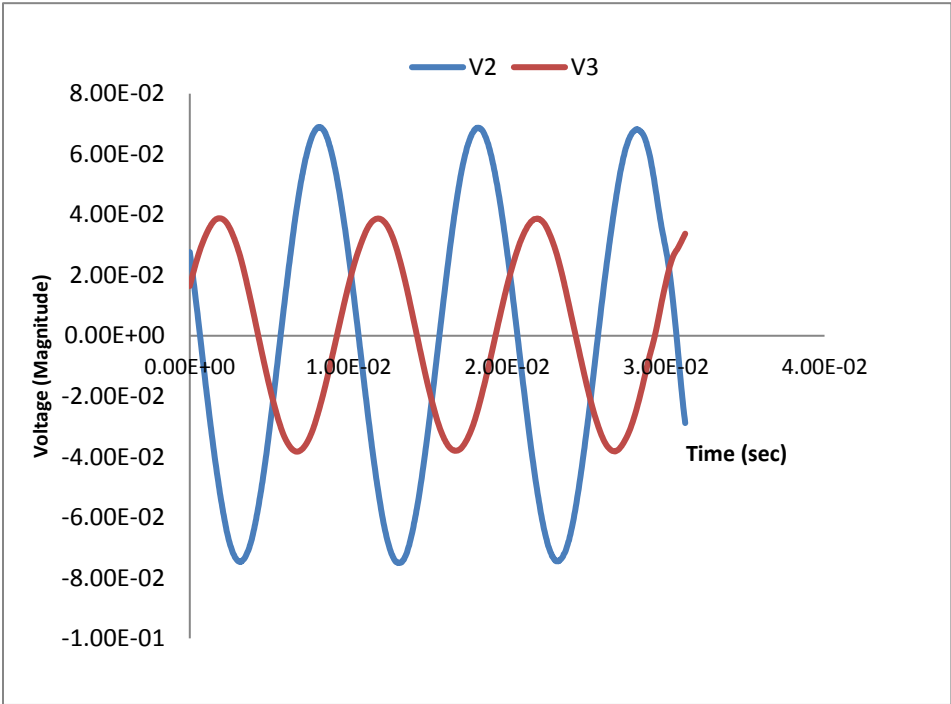


**Figure 3.28 – Time Response - (10,000 Ω Ohms - 100Hz - 1000mV)**
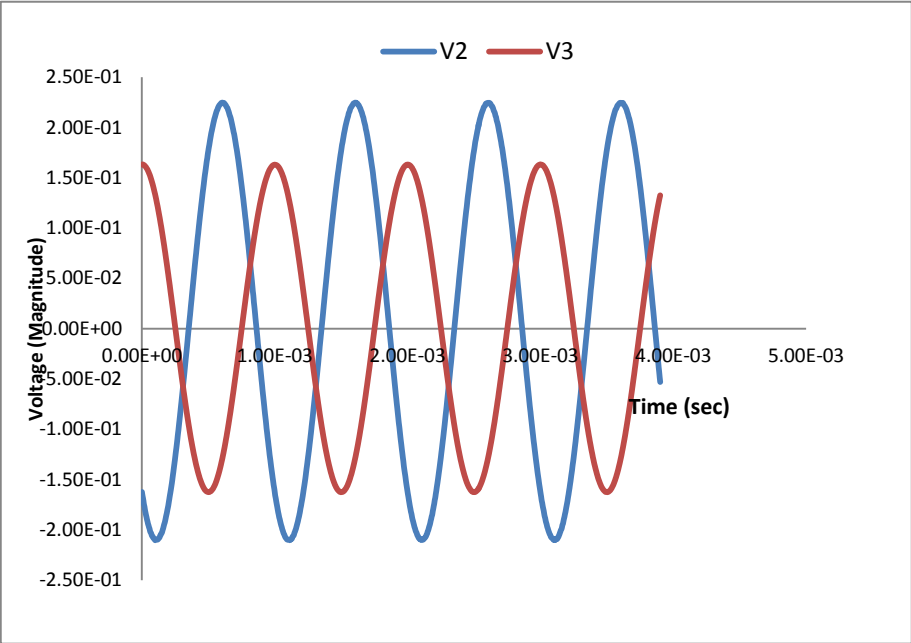
**Figure 3.29 –Time Response - (10,000 Ω - 1000Hz - 250mV)**
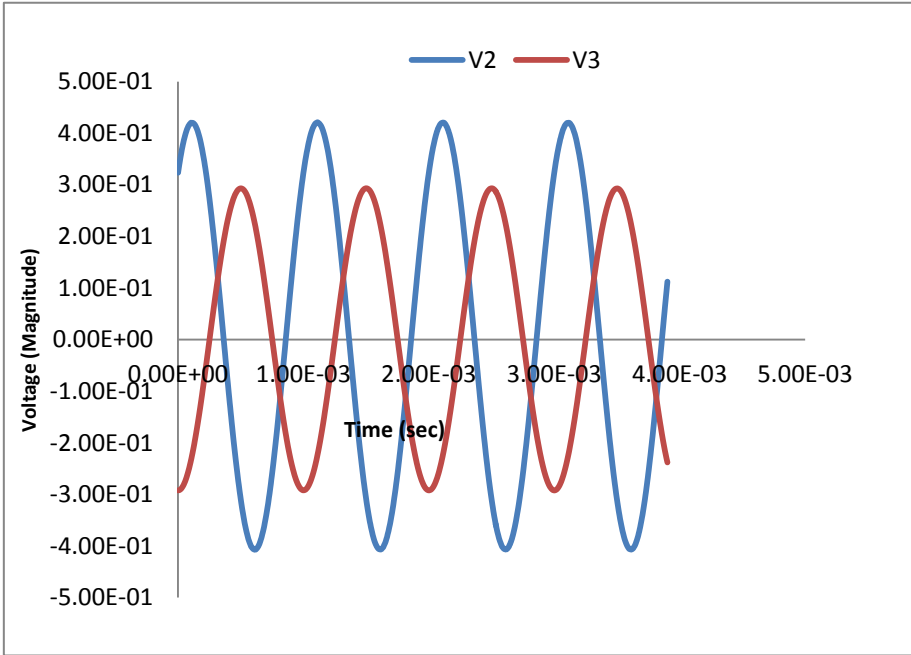


**Figure 3.30 –Time Response - (10,000 Ω - 1000Hz - 500mV)**
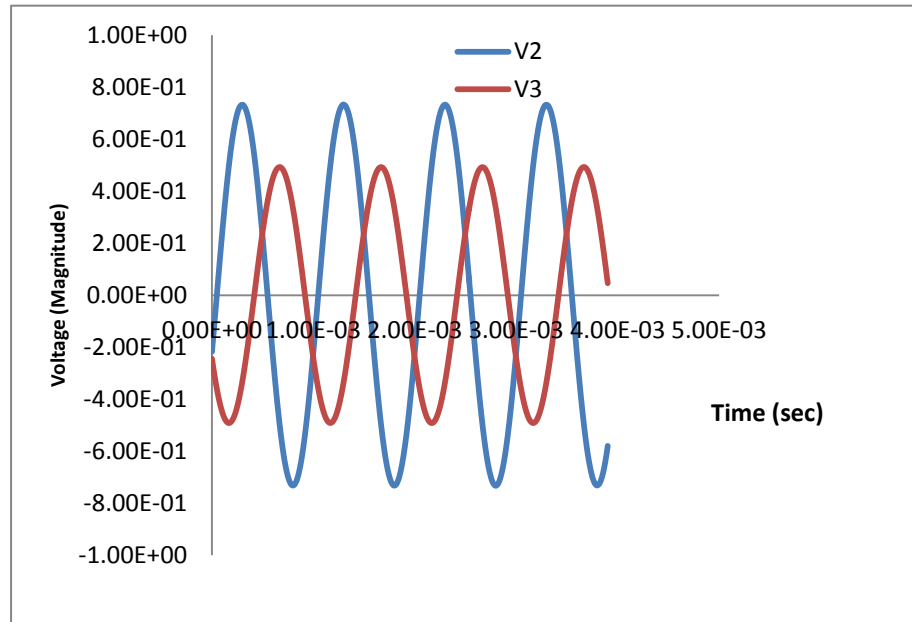
**Figure 3.31 –Time Response - (10,000 Ω - 1000Hz - 1000mV)**

Three plots can summarize the above 27 combinations of the potential difference across the second and third piezoelectric diaphragm of the acoustic cavity. Each of the three plots, represents one of the distinct combination of input magnitude.

Figure 3.31, 3.32 and 3.33 shows the effect on the ratio of the maximum voltage aptitudes in the second and third piezoelectric diaphragm against the change in the frequency.
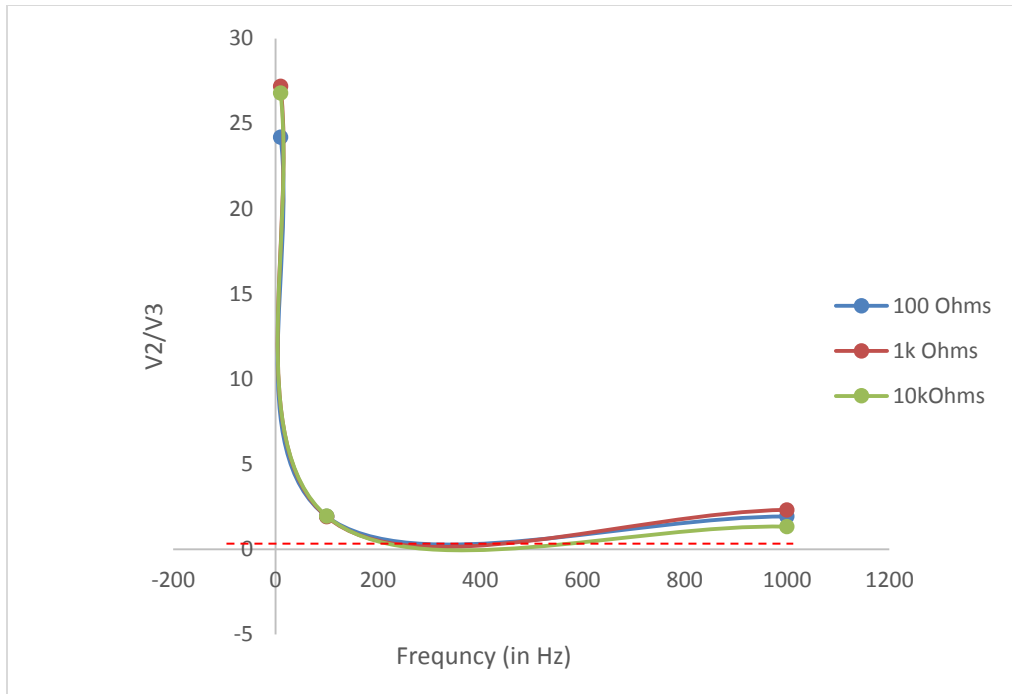
**Figure 3.32 –Frequency vs Voltage Amplitude Ratio for
250mV Input**
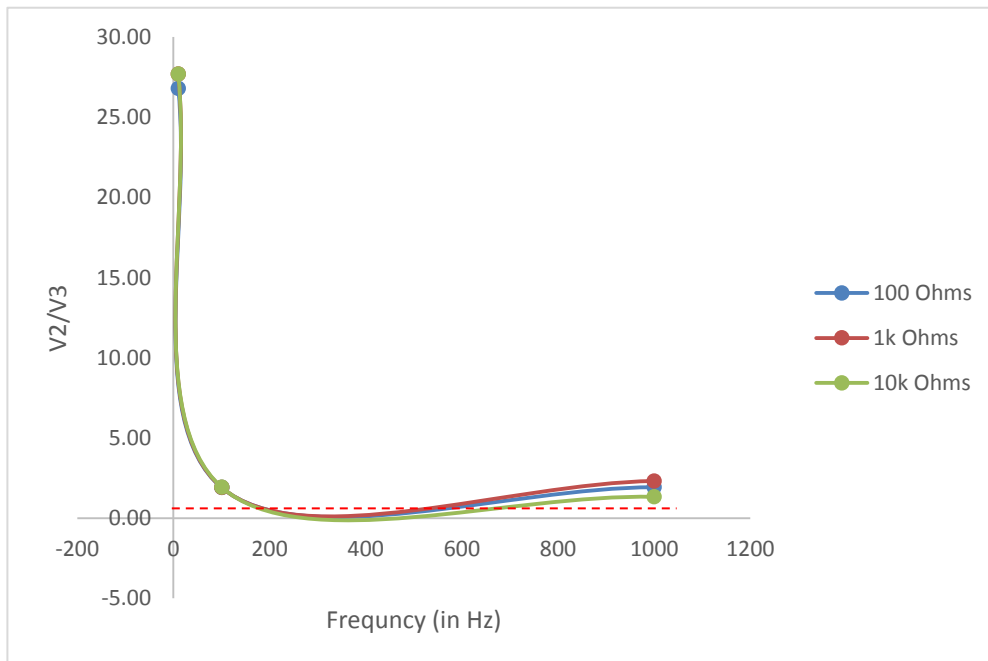


**Figure 3.33 – Frequency vs Voltage Amplitude Ratio for
500mV Input**
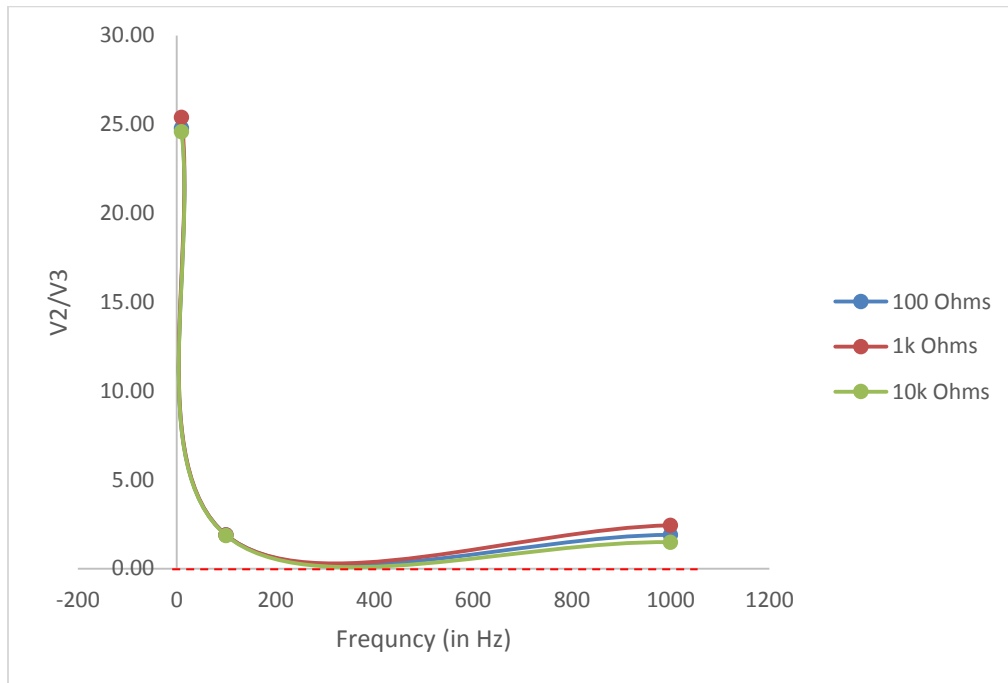
**Figure 3.34 – Frequency vs Voltage Amplitude Ratio for 1,000mV Input**

It is evident from Figure 3.31, Figure 3.32 and Figure 3.33 that the ratio between the voltage amplitude of the across the two piezoelectric diaphragms of the acoustic cell, is independent of the frequency, external resistance and the input voltage.   A couple of additional plots as shown Figure 3.34 and 3.35 relate the change in the output voltage amplitudes of the second and third piezoelectric diaphragms of the acoustic cavities.
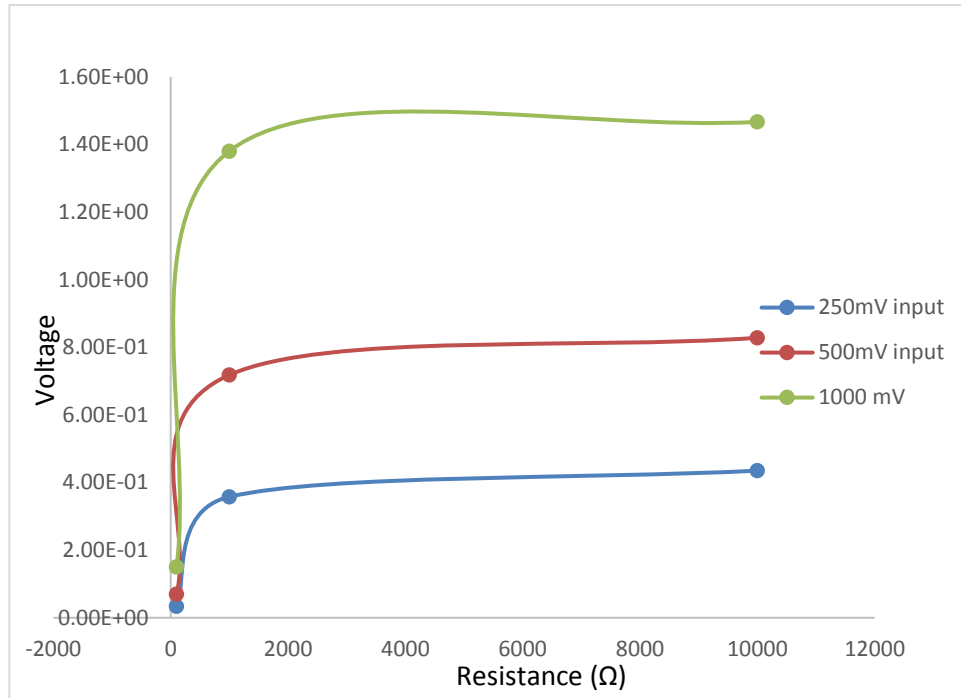
**Figure 3.35 –Resistance vs Voltage Amplitude across second piezoelectric diaphragm (sensor 1)**
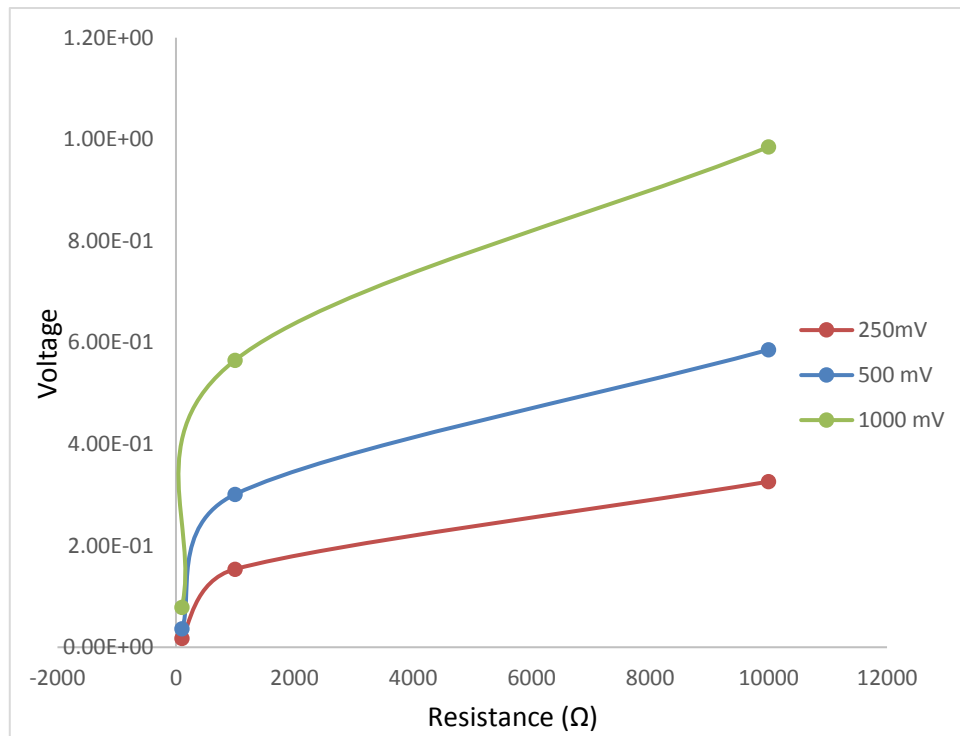


**Figure 3.36 –Resistance vs Voltage Amplitude across third piezoelectric diaphragm (sensor 2)**

Even though, not many resistances have been used to study the effect of resistance on the voltage amplitude of the two sensors of the acoustic cavity, yet it can be inferred from plots shown in figure 3.34 and figure 3.35 that the resistances and the voltage amplitude across the pressure sensors are related non-linearly.

### 3.2.2. Phase II: Switching Resistances:

After observing the effect of changing the resistance in the output, a combination of resistances were to be connected, but through a switch such as only one of those two resistance can remain connected to the circuit at a time. For this purpose a programmable switch was designed that can enable the circuit to switch between the two resistances. The output of the acoustic cavity, which is the pressure across the sensors of the piezoelectric boundaries is connected with the oscilloscope which reads the pressure (in terms of voltage) across the two pressure sensors. Figure 3.37 shows the photograph of what the experimental setup.

Function
Generator

Oscilloscope

Acoustic Cavity



Acoustic Cavity

LABVIEW Box



Switching
Device (Relay)
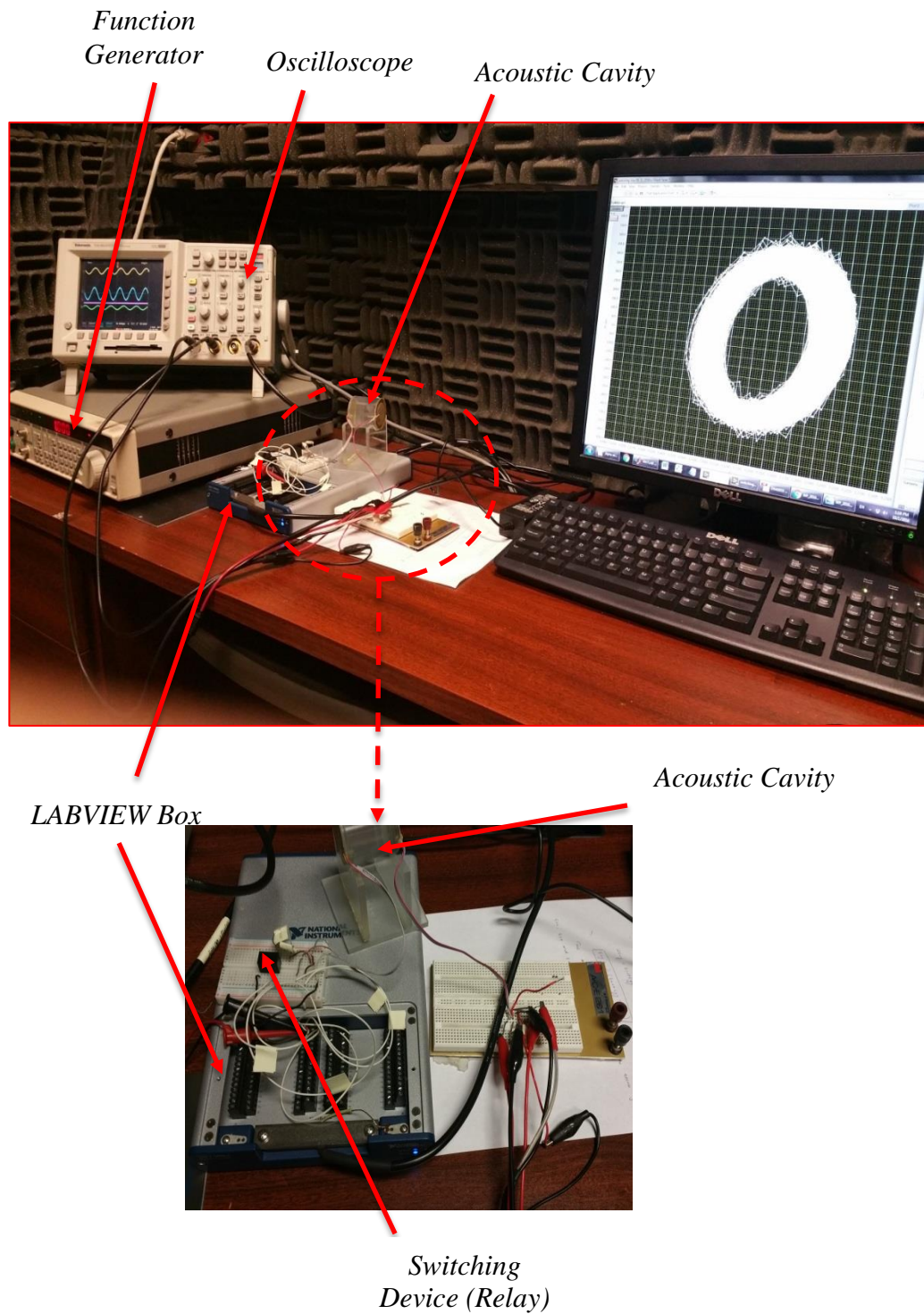
**Figure 3.37 – Photograph of the Experimental Setup
with programmable switching resistances**

### 3.2.2.1. Programmable Switch:

**a. Selection of the Resistances:**

The two resistances between which the switching needed to be done, are associated with the values of α. The two resistances were names $R_0$ and $R_1$. For each value of α, the values of the $R_0$ and $R_1$ can be calculated as;

$$R = R_0 = \frac{L_c}{\alpha} \tag{3.1}$$

$$R = R_1 < \frac{\alpha}{C_c\left(\alpha^2 + \frac{1}{C_c L_c}\right)} \tag{3.2}$$

A *MATLAB* code has been written which inputs the values of alpha and outputs the value of $R_0$ and $R_1$ which needs to be connected with the circuit. Below is the *MATLAB* code which has been written for this purpose.

```
clc
clear all
Lc = 2*24069;

Alpha = input('Please enter the value of Alpha you intend to use : ')

R0 = Lc/Alpha

Lp = 13456;
Cc = 1.85E-15;
Cp = 18.24E-9;

R1_max = Alpha/(Cc*(Alpha+1/(Cc*Lc)))
```

*MATLAB* Code for resistances calculation

Once the two resistances have been selected which corresponds to an alpha value, then a switch has been designed that enables allows the switching between the two resistances. This switch was later programmed using *LABVIEW*. For switching purposes, a relay has been used due to which the appropriate resistance becomes an active part of the circuit.

**b. Relay:**

A *SPDT 1-Amp 5V Relay switch* was used to switch the connections between $R_0$ and $R_1$. Basically this relay is initially connecting one of the three terminals. Once a potential difference of 5 Volts is supplied to it, it switches to the other terminal. Figure 3.38 shows schematic diagram how the circuit switches upon change in the voltage supplied.
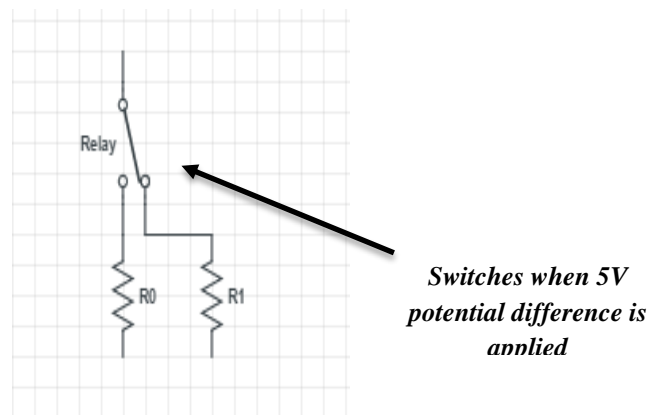


**Figure 3.38 – Schematic diagram of the relay switch**

**c. *LABVIEW* Based Code:**

A program on *LABVIEW* has been created that controls the switching of the switching controller. When using switching controller, the output from the third piezoelectric diaphragm is not only displayed at the oscilloscope's or signal analyzer's

screen but it plays the role of an input, for the *LABVIEW* program. The *LABVIEW* program not only controls the switch but it also plots the final output which is a plot between the voltage across third piezo ($V_3$) and the time derivative of the same quantity ($\frac{d}{dt}V_3$). Figure 3.3 shows the Block diagram of the *LABVIEW* program, which controls the switching of the resistances.

The output of the acoustic cavity, which is the pressure across the sensors of the piezoelectric boundaries is connected with the oscilloscope which reads the pressure (in terms of voltage) across the two pressure sensors. Figure 3.39 shows the photograph of what the experimental setup.
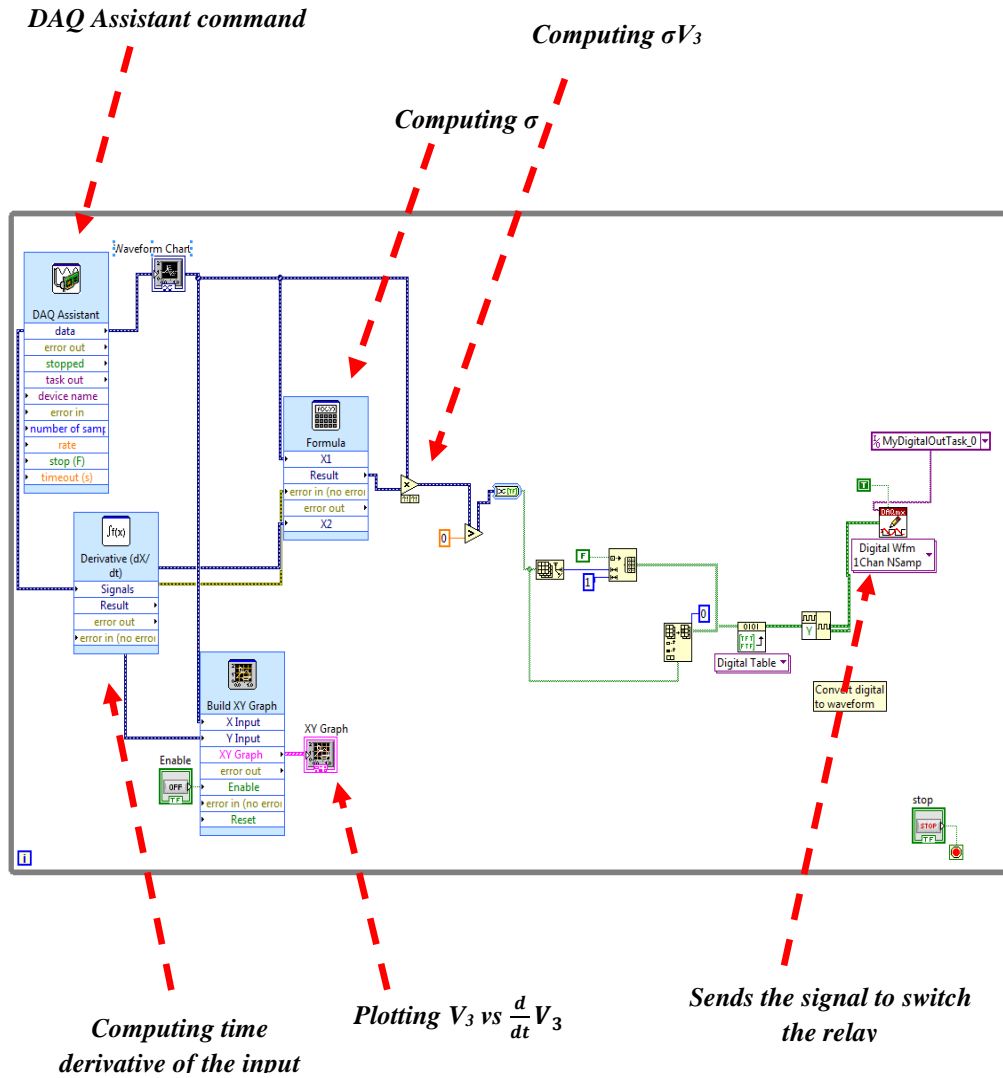
**Figure 3.39 – Block Diagram of the LABVIEW based program controlling the switching of resistances**

The portion of the *LABVIEW* code, which controls the switching between the external resistances is based on the following principle,

For this purpose, the oscilloscope and the input channel of the *LABVIEW* box are connected in parallel, which keeps the voltage obtained on the oscilloscope and voltage serving as receives the same potential difference. For validation purposes, the input of the *LABVIEW* has been plotted to make sure that it receives the exact same input as of the output as displayed on the screen of the oscilloscope or signal analyzer.

To obtain the data input a "*DAQ* Assistant Express VI" command of *LABVIEW* has been used. *DAQ* Assistant command was configured in the following way

*DAQ* Assistant command can read the signals from the specified channel of the *LABVIEW*. To obtain a precise and form of the data, 30,000 continuous samples were read at a sample rate of 25,000 *Hz*. Since the whole program has eventually been enclosed inside a while loop therefore this becomes a recurring process which continues until stopped manually. Due to this the *DAQ* Assistant command reads these signals continuously and the data is then further processed accordingly.

The data received by the *DAQ* assistant is first plotted which is duplicate of the time response which was seen on the signal analyzer / oscilloscope, after which its time derivative is calculated using the "Derivative function" of the *LABVIEW*. At this instant, the input voltage of the *LABVIEW* ($V_3$) and the time derivative of the same voltage $\left(\frac{d}{dt}V_3\right)$ which later contributes in the calculations too, are plotted.

**DAQ Assistant command**
**Used for reading the**

**Input signal waveform**
**generator**

**Time Derivative**

$V_3 vs \frac{d}{dt} V_3$   **Graphs Builder**
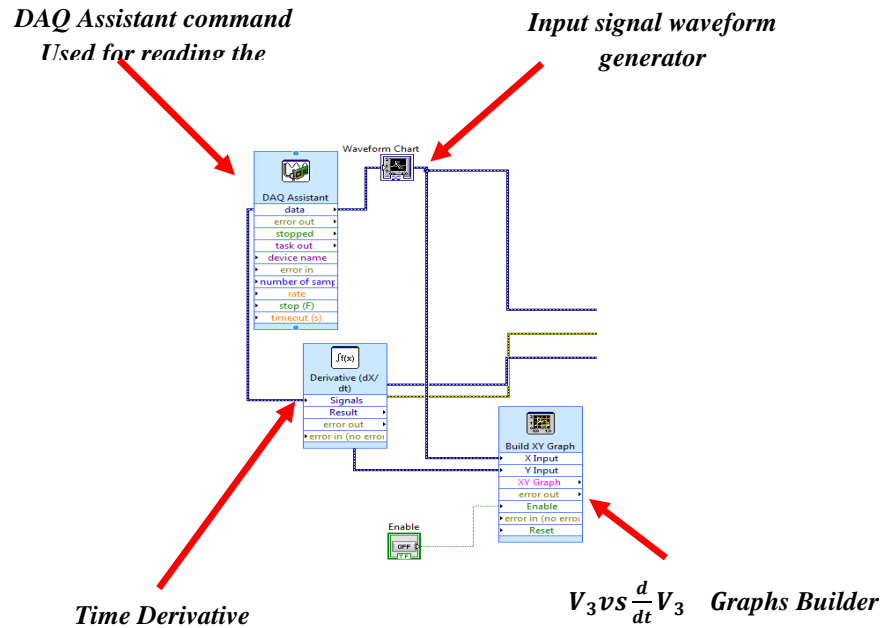
**Figure 3.40 –Portion of the *LABVIEW* block diagram used for plotting**

After plotting them both $\frac{d}{dt} V_3$ and the $V_3$ quantities go into a formula box where the value of σ is calculated using the following equation,

$$\sigma = \frac{d}{dt} V_3 + \alpha V_3$$

Once, σ has been calculated, sigma is again multiplied with $V_3$, and then using the following principles, the code continues,

If, $\sigma V_3 > 0$ , then Resistance used in circuit would be $R_0$. If not, the resistance in the used would be $R_1$. To establish this feature in *LABVIEW*, a Boolean True False command was used in the *LABVIEW*. If the value of $\sigma V_3 >$ zero, there is no change in the output, due to which resistance $R_0$ remains connected to the circuit. If the condition is not met, that means it turn out to be False for the *BOLEAN* true false function, then a voltage signal of

5 Volts is sent to the board through which the circuit is connected. Once a 5 Volts signal is sent to the port where the relay is attached, the relay switches itself that way the resistance $R_1$ gets connected to the circuit. A *DAQmx Write command* of *LABVIEW* has been used to send a 5V signal to the relay. For this specific case, we used *Digital Wfm 1 Chan N samples* type of the write command. As we wanted the data sent to the relay to be have no constraints in terms of sample size, therefore this specific type of write command has been selected. The type of write command function only accepts a digital waveform to write the task for which we used a series of some more *LABVIEW* commands that helped us in converting an array of the data to a digital waveform.

For the data conversion purposes, firstly a convertor was used that was able to convert the dynamic data into an array which was then connected with an array size adjustment command. Once the array size is adjusted, the data then goes through the process of initialization of arrays where every element is essentially initialized to its' related value. These initialized arrays are replaced by subarrays. Finally, the data goes through a convertor which converts a 2D Boolean array to a digital waveform which is followed by a waveform building command. This conversion of data makes it in a form which is acceptable by the write command of *LABVIEW* which basically send an on and off signal to the relay connected to the circuit.

The write commands has been associated with another True and False command due to which it only sends the signal when its required (i.e. when the switching condition is met) only.

For continuity, the *LABVIEW* based program has been constructed inside a while loop which enables the program to keep running until the stop button has been hit. A stop button at the bottom right corner has been inserted which stops the while loop.

### 3.2.2.2. Experimental Results from Phase II:

A series of α values, each corresponds to a unique value of $R_0$ and $R_1$, were used to observe the change in the two plots on varying the value of α. Since no significant switching was noticed experimentally for values of $\alpha$ above 1250 therefore, a series of $\alpha$ values were selected between 0 and 1250. For each α value, the following two plots were obtained.

- Time Response (Time *vs*. Potential Difference) across Third piezoelectric diaphragm
- Voltage *vs*. its Time derivative

Below mentioned plots indicate the experimental results that were obtained on using different values of α

As *LABVIEW* does not give many options pertaining to data analysis and plotting, therefore another *MATLAB* code was written after which the plots were brought to *MATLAB*. For the transformation of *LABVIEW* files to *MATLAB*, all the results with data points were initially obtained on an excel spreadsheet, which was then converted in a notepad (txt)file which was finally used as a data input file for the *MATLAB* code. The outputs of the *MATLAB* code were files that produces plots which are comparable to each other. This enables us to have multiple plots which can be compared together, each of them pertaining to a different couple of alpha values.

This time, the values of the input were not varied much. A single value of amplitude, *i.e.* 1V (pk to pk) was selected and the frequency of 1250 *Hz* was selected to see the variation in the Time response and size of the circle obtained from $mV_3$ *vs* $\frac{d}{dt}V_3$ graph. Figure 3.41 indicates the input signal provided to the acoustic cavity.
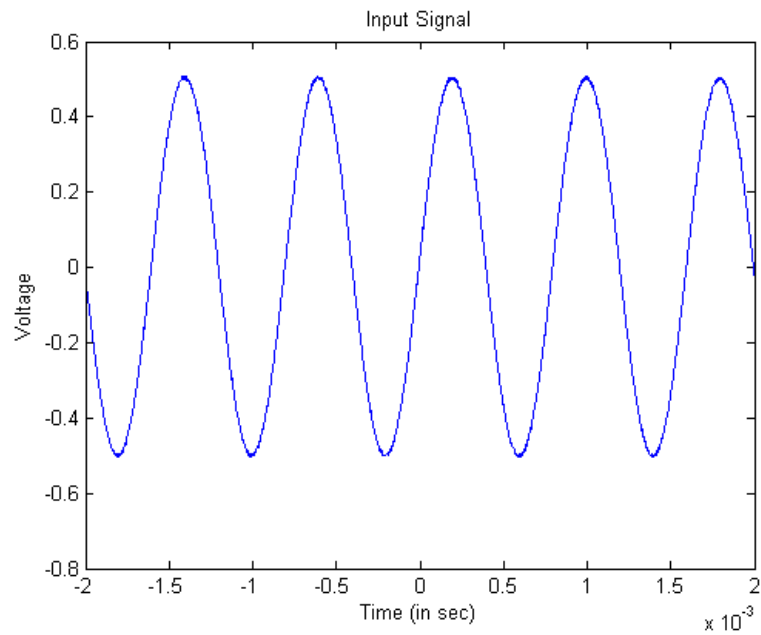


**Figure 3.41 – Time response of Acoustic cavity's input signal**

As each α is associated with a unique value of $R_0$ and a maximum value of $R_1$, therefore multiple values of $R_1$ have been taken due to which we have obtained plots for each value of α.

Below are the plots for different values of the slope of the switching line (α).

**Table 3.2 – Parameters of the Controller for $\alpha$=4.8138, $R_0$=10,000$\Omega$ and $R_1$=1,000 $\Omega$**

| $\alpha$ | 4.8138 | $R_{1\ (max)}$ | $2.317 \times 10^5\ \Omega$ |
|---|---|---|---|
| $R_0$ | 10,000 $\Omega$ | $R_{1(used)}$ | 1,000 $\Omega$ |



*Sliding Line*

(a)



(b)
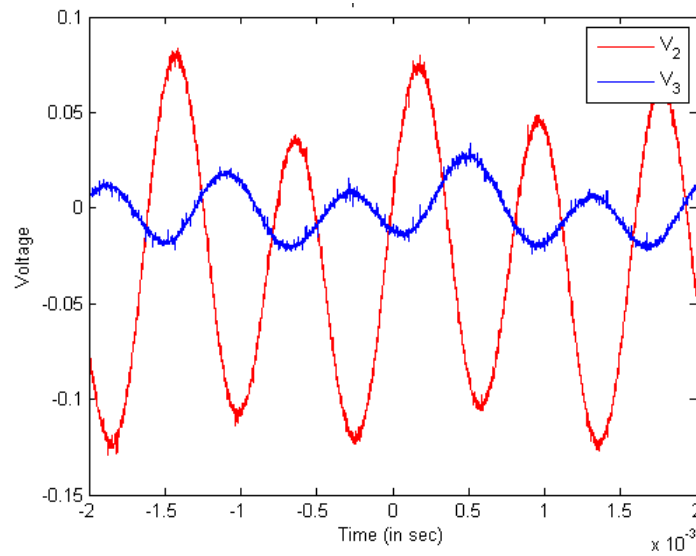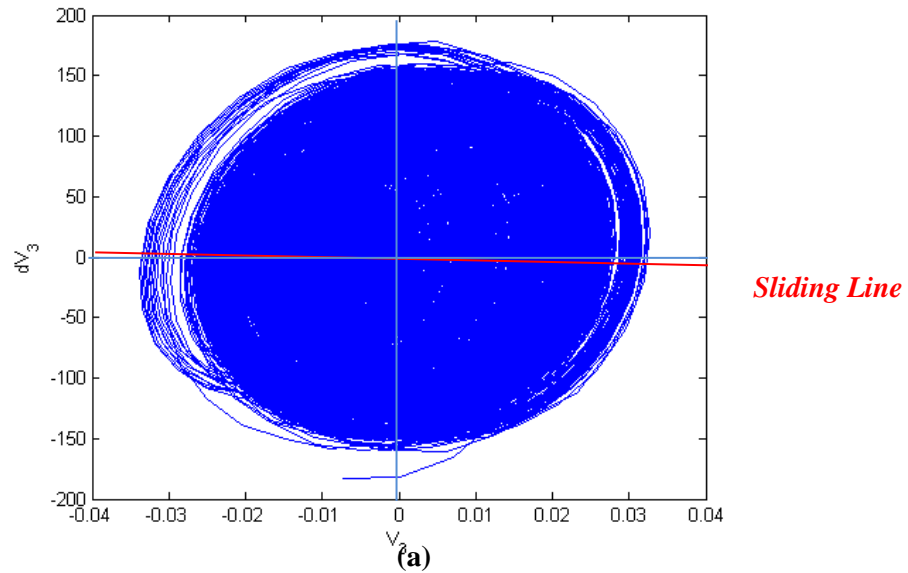
**Figure 3.42 - The phase plane (a) and the time response of the input/output (b) for $\alpha$=4.8138, $R_0$=10,000$\Omega$ and $R_1$=1,000 $\Omega$**

**Table 3.3 – Parameters of the Controller for $\alpha$=4.8138, $R_0$=10,000$\Omega$ and $R_1$=10,000$\Omega$**

| $\alpha$ | 4.8138 | $R_{1\ (max)}$ | $2.317 \times 10^5\ \Omega$ |
|---|---|---|---|
| $R_0$ | 10,000 $\Omega$ | $R_{1(used)}$ | 10,000 $\Omega$ |



**(a)**



**(b)**
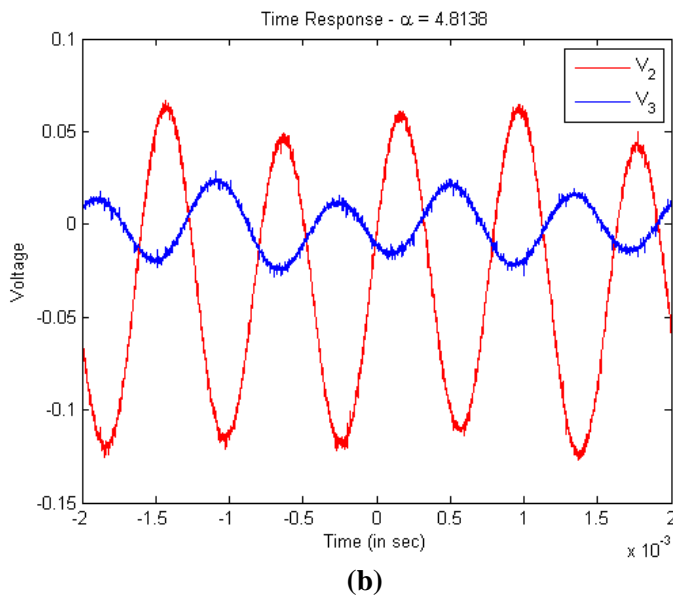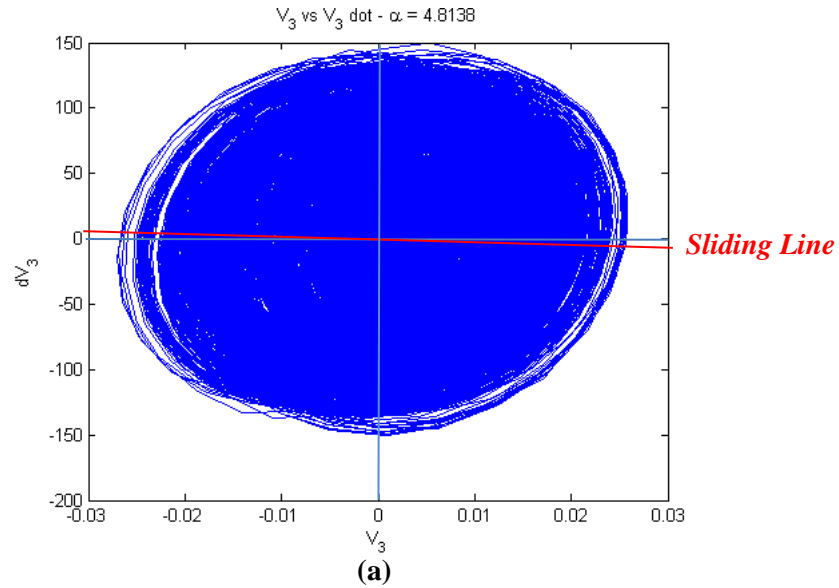
**Figure 3.43 - The phase plane (a) and the time response of the input/output (b) for $\alpha$=4.8138, $R_0$=10,000$\Omega$ and $R_1$=10,000 $\Omega$**

**Table 3.4 – Parameters of the Controller for $\alpha$=4.8138, $R_0$=10,000$\Omega$ and $R_1$=0.22$M\Omega$**

| $\alpha$ | 4.8138 | $R_{1\,(max)}$ | $2.317\times10^5\ \Omega$ |
|----------|--------|----------------|---------------------------|
| $R_0$ | 10,000 $\Omega$ | $R_{1(used)}$ | 0.22 M$\Omega$ |
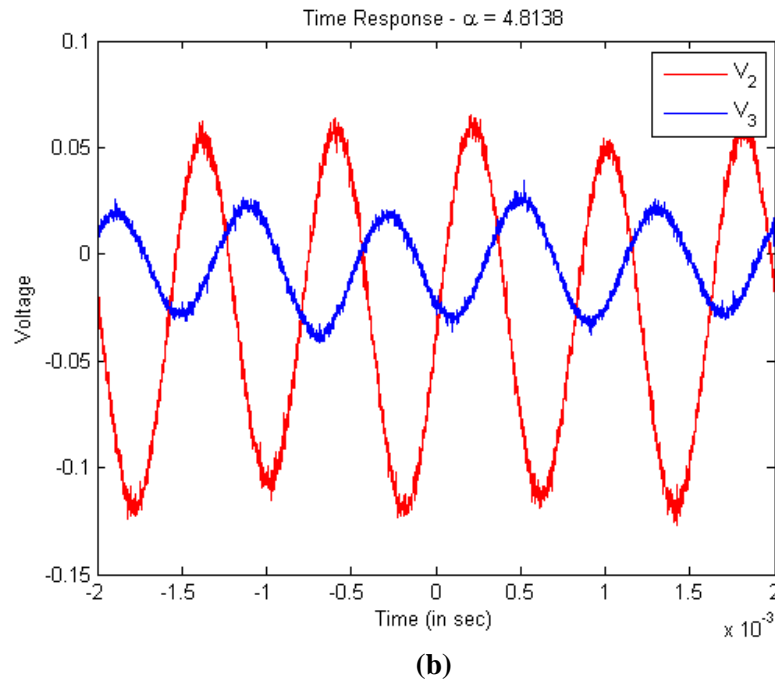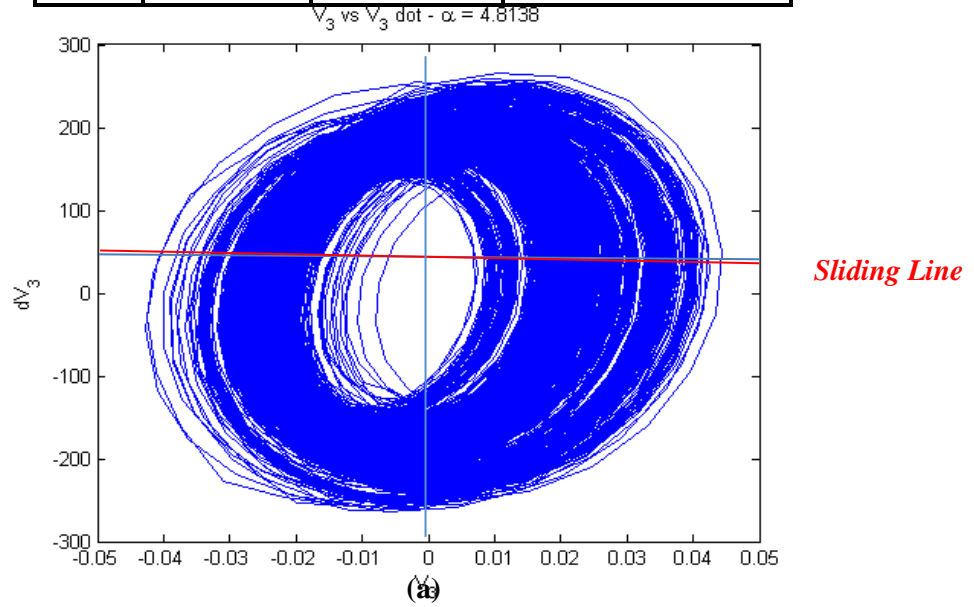


**Figure 3.44 - The phase plane (a) and the time response of the input/output (b) for $\alpha$=4.8138, $R_0$=10,000$\Omega$ and $R_1$=0.22$M\Omega$**

**Table 3.5 – Parameters of the Controller for $\alpha$=48.138, $R_0$=10,000$\Omega$ and $R_1$=100k$\Omega$**

| $\alpha$ | 48.138 | $R_{1\,(max)}$ | $2.317\times10^6$ $\Omega$ |
|---|---|---|---|
| $R_0$ | 1,000 $\Omega$ | $R_{1(used)}$ | $1\times10^5$ $\Omega$ (100 kOhms) |



**(a)**



**(b)**
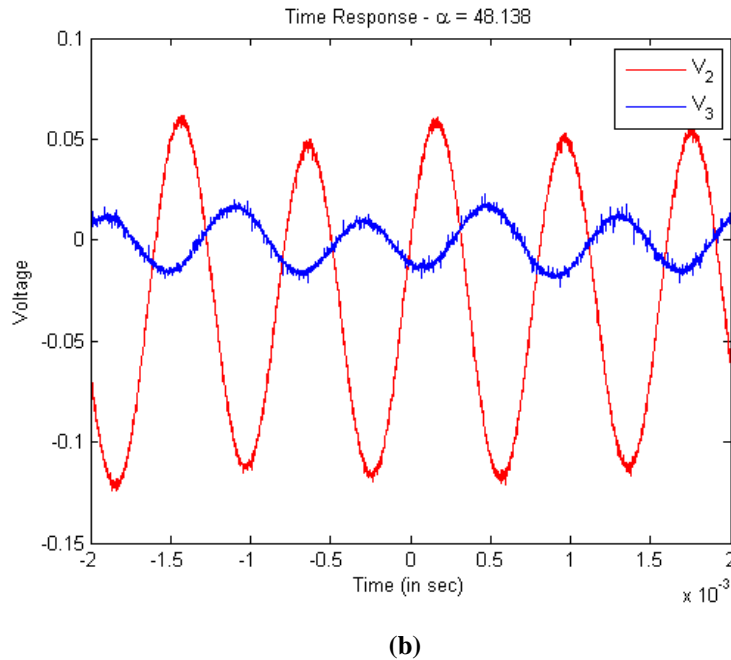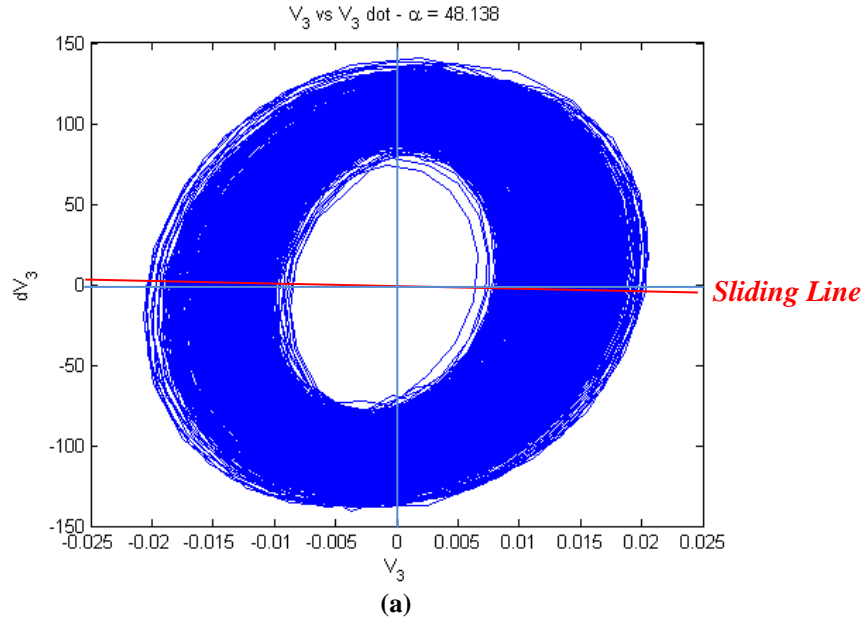
**Figure 3.45 - The phase plane (a) and the time response of the input/output (b) for $\alpha$=48.138, $R_0$=1,000$\Omega$ and $R_1$=100K$\Omega$**

65

**Table 3.6 – Parameters of the Controller for *α*=48.138, *R₀*=1,000*Ω* and *R₁*=1,000*KΩ***

| $\alpha$ | 48.138 | $R_{1\ (max)}$ | $2.317 \times 10^6\ \Omega$ |
|---|---|---|---|
| $R_0$ | 1,000 $\Omega$ | $R_{1(used)}$ | $1 \times 10^6\ \Omega$ |



**(a)**



**(b)**
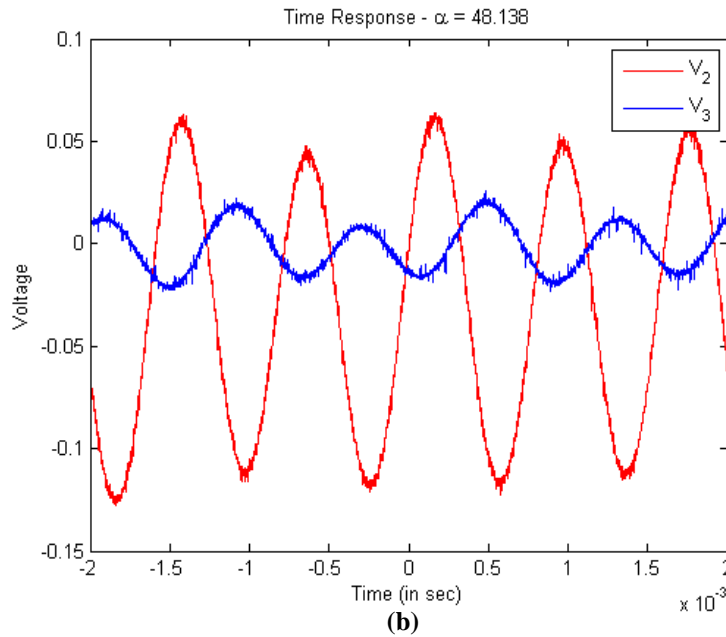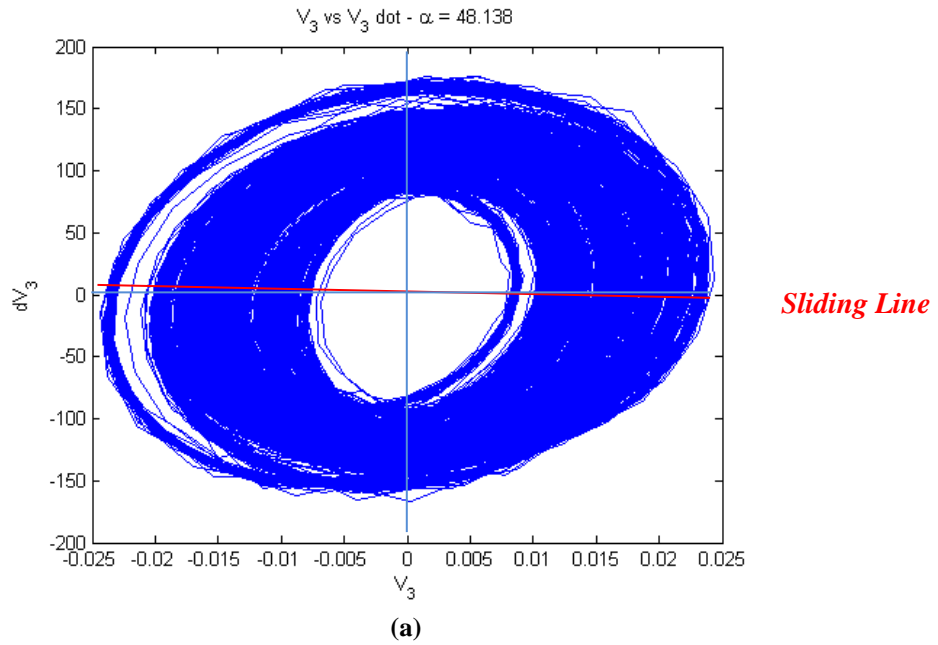
**Figure 3.46 - The phase plane (a) and the time response of the input/output (b) for *α*=48.138, *R₀*=1,000*Ω* and *R₁*=1MΩ**

**Table 3.7 – Parameters of the Controller for *α*=481.38, *R₀*=100*Ω* and *R₁*=1 M*Ω***

| *α* | 481.38 | *R₁ (max)* | $2.317 \times 10^6$ Ω |
|-----|--------|------------|------------------------|
| *R₀* | 100 Ω | *R₁(used)* | $1 \times 10^6$ Ω |



**(a)**



**(b)**
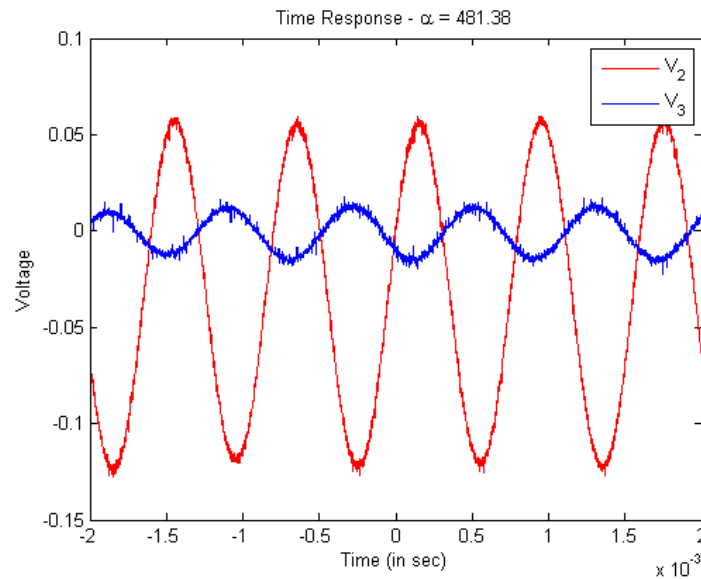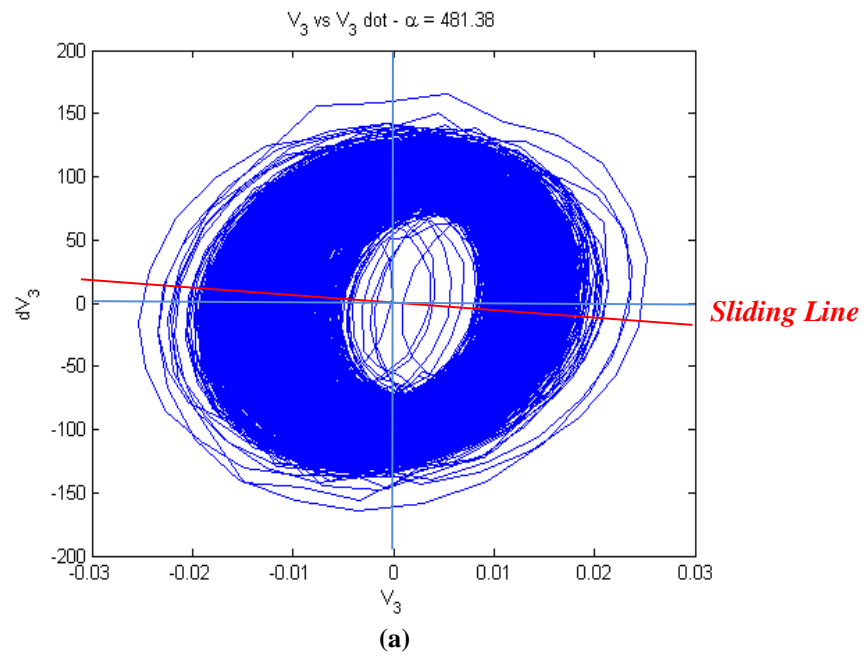
**Figure 3.47 - The phase plane (a) and the time response of the input/output (b) for α=48.138, R₀=100Ω and R₁=1MΩ**

**Table 3.8 – Parameters of the Controller for $\alpha$=481.38, $R_0$=100$\Omega$ and $R_1$=10$M\Omega$**

| $\alpha$ | 481.38 | $R_{1\ (max)}$ | $2.317{\times}10^7\ \Omega$ |
|---|---|---|---|
| $R_0$ | 100 $\Omega$ | $R_{1(used)}$ | $1{\times}10^7\ \Omega$ |



*Sliding Line*

**(a)**



**(b)**
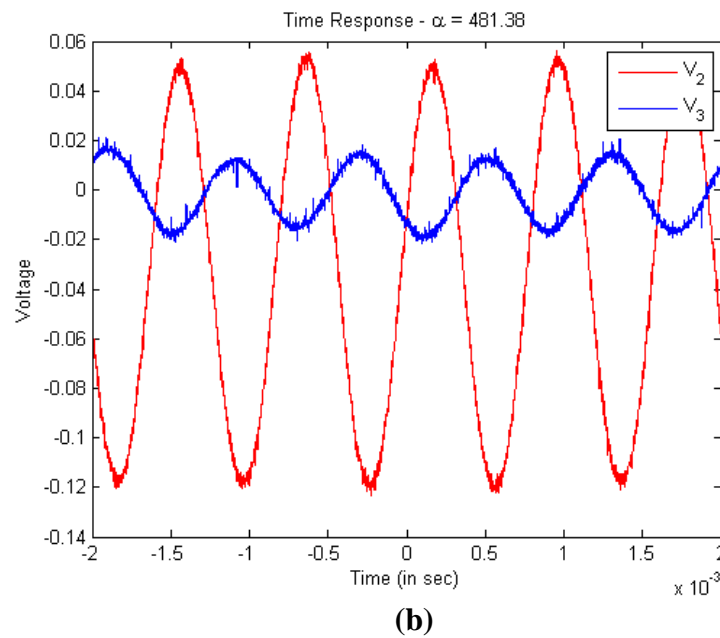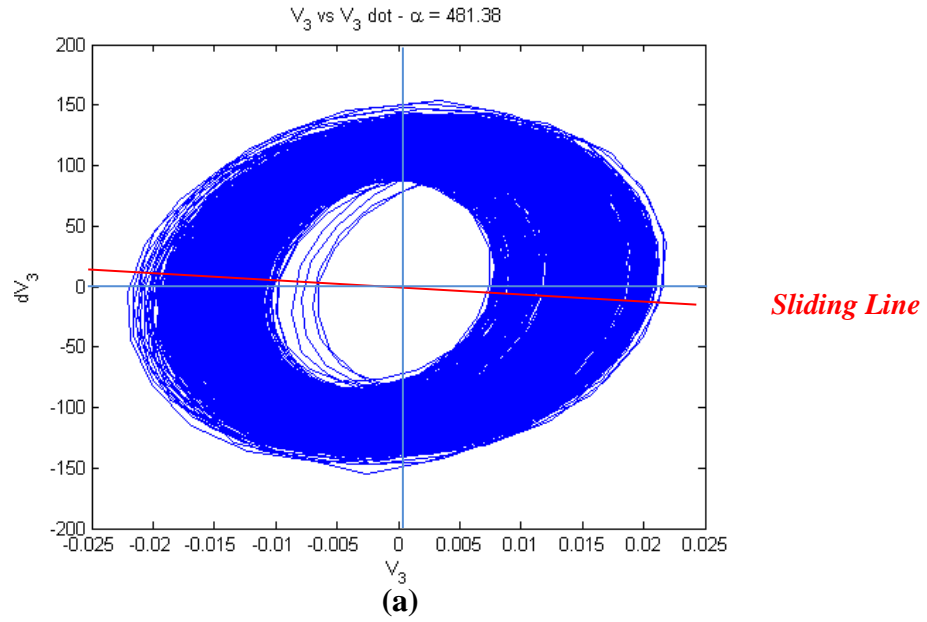
**Figure 3.48 - The phase plane (a) and the time response of the input/output (b) for $\alpha$=481.38, $R_0$=100$\Omega$ and $R_1$=10$M\Omega$**

After trying multiple values of α, each with different values of Resistances, the two extreme values of *α i.e.* 0.1 and 1250 were chosen at which the switch was able to work precisely. The results displayed in figure 3.49 show the two plots for both values of *α*.
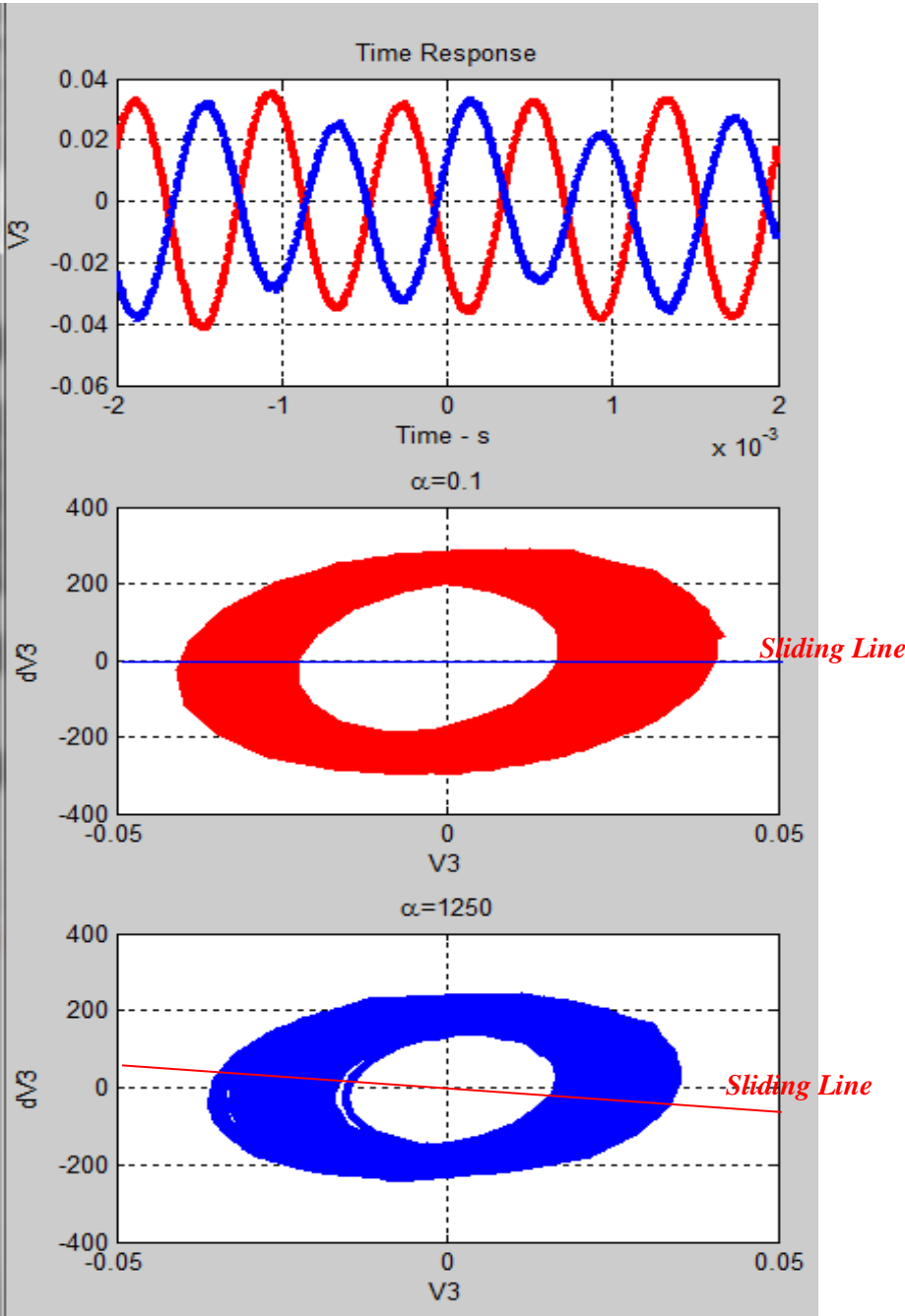


**Figure 3.49 – Comparison between the phase plane plots
and time response for values of α = 0.1 and α =1250**

## 3.3. Summary:

This section includes a summary of the obtained experimental results from different phases of the experiment. The theoretical predictions of the lumped-parameter mathematical models have been validated experimentally using prototypes *ANAM*. The variation in the non-reciprocity conditions of the experiments with the variation in $\alpha$, confirms the theory of the structure which has been discussed in the earlier chapters.

# Chapter 4

# *PSPICE* SIMULATIONS

## 4.1. Introduction:

*PSPICE* is one of the computer programs which allows the users to simulate an electrical circuit on their computers. It is often used for testing the way a circuit will simulate.

It is widely used in the field of electronics. *PSPICE* basically stands for Program Simulation with Integrated Circuit Emphasis. In this software the users can draw the desired circuit using the toolbars offered by *PSPICE*. The values can many other details can be set by the users. Once the desired circuit is constructed, users can perform different types of analysis. One of the *PSPICE* offered analysis that we have been interested in is transient analysis.

## 4.2. Transient Analysis in *PSPICE*:

Transient Analysis is one of the Analysis options in *PSPICE* in which the users are allowed to analyze their circuits in time domain. *PSPICE* also allows their users to select the time step size and the maximum time to run. Figure 4.1 shows the *PSPICE* screen of Analysis which gives you an option of doing a customized analysis.
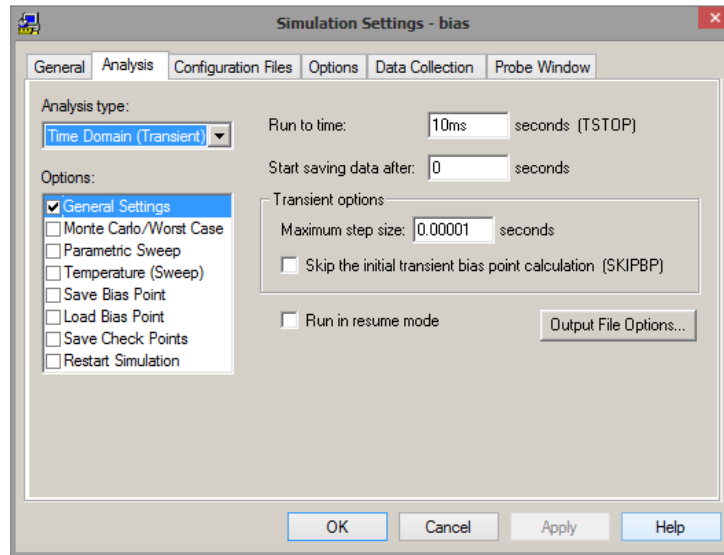
**Figure 4.1 - PSPICE Transient Analysis settings**

Since, we have mainly been willing to obtain time response of the third piezoelectric diaphragm of the acoustic cavity, we are interested in the transient analysis. This option of *PSPICE* allows the user to plot bunch of parameters of the circuit against time. In addition, the user can setup the number of points and the maximum time for which the user want to run the simulation.

In our case, we had to run the simulation once for the time response graph and then keeping all the parameters unchanged, we performed a transient analysis to obtain a graph between time *vs* $\frac{d}{dt}V_3$.

As none of the parameter including time step and total time of analysis were changed, both plots, *i.e*. Time *vs* voltage across third piezo electric diaphragm (time response) and time *vs* the derivative of the voltage across third piezo electric diaphragm (time *vs* $\frac{d}{dt}V_3$ ) had the exact same data points for time.

As the data points were the same for the independent quantities of bot plots, the same set of data was capable of being used to obtain a plot between voltage ($V_3$) and its time derivative ($\frac{d}{dt} V_3$)

## 4.3. AC Sweep Analysis in *PSPICE*:

As we had also been interested in getting the frequency sweep, which is operated in the frequency domain of *PSPICE*, one of the possible options we had, which was also used was the AC Sweep Analysis option of *PSPICE*. It allows you to obtain a frequency sweep option of your circuit which can help you in determining the pass bands and stop bands of your circuit. It allows its' users to set the frequency range they want to run the frequency sweep for.

**4.4. Construction of Circuit in *PSPICE*:**

As discussed in earlier chapters that the equivalent electric circuit of the acoustic cavity will be similar to the circuit shown in Figure 4.2.
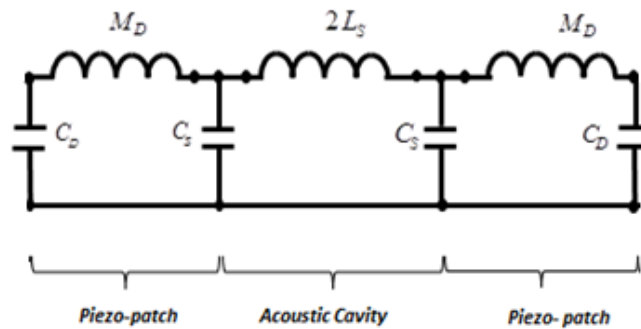


**Figure 4.2 - Equivalent circuit of Acoustic cavity**

To construct a similar circuit in *PSPICE*, a circuit library needs to be downloaded first. Once the circuit library is downloaded, the user can now construct a circuit in the schematic page of *PSPICE*.

Now, in this schematic window the circuit was constructed as shown in Figure 4.3. For this purpose, an appropriate voltage source was to be selected. In our case, this selected voltage source was a sinusoidal voltage source. We could also have selected an *AC* source as both *AC* and sinusoidal source give the same output. The only difference is that sinusoidal option allows you to be more specific. If we select sinusoidal source, we can set things like frequency, offset voltage etc. based on our requirement.

As experimentally we had selected a frequency of 1250$Hz$, therefore we setup the Sinusoidal source frequency to be 1250 $Hz$. Similarly, we had used 1V peak to peak voltage during the experimental runs, therefore the Amplitude of sinusoidal source in PSPSICE was also set to be 0.5V which makes 1V peak to peak.

Once the voltage source has been selected the rest of the circuit gets easier to build. From the circuit library offered *PSPICE* resistances, inductances and capacitances can be selected and assigned the values correspondingly.

Figure 4.3 displays the values of the resistances, inductances and capacitances that have been assigned in this circuit. Once all these components are selected, assigned values and arranged, they can be connected through a wire by using 'place wire' option given in the *PSPICE* library. Figure 4.3 represents the final circuit which was obtained in *PSPICE* which was basically used to were run simulations,
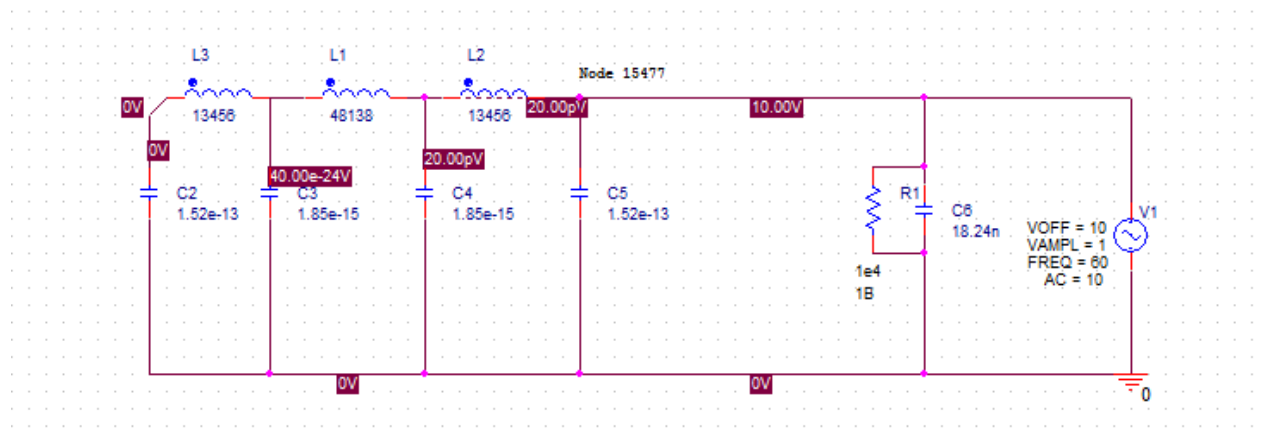


**Figure 4.3 – PSPICE circuit used for simulations**

## 4.5. AC Sweep Plots obtained from *PSPICE*:

Before adding an external resistance to it, a frequency sweep was obtained to determine the pass bands and stop bands of the circuit. Figure 4.4(a) shows the frequency sweep plot of the circuit. In addition, Figures 4.4(b) and 4.4(c) shows the zoomed in picture of the stop band.
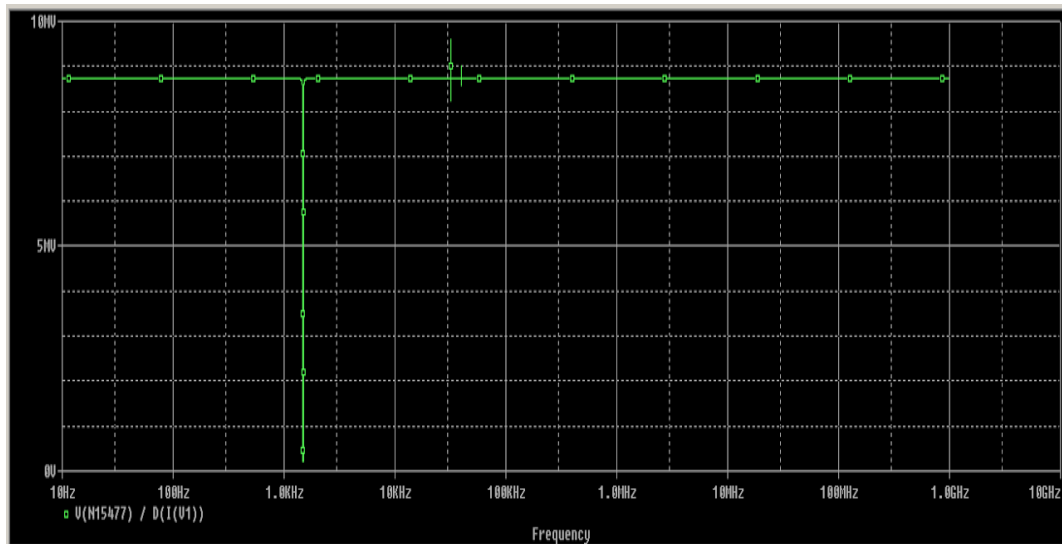


*(a) – Frequency sweep original plot between 10Hz to 1.0HHz*
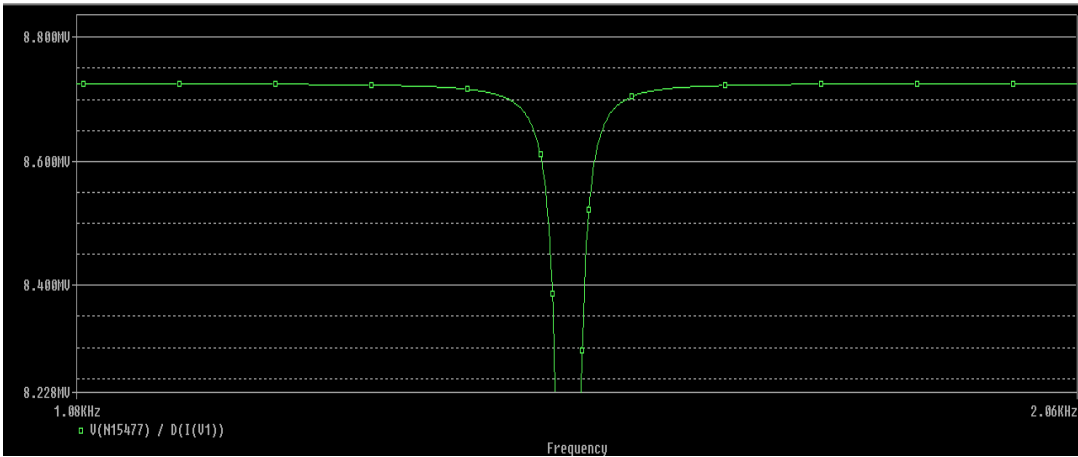
*(b) – AC sweep plots with zoomed in view of resonace
between 1.08KHz and 2.06 kHz*
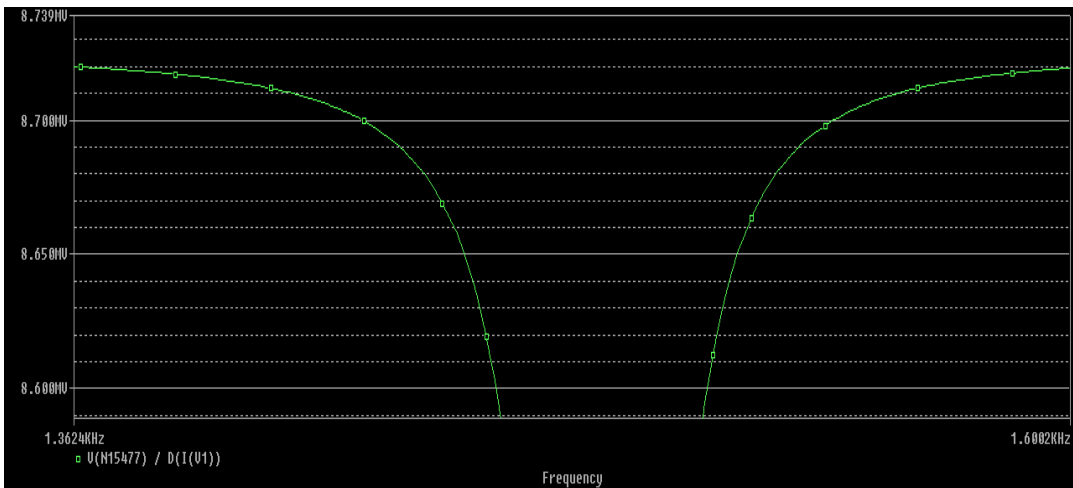


*(c) – AC sweep plots with zoomed in view of resonance
between 1.362KHz and 1.602 kHz*

**Figure 4.4. – AC sweep plots for the equivalent circuit of the**

**4.6. Switching Resistances:**

The graphs that were obtained from *PSPICE* were transformed into *MATLAB* files, for the following reasons,

1) *PSPICE* does not have an option of that's easily accessible which can allow switching resistances based on the required conditions

2) To compare the plots with experimental results we needed to have similar linewidth and other plotting features, to what we had from experimental results.

3) In transient analysis of *PSPICE*, *x*-axis quantity is setup as time by default. Since it was also required to see a plot between Voltage and its time derivative to have a comparison, the requirement was to have voltage ($V_3$) on the *x*-axis of the plot.

The plots that that are obtained from *PSPICE* were exported into 'txt' files which eventually were used as an input file in *MATLAB*. The txt files obtained from *PSPICE* basically contains all the data points that have been used by *PSPICE* to plot the graphs. Each txt file contains two columns from which one of them is the data points used for *x*-quantity and the other is for *y*-quantity.

A *MATLAB* code has been written in *MATLAB*, which not only switches between the resistances based on the required programmed condition, but it also plots the data points after switching. Below is the *MATLAB* code written for the switching and plotting. For each case, the values of alpha and resistances change,

```
clc
clear all
close all

% Defining the value of /alpha
alpha = 0.1;

% Loading the two files
load r481380.txt
load r4813.txt

load r38A.txt
load r6e7A.txt

load dt481380.txt
load dt4813.txt
```

```matlab
% Defining the columns used
r0_time = r481380(:,1);
r0_voltage = r481380(:,2);
r1_time = r4813(:,1);
r1_voltage = r4813(:,2);

dtr0_time = dt481380(:,1);
dtr0_dt = dt481380(:,2);
dtr1_time = dt4813(:,1);
dtr1_dt = dt4813(:,2);

sigma = dtr0_dt(1,1) + alpha*r0_voltage(1,1);

% ******************************************
% *** Programming switching controller ******
% ******************************************

for ii = 1:length(r0_voltage)

    if sigma*r0_voltage(ii) > 0;
        v3(ii) = r0_voltage(ii);
        v3_dot(ii) = dtr0_dt(ii);
    else
        v3(ii) = r1_voltage(ii);
        v3_dot(ii) = dtr1_dt(ii);
    end

    sigma = v3_dot(ii) + alpha*v3(ii);

end

% ********************
% ****** PLOTS *******
% ********************
plot(smooth(v3(55:length(v3))),smooth(v3_dot(55:length(v3_dot))))
xlabel('V_3 - Theoritical')
ylabel('dV_3')
title('V_3 vs V_3 dot - \alpha = 0.1')


% figure(4)
% hold on
plot(r0_time,(v3),'blue','linewidth',1)
xlabel('Time')
ylabel('V_3')
title('Time response - \alpha = 0.1 (from pspice)')
```

*MATLAB* **Code written for switching and plotting**

**4.7. Simulation Results (*PSPICE* and *MATLAB*):**

As mentioned earlier, *PSPICE* files were brought to *MATLAB* from where not only switching of the resistances was done, but the final data was also used to obtain the plots. Multiple values of $\alpha$, each of them corresponds to unique values of resistances ($R_0$ and $R_1$) were taken into consideration due to which plots were obtained. One of the reasons of take multiple α values to verify that the increasing the value of α leads to the decrease in the size of the closed circle obtained in pressure and pressure rate plots.

Quantities similar to experimental plots' parameters (pressure rate against pressure and time response) were plotted to make the plots comparable. Following plots represent the *PSPICE* results for both, time response and Voltage *vs* its time derivative for a bunch of α values

*Sliding Line*
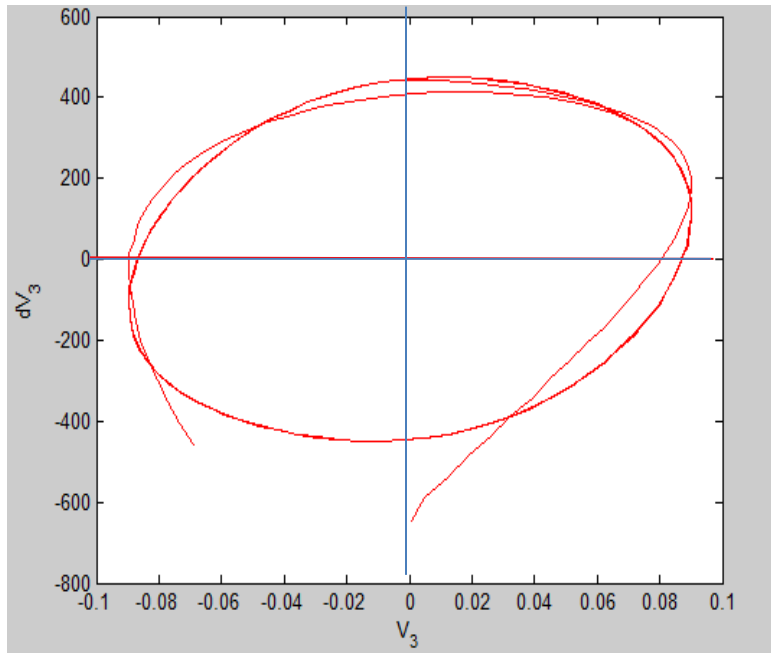
*(a)*
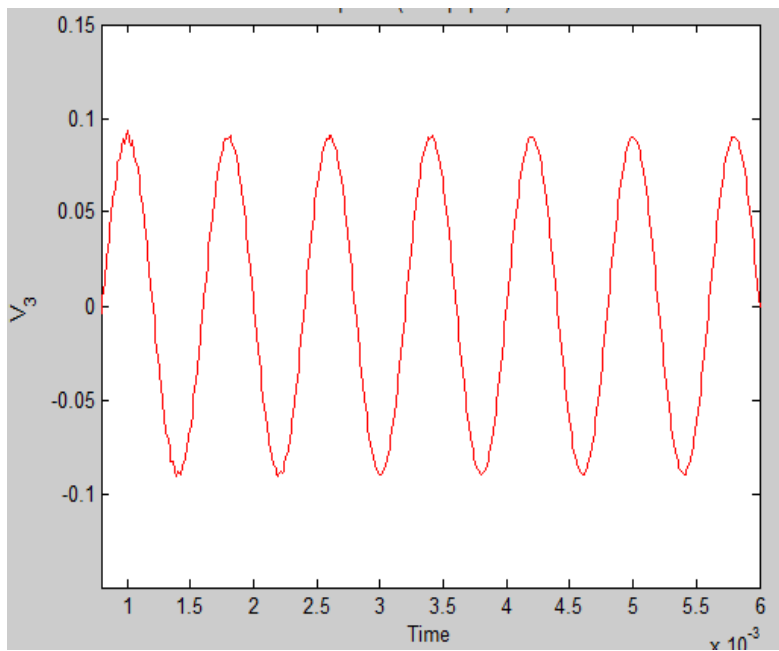


*(b)*

**Figure 4.5 - The *PSPICE* phase plane (a) for α = 0.1  (b) for the time response of the input/output**
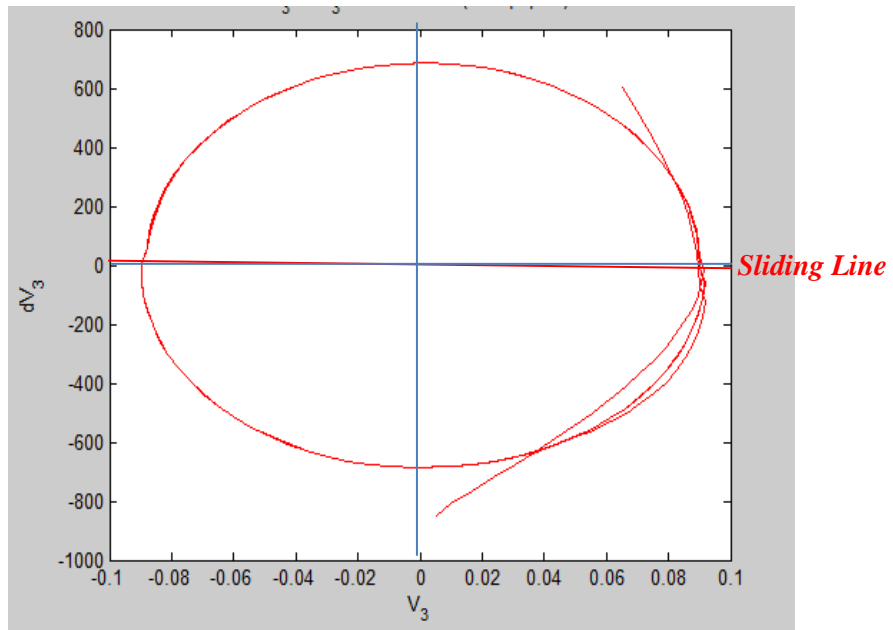
*(a)*
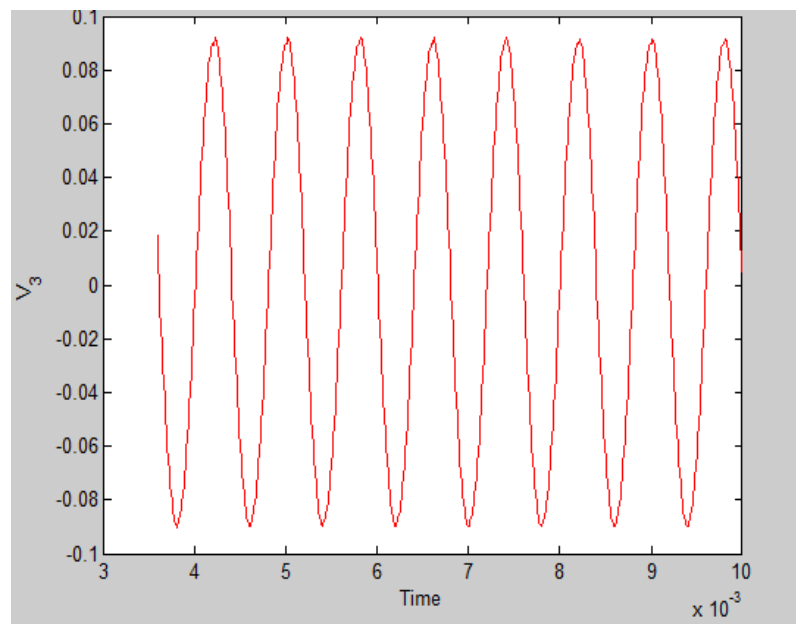


*(b)*

**Figure 4.6 - The *PSPICE* phase plane (a) for α = 100 (b) for the time response of the input/output**

83

Sliding Line
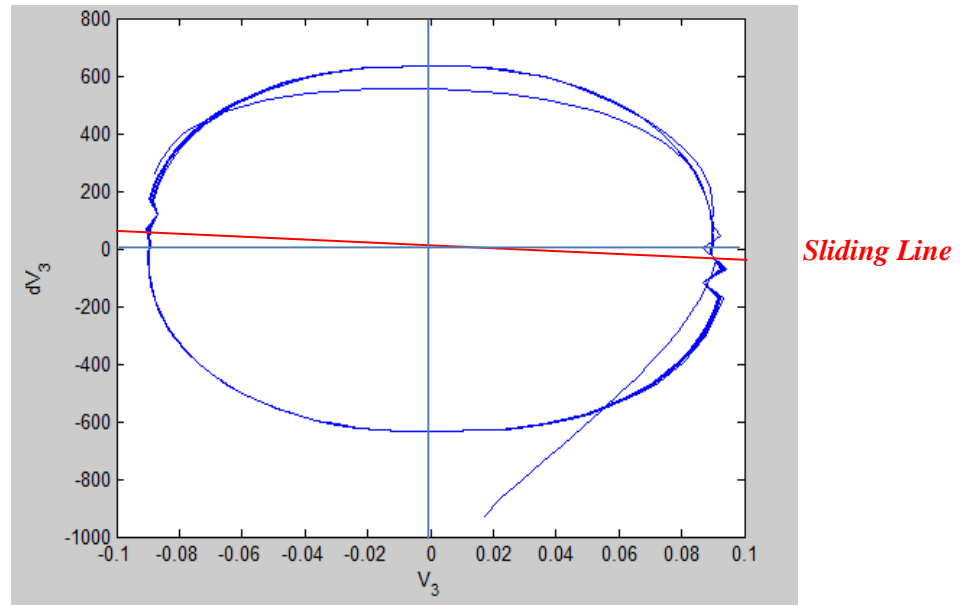
*(a)*
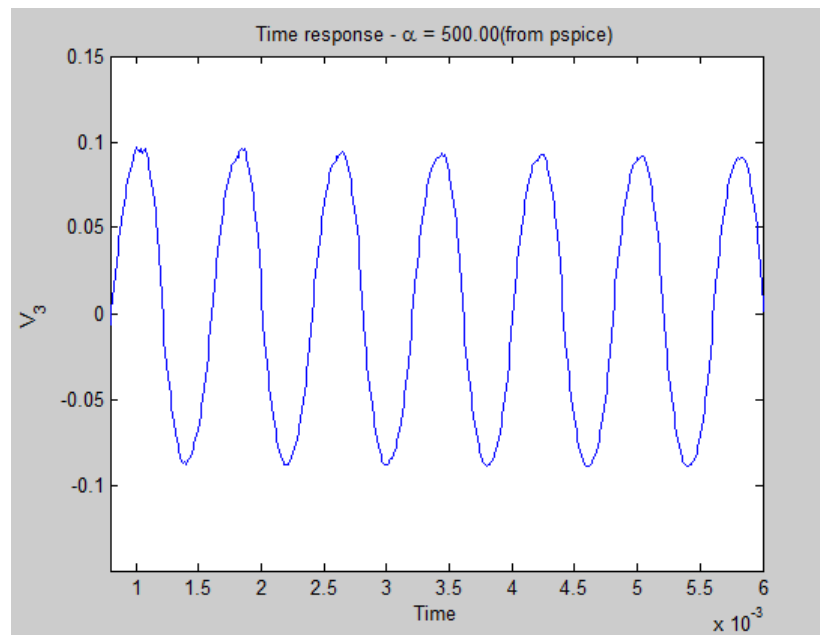


*(b)*

**Figure 4.7 - The *PSPICE* phase plane (a) for α = 500 (b) for the time response of the input/output**
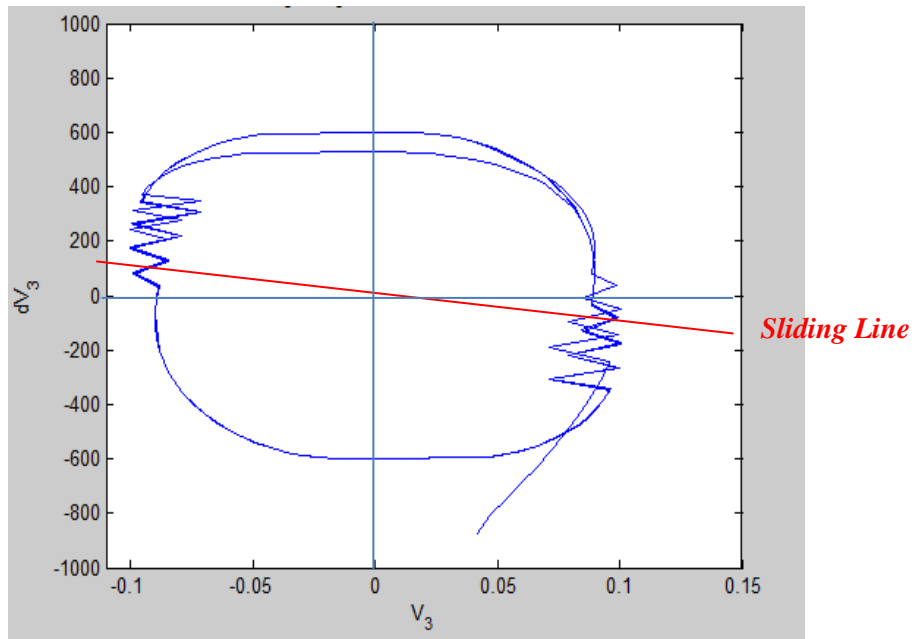
*(a)*
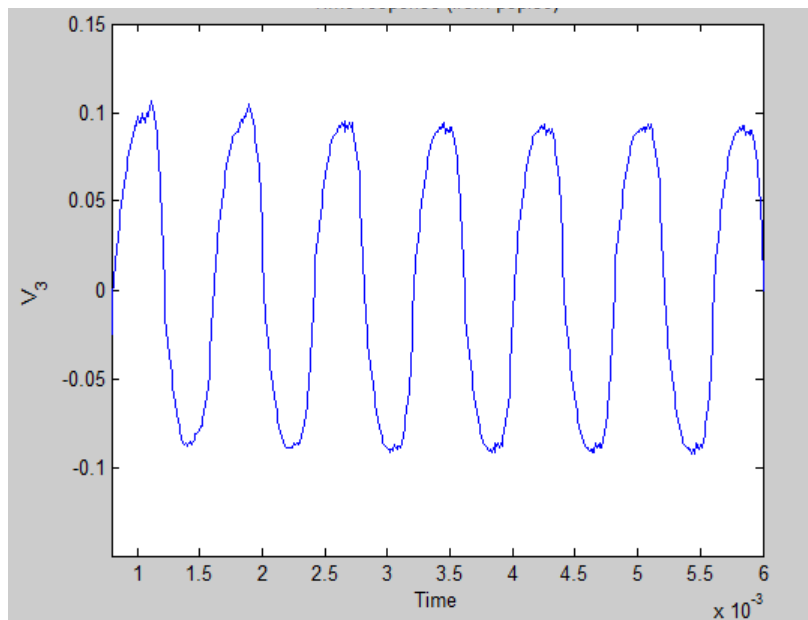


*(b)*

**Figure 4.8 - The *PSPICE* phase plane (a) or α = 1250 (b) for
the time response of the input/output**

**4.8. Results obtained from switching the Input Source Position:**

**a. With Ground connected with right actuator :**

A few simulations were also run, after changing the position of the input to the second piezoelectric diaphragm. And there were further two cases simulated, in the first one the ground was connected with the forth piezoelectric diaphragm (capacitance in *PSPICE*), as shown in Figure 4.12 (a).
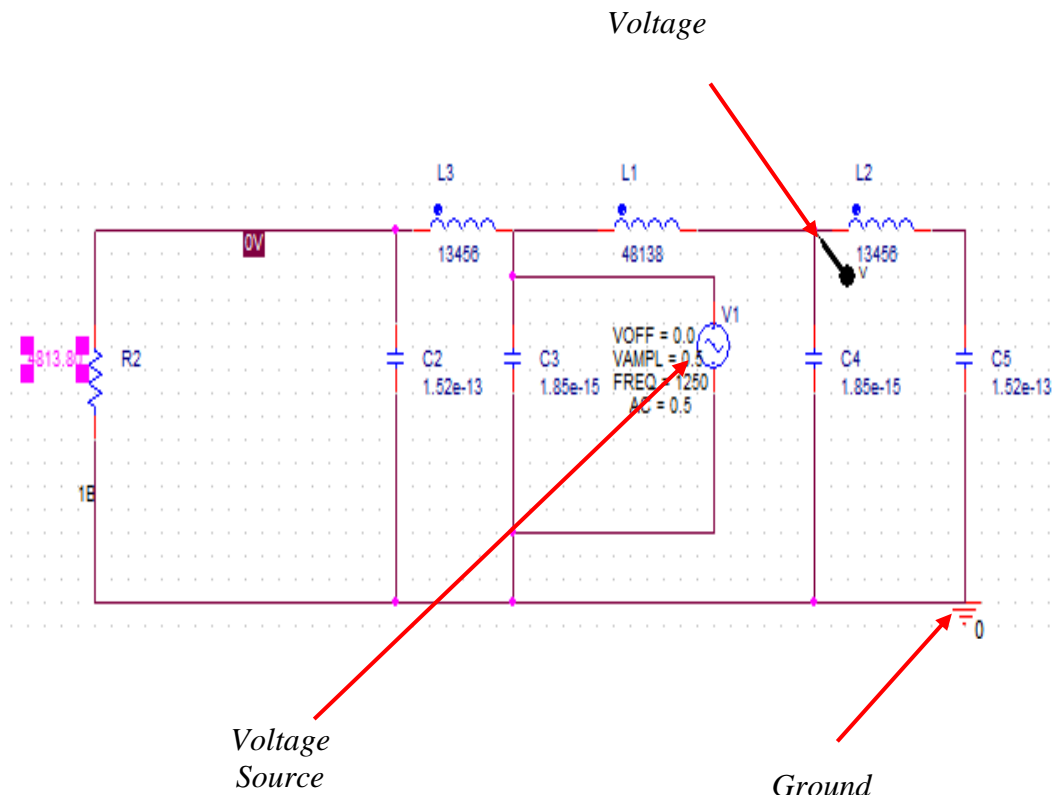


**Figure 4.9 – PSPICE circuit after switching input position and with voltage marker to $V_3$**

Figure 4.10 represents a plot of *V3 vs* $\frac{d}{dt}V_3$ and the time response obtained after time response obtained after switching the resistances. A range of α was used resulting in no change for time response or Voltage *vs* its time derivative's graph.
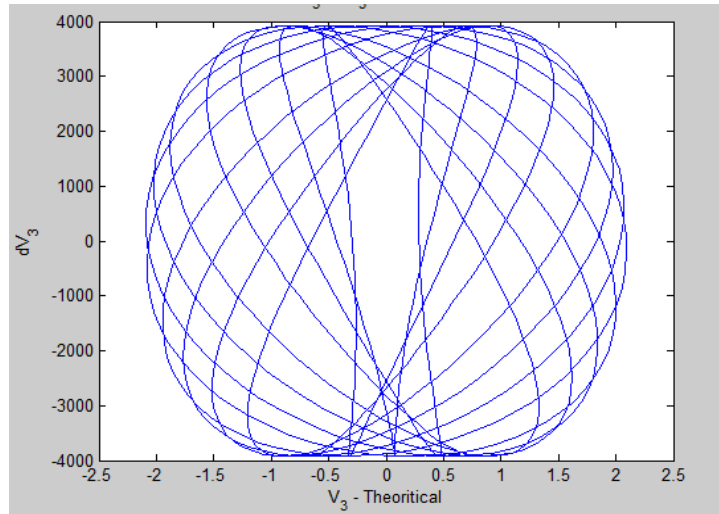


*(a)*
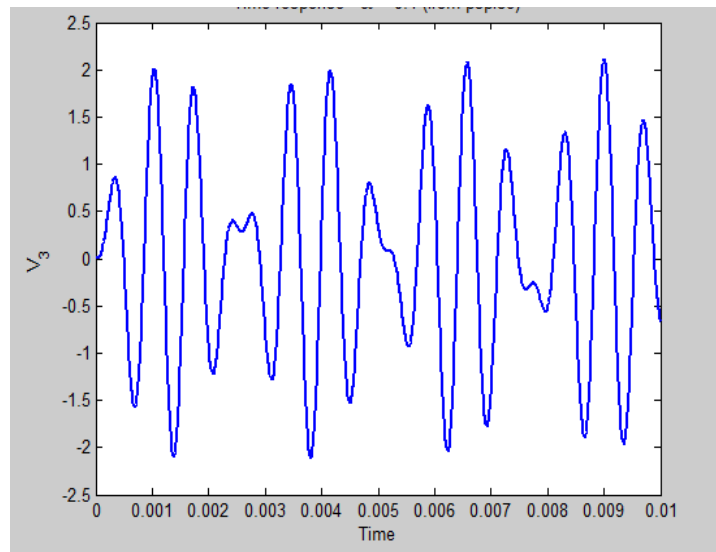


*(b)*

**Figure 4.10 - The *PSPICE* phase plane after switching ground position (a) or multiple α values (b) for the time response**

In addition to trying different values of α, the position of voltage marker in *PSPICE* was also changed to the forth piezoelectric diaphragm but there was no noticeable difference in the results. Figure 4.11 shows the *PSPICE* circuit obtained after switching the voltage source and the plots obtained for the circuit have been displayed in Figures 4.12(a) and 4.12 (b)
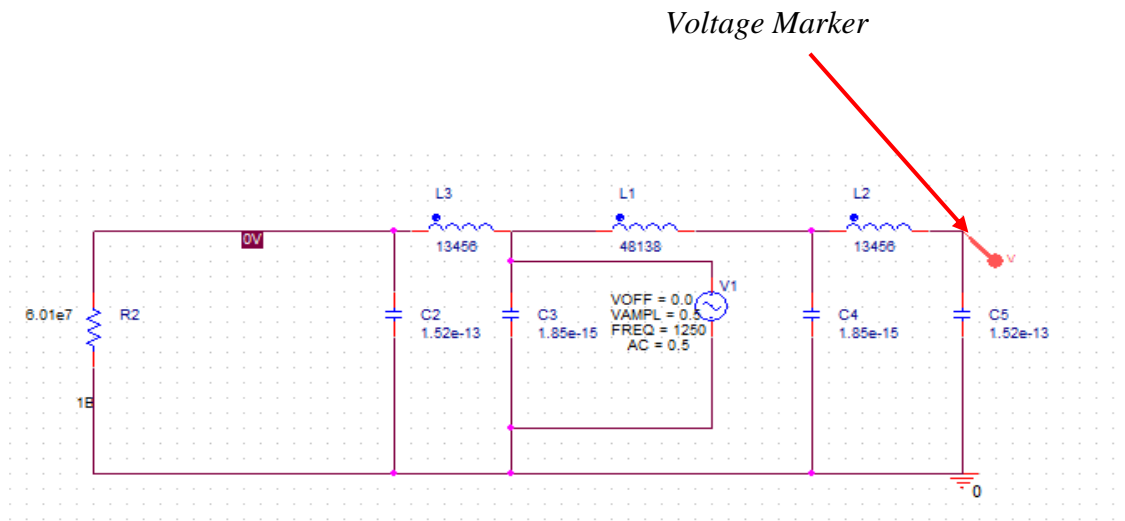


*Figure 4.11 – PSPICE* **circuit after switching input position and with voltage marker at** $V_3$
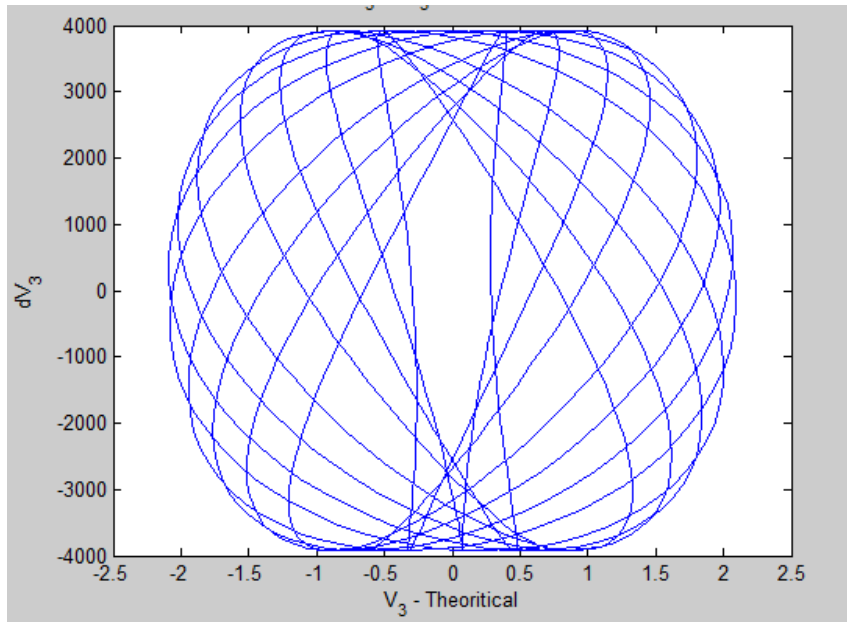
*(a)*
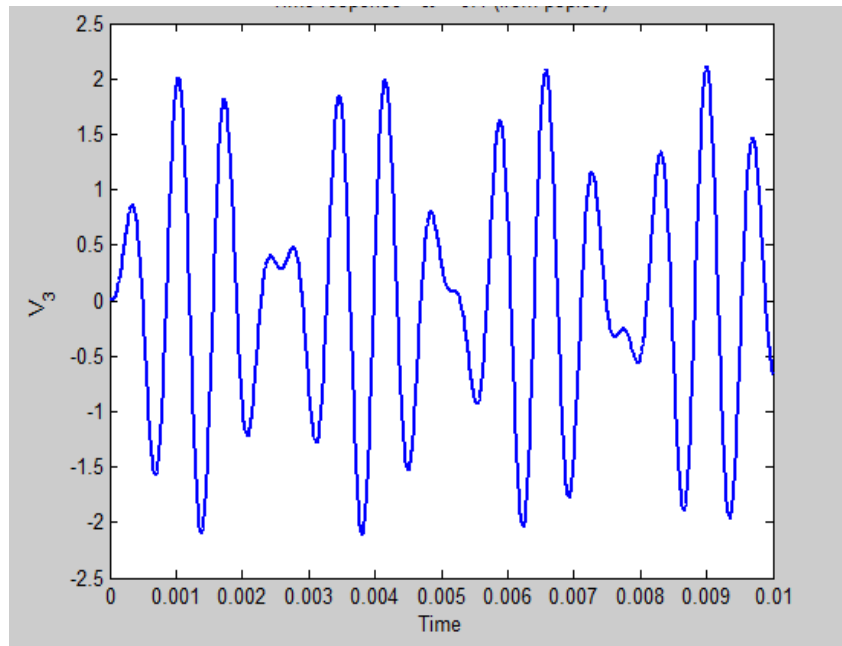


*(b)*

**Figure 4.12 - The *PSPICE* phase plane with voltage market across inductor (a) for multiple alpha values (b) for the time response of the input/output**

**b. With Ground connected in a separate loop :**

Very similar cases were worked upon with the ground connected separately in a loop. A very minor resistances was added in series combination as recommended by *PSPICE*. Figure 4.13 shows the *PSPICE* circuit after changing the ground position.



*Series*          *Voltage marker*

*Input voltage*

*Ground*
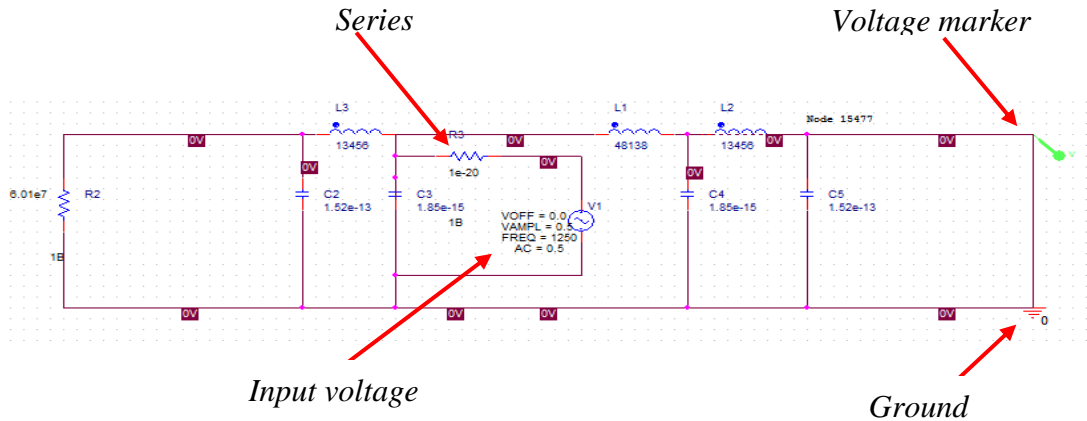
**Figure 4.13 – *PSPICE* circuit after switching input position and with voltage marker outside**

Figure 4.14 shows the time response, gotten from the circuit pertaining as shown in Figure 4.13.
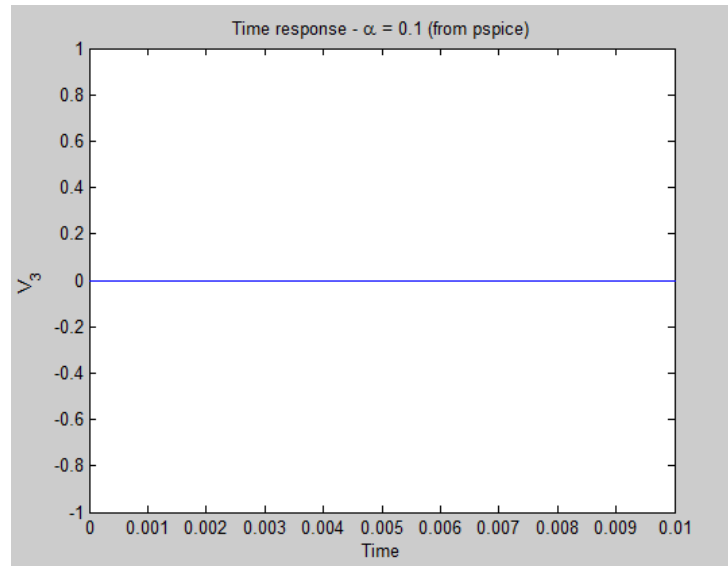


**Figure 4.14- Time response obtained from *PSPICE* with voltage market across inductor and ground outside the loop**

Multiple values of α were taken but no change in the any of the plots were noticed. Also, the value of $\frac{d}{dt}V_3$ were all zero as there's no change in $V_3$. So essentially the graph between $V_3$ and $\frac{d}{dt}V_3$ turns out to be a point circle at origin.

This practice was repeated after changing the position of the voltage marker as shown in the Figure 4.16, but the plots were no different.
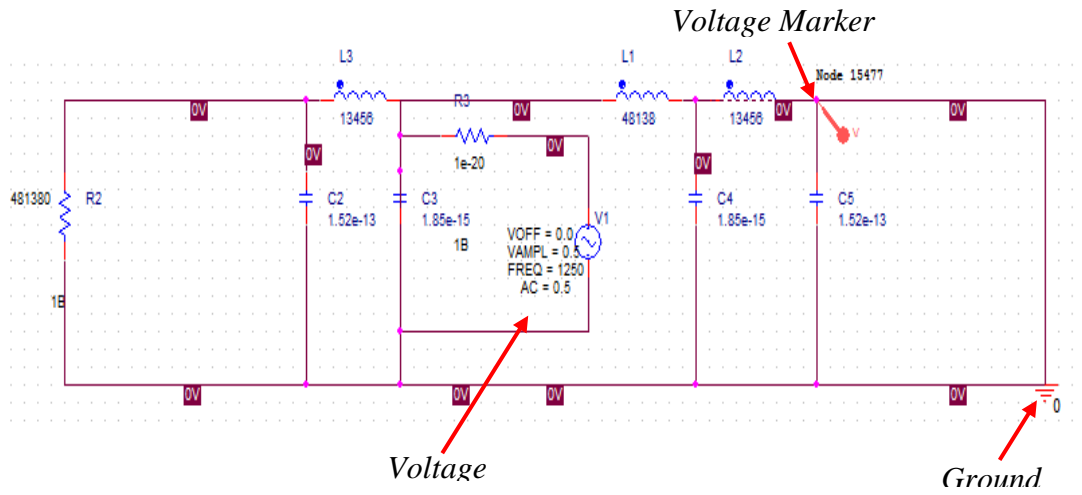
*Figure 4.15 – PSPICE* **circuit after switching input position and with voltage marker at 4th piezoelectric diaphragm**
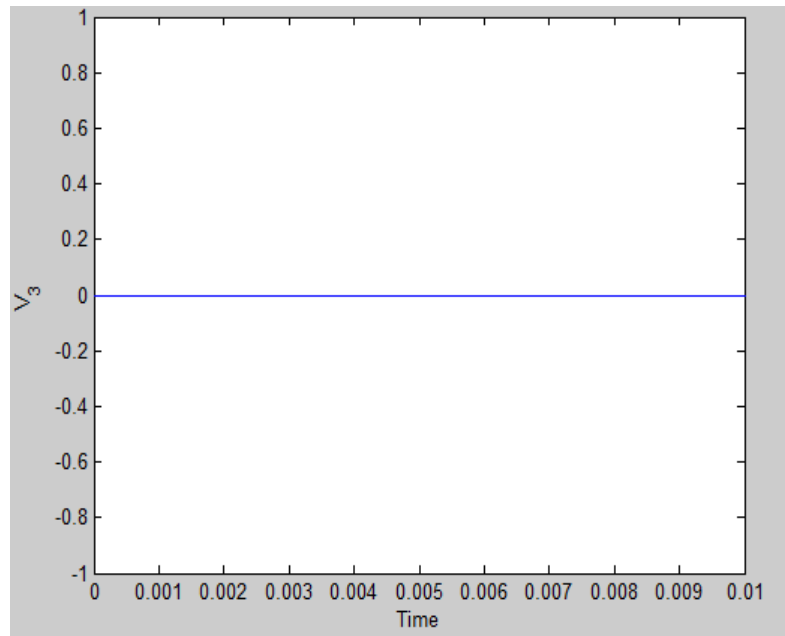


**Figure 4.16 - Time response obtained from *PSPICE* with voltage marker across capacitor and ground inside the loop**

## 4.9. Comparison of Experimental Results and *PSPICE* Results:

The two extreme values of α, each corresponding to a time response plot and a plot which was between $V_3$ and $\frac{d}{dt}V_3$ have been putte together to compare the plots for two same values of α obtained from Experiment and from *PSPICE*.



*(b)*
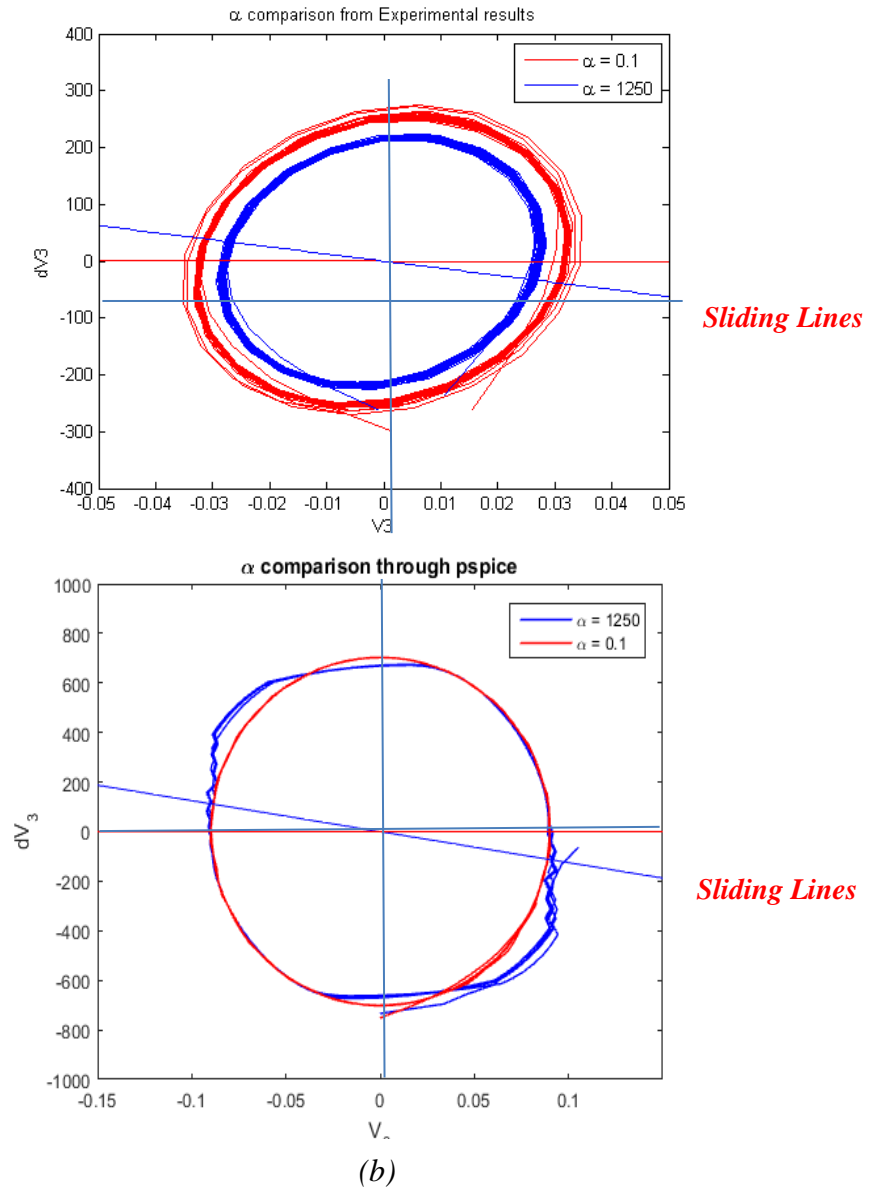
**Figure 4.17 – Comparison of plane phase between experimental and PSPICE**
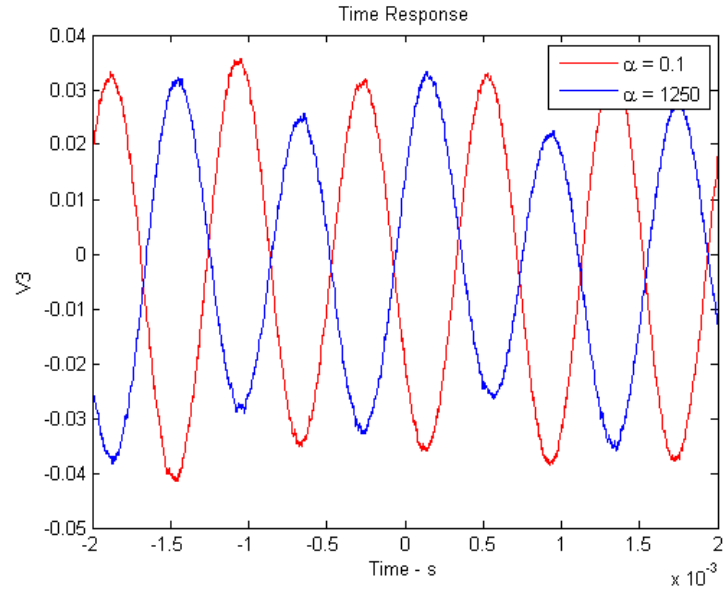
*(a)*
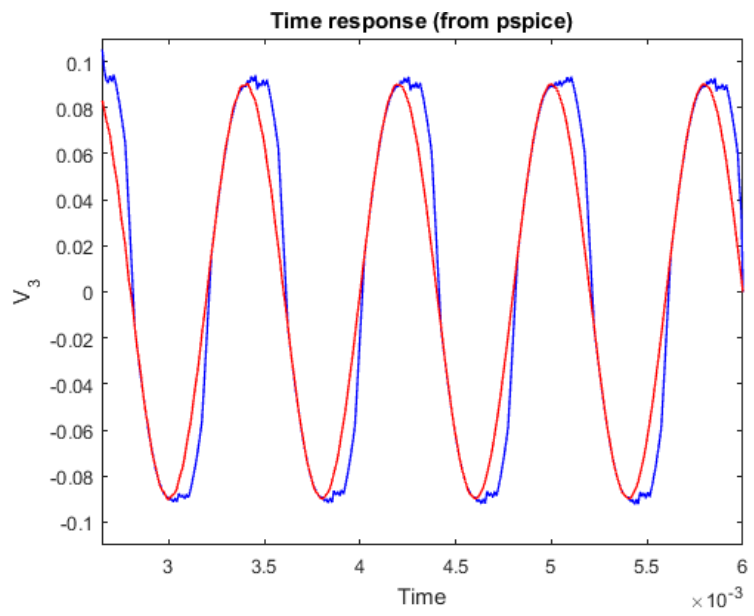


*(b)*

**Figure 4.18 – Comparison of Time Response between Experimental and PSPICE Results**

**4.10. Summary:**

In conclusion, the electrical equivalent of the Active Nonreciprocal Acoustic Metamaterial was constructed in *PSPICE*, an electrical circuit's simulations and analysis software. Similar inputs were used in the simulation as given the Active Acoustic Nonreciprocal Metamaterial cell experimentally. Different values of $\alpha$ were used which were associated with different external resistance values and the results were plotted. On comparing the results of the experiments and the simulations obtained, it can be inferred that the results obtained from *PSPICE* simulations and experiments conducted are in agreement with each other.

# Chapter 5

# CONCLUSIONS AND RECOMENDATIONS FOR FUTURE WORK

## 5.1. Conclusions:

As an *'electrical diode'* can work as an open switch and a close switch, i.e. it can work be used to flow the electric charges from one point to another and if revered, the same device can also be used as something which stops the electrical current from flowing. Similarly, an acoustic diode, Active Non-reciprocal Acoustic Metamaterial *(ANAM)* has been presented in this thesis. This device can also be used as an open switch and/or a closed switch depending on the requirements. Unlike electrical diode, this device can be programmed and through which desirable non-reciprocity characteristics can be achieved.

Comprehensive studies, which includes experimental validations, mathematical models development, prototypes developments and simulation have been done to study and validate the non-reciprocal characteristics behavior of the Active Non-reciprocal Acoustic Meta-material. Through active and passive nonreciprocal acoustic metamaterials *(ANAM)*, a device has been created which possess programmable characteristics to enable operation over broad frequency band unlike all available hard wired nonreciprocal metamaterials which operate over limited frequency bands.

Various nonlinear analog alternatives have been considered for generating desirable dissipation-pressure characteristics of the *ANAM*. Lumped-parameter mathematical models have been developed to describe the interactions of the control alternatives with the dynamics of the *ANAM* components including the acoustic cavities and the flexible piezoelectric boundaries.

Time and frequency domains performance characteristics have been investigated of the *ANAM* when coupled with the various nonlinear analog and digital control alternatives as influenced by the design parameters of both the *ANAM* and the controllers.

This study of a new class of active nonreciprocal acoustic metamaterial (*ANAM*) platforms that can be programmed to achieve reversible transmission and/or attenuation of acoustic wave propagation in structures. The presented *ANAM* can find its applications in interior and exterior noise mitigation.

For example, the *ANAM* can be used to manufacture aircraft fuselage to isolate the engine and flow noise from propagating to the interior of the fuselage and enabling any noise generated inside the fuselage to escape to the surrounding medium. Also, the *ANAM* can be employed in underwater vehicles in order to isolate the engine and flow noise from propagating to the exterior of the vehicle to ensure stealth operation. Between these two extreme cases, there are many others that are only limited by human imagination.

## 5.2. Recommendations for Future Work:

Although this thesis has presented a detailed theoretical and experimental development of the concept of active nonreciprocal acoustic metamaterials (*ANAM*), it has opened the door for many new directions that can be pursued in the future.

Distinct among these new directions is the need to extend the present work to studying the performance of the *ANAM* when the unit cell is subjected to either transient or random incident acoustic waves.

More work is needed to rigorously establish the optimal slope of the switching line of the sliding mode controller that quantifies its effect on the non-reciprocity of the *ANAM*.

Further work is needed to modeling and testing 2D arrays of *ANAM*. This extension will ensure the applicability of the *ANAM* to many practical and important problems.

Work is also needed to compare between the performance characteristics of the different approaches of the *ANAM* in order to determine their limits and merits.

# References

1.  **Lorentz H. A.,** "The theorem of Poynting concerning the energy in the electromagnetic field and two general propositions concerning the propagation of light," Amsterdammer Akademie der Wetenschappen, Vol. 4, p. 176, 1896.

2.  **Helmholtz, H**. Theorie der Luftschwingungen in Röhren mit offenen Enden. Journal für die reine und angewandte Mathematik, Vol. 57, pp. 1-72, 1860.

3.  **Rayleigh J. W.S.,** "On the magnetic rotation of light and the second law of thermodynamics", Nature (London), Vol. 64, p. 577, 1901.

4.  **Rayleigh J. W. S.**, The Theory of Sound, Dover Publications; 2nd edition, 1945.

5.  **Siegman A.E.**, Lasers, University Science Books, Sausalito, CA, 1986.

6.  **Jalas D. *et al*.** , "What is — and what is not — an optical isolator", *Nature Photonics*, Vol. 7, No. 8, pp. 579–582, 2013.

7.  **Dames C.**, "Solid-state thermal rectification with existing bulk materials," *ASME Journal of Heat Transfer,* Vol. 131, pp. 061301, 2009.

8.  **Liu C. *et al.,*** "Frequency-Preserved Acoustic Diode Model with High Forward Power-Transmission Rate", *Physical Review Applied*, Vol. 3, pp. 064014, 2015.

9.  **Popa B.-I. and Cummer S. A.**, Non-reciprocal and highly nonlinear active acoustic metamaterials", *Nature Communications*, Vol., 5, pp. 3398 | DOI: 10.1038, 2014

10. **Gu Z.-M *et al.*,** "Broadband non-reciprocal transmission of sound with invariant frequency", http://arxiv.org/ftp/arxiv/papers/1506/1506.01049.pdf, 2015.

11. **A. Baz**, "The Structure of an Active Acoustic Metamaterial with Tunable Effective Density", *New Journal of Physics*, Vol 11, 1230102009, 2009.

12. **A. Baz**, "An Active Acoustic Metamaterial with Tunable Effective Density", *ASME Journal of Vibration & Acoustics*, Vol. 132, No. 4, 041011 1-9 , 2010.

13. **W. Akl, and A. Baz**, "Multi-cell Active Acoustic Metamaterial with Programmable Bulk's Modulus", *Journal of Intelligent Material Systems and Structures*, Vol. 21, pp. 541-556, March 2010.

14. **W. Akl and A. Baz**, "Analysis and experimental demonstration of an active acoustic metamaterial cell", *J. Appl. Phys*. Vol. 111, No. 4, 044505, 2012.

15. **W. Akl and A. Baz**, "A technique for physical realization of anisotropic density matrices with application to acoustic beam shifters", *J. Appl. Phys*., Vol. 111, No. 2, 024907, 2012.

16. **W. Akl and A. Baz**, "Experimental characterization of active acoustic metamaterial cell with controllable dynamic density", *J. Appl. Phys*., Vol. 112, 084912, 2012.

17. **W. Akl, A. Elsabbagh, and A. Baz**, Acoustic metamaterials with circular sector cavities and programmable densities", *Journal of the Acoustical Society of America*, Vol. 132, No. 4, Pt. 2, pp. 2857-2865, October 2012.

18. **W. Akl and A. Baz**, "Multicell active acoustic metamaterial with programmable effective densities", *ASME Journal of Dynamic Systems, Measurement, and Control*, Vol. 134 , No. 6, pp. 061001-(1-11), 2012.

19. **W. Akl and A. Baz**, "Active Acoustic Metamaterial with Simultaneous Programmable Density and Bulk Modulus", *ASME Journal of Vibration & Acoustics*, Vol. 135, No. 3, 031001, 2013.

20. **W. Akl and A. Baz**, "Active Acoustic Metamaterial With Simultaneously Programmable Density and Bulk Modulus", *ASME Journal of Vibration and Acoustics*, Vol. 135, No. 3, 031001, 2013.

21. **M. Nouh, O. Aldraihem, and A. Baz**, "Vibration characteristics of metamaterial beams with periodic local resonances", *ASME Journal of Vibration and Acoustics*, 136(6), 061012 (2014).

22. **Althamer S. and Baz A.**,"Active acoustic metamaterial with fractional derivative controller", *Proc. of Smart Structures and Materials Conf.*, SPIE 9064, Health Monitoring of Structural and Biological Systems 2014, 90641V, DOI: 10.1117/12.2046424, ed. by Tribikram Kundu, San Diego, CA, 9 March 2014.

23. **W. Akl and A. Baz**, "Interior Acoustic Cloak", *AIP Advances* 4, 124305, 2014, http://dx.doi.org/10.1063/1.4902100.

24. **W. Akl and A. Baz**, "Active Acoustic Metamaterials", in *Theory and Design of Acoustic Metamaterials,* Editor(s): P. Frank Pai and Guoliang Huang, SPIE Press, Bellingham, WA, Volume: PM260, 2015

25. **M. Nouh, O. Aldraihem, and A. Baz**, "Wave propagation in metamaterial plates with periodic local resonances", *Journal of Sound and Vibration*, 341, 53:73 (2015).

26. **M. Nouh, O. Aldraihem, and A. Baz**, "Periodic metamaterial plates with smart tunable local resonators", *Journal of Intelligent Material Systems and Structures*, DOI: 10.1177/1045389X15615965, 2016.